March 2024

QUANTUM CHAOS, INTEGRABILITY, AND HYDRODYNAMICS IN NONEQUILIBRIUM QUANTUM MATTER

Javier Lopez Piqueres
University of Massachusetts Amherst

QUANTUM CHAOS, INTEGRABILITY, AND HYDRODYNAMICS IN NONEQUILIBRIUM QUANTUM MATTER

A Dissertation Presented

by

JAVIER LOPEZ PIQUERES

Submitted to the Graduate School of the
University of Massachusetts Amherst in partial fulfillment
of the requirements for the degree of

DOCTOR OF PHILOSOPHY

February 2024

Physics

QUANTUM CHAOS, INTEGRABILITY, AND HYDRODYNAMICS IN NONEQUILIBRIUM QUANTUM MATTER

A Dissertation Presented

by

JAVIER LOPEZ PIQUERES

Approved as to style and content by:

Romain Vasseur, Chair

Nikolay Prokofiev, Member

Benjamin Davidovitch, Member

Sarang Gopalakrishnan, Member

Anthony D. Dinsmore, Department Chair
Physics

ACKNOWLEDGMENTS

I would like to thank my adviser, Romain Vasseur, for support throughout these years. It has been a true privilege working under him. I would also like to thank the committee members, Benjamin Davidovitch, Nikolai Prokofiev, and especially Sarang Gopalakrishnan, with whom I have benefited from exciting research collaborations in the past. I would also like to thank the rest of the group members for fruitful in-and-out-of-office discussions: Hans Singh, Utkarsh Agrawal, Abhishek Kumar, Catherine McCarthy, Ewan McCulloch, Fergus Barratt, Brayden Ware, and Aaron Friedman. It was also a pleasure sharing the 402 office throughout the years with other grads: Ke Wang, Vahini Reddy, Chris Amey, Xiansheng Cai, and Tao Wang. Some words of gratitude go towards other members of the Physics department who made graduate school life run smoother: Narayanan Menon, and Anthony Dinsmore, for their availability when I needed help with bureaucratic matters; and Heath Hatch, and Brook Toggerson for their support during my first semester teaching Physics 131. Many thanks go to Katie Bryant as well for making sure all administrative matters ran smoothly.

Life in Amherst over these years would have not been as fulfilling without the company of friends and partners I've had. Despite being thousands of miles away, I feel also very lucky to have maintained such strong bonds with my family and friends from back home. I am especially thankful to my parents and two sisters for their support and encouragement over the years.

ABSTRACT

QUANTUM CHAOS, INTEGRABILITY, AND HYDRODYNAMICS IN NONEQUILIBRIUM QUANTUM MATTER

FEBRUARY 2024

JAVIER LOPEZ PIQUERES

B.Sc., UNIVERSIDAD AUTÓNOMA DE MADRID

M.Sc., ÉCOLE NORMALE SUPÉRIEURE, PARIS

Ph.D., UNIVERSITY OF MASSACHUSETTS AMHERST

Directed by: Professor Romain Vasseur

It is well-known that the Hilbert space of a quantum many-body system grows exponentially with the number of particles in the system. Drive the system out of equilibrium so that the degrees of freedom are now dynamic and the result is an extremely complicated problem. With that comes a vast landscape of new physics, which we are just recently starting to explore. In this proposal, we study the dynamics of two paradigmatic classes of quantum many-body systems: quantum chaotic and integrable systems. We leverage certain tools commonly employed in equilibrium many-body physics, as well as others tailored to the realm of non-equilibrium scenarios, in order to address various problems within this evolving field. Our contributions are the following:

Inspired by random matrix theory and random unitary circuits subject to projective measurements, we first uncover a novel phase transition in a model of random

tensor networks separating an area-law from a logarithmic-law in the scaling of entanglement entropy of a many-body wavefunction. Next, we study transport in the Rule 54 cellular automaton, a paradigmatic integrable model displaying just two species of solitons of different chiralities. Our contribution here is a sound numerical verification of some of the formulas for transport coefficients recently derived within a *generalized hydrodynamic* approach valid for integrable systems. Using the equations of generalized hydrodynamics as a starting point we then propose a new phenomenological scheme based on a relaxation-time approximation widely used in kinetics, but fundamentally different, to study the experimentally relevant regime where only a few conservation laws are present. We then aim at uncovering the hydrodynamics of integrability-breaking starting from fully microscopic dynamics. To do so we study a noisy version of the Rule 54 model and of the hard-rod gas, where the source of noise in both models is backscattering of solitons. We find that these models of integrability-breaking are atypical in that in the former relaxation occurs at long time scales owing to the presence of kinetic constraints, and the latter displays singular transport signatures as a result of infinitely many conserved charges despite the model being nonintegrable. Finally, we conclude by studying operator spreading in both integrable and chaotic quantum chains. Using hydrodynamics and tensor network simulations we find distinctive signatures of these two classes of models when looking at their operator front.

TABLE OF CONTENTS

LIST OF TABLES

Table **Page**

LIST OF FIGURES

Figure **Page**

INTRODUCTION

It is known in popular folklore that the *three body problem* was the only problem to ever give Newton headaches [Tao14]. The only major progress on this problem had to wait a couple centuries, when Poincaré, despite not being able to find a closed-form solution to the problem, laid the foundations of *chaos theory* (all the while revolutionizing various areas of mathematics) [Che15]. Fast forward into the present and the $n \geq 3$ *body problem* is still a mystery. The inability to solve the problem of many interacting objects is sometimes known as the *curse of dimensionality*. Despite this natural obstruction, different ideas and methods have been developed to tackle seemingly complex problems involving many degrees of freedom interacting with each other. Ideas based on universality, the renormalization-group, perturbative and variational methods, etc; have proved successful in determining macroscopic properties of such complex systems; only at *equilibrium*. Away from it, much less is known: the added layer of complexity that stems from *temporal* (and not just *spatial*) correlations yields room for new and unexpected phenomena with no equilibrium counterpart. At the same time, many of the ideas that work in the equilibrium scenario may fail terribly in the nonequilibrium context (such as is the case of many perturbation theory based methods [Mac07]), or simply not work at all (it is not clear what the relevant variational manifold of physical states should look like away from equilibrium). Nevertheless, one hopes that such exponential complexity could be possibly compressed in such a way we can at least accurately simulate these systems on a computer, either by using *equilibrium-inspired* methods, or by means of completely new frameworks with no equilibrium counterpart.

This work fits within the general paradigm of finding new efficient representations of underlying highly complex, dynamical phenomena. We study quantum many-body systems out of equilibrium inspired in part by methods that have proven to work in the equilibrium setting, such as is the case of tensor network based methods, as well as tools particular to the nonequilibrium setting, such as is the case of hydrodynamic based approaches.

In Chapter 1 we discuss the basics of quantum chaotic systems. We explore a novel *entanglement phase transition* in a system of random tensor networks that reproduces some universal properties of quantum many-body chaotic systems and that shares many properties with a system of *qudits* (d-level quantum systems) evolved under random unitary gates subject to random measurements. Using the cavity method from spin-glass theory and arguments based on universality, we analytically extract the critical properties of the entanglement phase transition when the topology of the tensor network is that of a tree, finding that the transition belongs to the universality class of the n-state Potts model. Based on this, we conjecture our results provide the basis for the *mean-field* universality class of entanglement phase transitions.

In Chapter 2 we discuss integrable systems. Despite having been studied for many decades in the context of their thermodynamic properties, it has only been just recently that much progress has been made in their study away from global equilibrium. A new hydrodynamic approach, dubbed *generalized hydrodynamics* (or GHD for short) – named that way as a natural extension of the standard theory of hydrodynamics of integrable systems (systems with *infinitely* many *local* conservation laws) – has shed new light into the nonequilibrium properties of such systems. Here we put this hydrodynamic theory to test, by studying a very simple integrable model, the Rule 54 cellular automaton where many of the GHD formulas can be put to scrutiny numerically.

It is in Chapter 3, where we discuss the core work of the Thesis. Using the GHD framework as a starting point, we explore the physics of more realistic systems, that are strongly interacting, far-from-equilibrium, but *not* integrable. Using the equations of generalized hydrodynamics as a starting point we then propose a new phenomenological scheme based on a relaxation-time approximation widely used in kinetics, but fundamentally different, to study the experimentally relevant regime where only a few conservation laws are present. This hydrodynamic approach is verified to work extremely well when compared with first-principle based numerical simulations using tensor networks. We then aim at uncovering the hydrodynamics of integrability-breaking starting from fully microscopic dynamics. To do so we study a noisy version of the Rule 54 model where the source of noise is backscattering of solitons. This perturbation has the effect of preserving the conservation in the number of the total number of solitons of both chiralities, while forcing the imbalance of both chiralities to decay. We show that while the dynamics of the tagged quasiparticles is well-captured by our theory, transport on the other hand evades a full analytical treatment owing to the presence of kinetic constraints. In order to have a full analytical-handle of transport in an interacting system away from integrability we study backscattering again, this time in the hard-rod gas. The hard-rod gas is a simpler model than that of Rule 54, yet it shares many properties with most integrable models. We successfully describe transport analytically in this noisy version of the hard-rod gas in the limit of small noise, providing, to the best of our knowledge, the first fully analytically tractable model of transport of an interacting, nearly integrable model where integrability-breaking leads to large momentum transfer, going beyond the types of perturbations currently tackled by the *form-factor* expansion formalism. Furthermore, the resulting model answers the intriguing question of what happens when the integrablity-breaking perturbation breaks infinitely many charges, while preserving infinitely remaining ones.

In Chapter 4 we again study chaotic as well as integrable systems, this time within the context of operator spreading. Using GHD we show that the *right-weight* – a measure of operator spreading, has a front that decays anomalously for all accessible time scales, in contrast with quantum chaotic systems that are governed by a decay consistent with a purely gaussian front. We also give numerical evidence that while small bond dimension matrix product operators are sufficient to capture the exponentially decaying tail of the front, they lead to significant quantitative and qualitative errors for the actual front.

We close in Chapter 5 with some conclusions from the work presented in this Thesis.

CHAPTER 1

QUANTUM CHAOTIC SYSTEMS

In the first part of this Chapter, we give a brief exposition of the main ideas behind the theory of quantum chaos, focusing on two of its pillars, the *eigenstate thermalization hypothesis*, and *random matrix theory*. We then move on to describe *random unitary circuits* and *random tensor networks*, which are models inspired by random matrix theory with the added constraint of locality. We shall outline as well the basics of tensor network theory. In the last part of the Chapter, we work out a model of random tensor networks that feature an *entanglement phase transition* between an area-law to a logarithmic-law in entanglement entropy when the bond dimension of the network is tuned. The results of that section follow [LPWV20].

1.1 Eigenstate Thermalization Hypothesis and Random Matrix Theory

Roughly speaking, quantum chaotic systems comprise quantum systems with very few or no conservation laws. Defining precisely quantum chaos is a bit subtle. While there exists a precise definition of *classically* chaotic systems, the same is not true in the quantum case. Chaoticity in classical systems is the result of nonlinearity in the evolution of a dynamical system and extreme sensitivity to the initial conditions [1]. The main consequence of this is that any chaotic system will reach a unique stationary state after long enough times, from which we can characterize the statistical properties

[1] Extreme sensitivity here can be quantified in terms of a positive Lyapunov exponent.

of the system after equilibrium is reached [Rue78, Gal13]. We then say the system *thermalizes*. The main feature of nonlinear dynamics is phase space mixing, and it is what ultimately leads to positive entropy production and loss of information of the initial state [KS12]. It is this basic feature that questions the mere existence of chaos in the quantum context, as the Schrödinger equation is linear and so one would think that no chaos can ever be present in a quantum system. Further, time evolution is unitary and so no information can ever be lost. The resolution to this little paradox was given by von Neumann in his famous work [Neu29]. He gives a natural notion of ergodicity in the quantum context, whereby instead of focusing on *states* evolved under the Schrödinger equation, one should pay instead attention to local *observables*. In looking at local observables at long times, the system behaves as if ergodic, this is, the time average of an observable at long enough times and w.r.t. an initial state within a given energy shell $[E, E+\delta E]$, should be equal to the average of that observable w.r.t. the microcanonical ensemble at that energy E [PSSV11].

Recent years have witnessed a revival in interest in understanding the emergence of statistical mechanics in quantum many-body systems, sparked in great part by remarkable experimental progress [KWW06, HLF$^+$07, BDZ08] (see also the reviews [DKPR16, GE16, Deu18]). A major breakthrough was achieved with the inception of the Eigenstate Thermalization Hypothesis (ETH) as a promising candidate to explain the microscopic origin of thermalization in generic closed quantum many-body physics [Deu91, Sre94, Sre99, RDO08a]. ETH can be succinctly expressed by the following formula for the matrix elements of a few-body local observable $\hat{\mathcal{O}}$ in the basis of energy eigenstates $\{|E_\alpha\rangle\}$ [Sre99]

$$\mathcal{O}_{\alpha\beta} \equiv \langle E_\alpha|\hat{\mathcal{O}}|E_\beta\rangle = \mathcal{O}_{\rm mc}(E)\delta_{\alpha\beta} + e^{-S(E)/2} f_{\hat{\mathcal{O}}}(\omega, E) R_{\alpha\beta}, \tag{1.1}$$

where $E = \frac{E_\alpha + E_\beta}{2}$ is the energy average, $\omega = E_\alpha - E_\beta$ is the energy difference, S is the thermodynamic entropy, and $R_{\alpha\beta}$ are random numbers that average to zero and have

variance equal to one. Both the microcanonical average $\mathcal{O}_{\rm mc}(E)$ as well as the spectral function $f_{\hat{\mathcal{O}}}$ are some smooth functions. The formula (1.1) in particular shows that the microcanonical average centered around the eigenenergy E_α can be found by picking up *any* eigenstate within an energy window $[E_\alpha - \delta E_\alpha, E_\alpha + \delta E_\alpha]$ with δE_α sufficiently small in a sense specified in [RDO08a], in other words, $\langle E_\alpha|\hat{\mathcal{O}}|E_\alpha\rangle \approx \mathcal{O}_{\rm mc}(E_\alpha)$, where the $\approx$ should be understood as equality up to exponentially small errors.

Eq. (1.1) is very similar to the predictions from Random Matrix Theory (RMT) for what the components of a given observable should be between eigenstates of the Hamiltonian, namely,

$$O_{\alpha\beta} \approx \overline{\mathcal{O}}\delta_{\alpha\beta} + \sqrt{\frac{\overline{\mathcal{O}^2}}{\dim\mathcal{H}}}R_{\alpha\beta}, \tag{1.2}$$

where $\dim\mathcal{H}$ is the dimension of the Hilbert space. The similarity between the RMT and ETH predictions for the components of local observables is not mere coincidence, and in fact, the ETH ansatz reduces to that of RMT when restricted to a very narrow energy window so that $f_{\hat{\mathcal{O}}}(\omega, E)$ is constant in Eq. (1.1) [RDO08a]. The difference in content between ETH and RMT goes beyond the scope of the Thesis and we refer the interested reader to the review article [DKPR16]. The main point to make here is that RMT and ETH make universal predictions of *generic* quantum systems, where energy is the only conserved quantity. There are many systems where the presence of extra conserved quantities render the predictions from ETH and RMT inapplicable. Of particular relevance are integrable systems, which we discuss in the next Chapter, and many-body localized systems (see Ref. [AL18, AABS19] for recent reviews on the subject).

1.2 Random Unitary Circuits, (Random) Tensor Networks, & Entanglement Phase Transitions

Very recently the attention has been veered towards cooking up minimal models of quantum many-body systems embodying certain aspects of RMT, such as is the

case of random unitary circuits (RUCs). The extra ingredient in these systems is locality, enforced by the presence of local unitary gates that entangle two nearby qudits. These models have proved useful when studying out-of-equilibrium dynamics, as their simplicity allows for predictions for entanglement growth [NRVH17, ZN19a] and out-of-time-ordered correlators [NVH18a, vKRPS18a].

Consider a one dimensional array of qudits initially unentangled. Applying consecutive layers of two-qudit random unitary gates acting on two consecutive qudits as shown in Fig. 1.1 will produce a highly entangled state over time. The information about the initial state of the system becomes, at long enough times, *scrambled*, that is, hidden from local observables, and consequently one speaks of the system being thermalized [2]. This is because stationary states in this setup become volume-law entangled, in accordance with our expectations that thermal states have extensive entropy proportional to the volume of the system.

While RUCs give insight into the process of how quantum systems may eventually thermalize, recent attention has been directed towards studying under which conditions a system *fails* to thermalize and produce area-law entanglement at long enough times, as opposed to volume-law entanglement. Interspersing random measurements at a rate p with unitary gates, the resulting wavefunction may collapse to an area-law state if p is large enough (see Fig. 1.1). On the other hand, if p is low enough, the state should thermalize, that is, should have volume-law entanglement [3]. The expectation is thus that the competing action of disentangling projective measurements and entangling unitary dynamics should yield a *phase* transition at a critical measurement rate p_c between area-law and volume-law entanglement states. This is

[2]Note that the converse may not be true, since a thermalizing system may not necessarily imply it is scrambling, as is the case of Clifford circuits [VKRPS18b].

[3]The fact that one should generally have volume-law entanglement at a small non-zero measurement rate is a non-trivial statement, and in fact earlier works (mistakingly) suggested that any small amount of measurements is enough to maintain an area-law state in general [CNPS19].

indeed the case, and such phenomenon is for obvious reasons dubbed *measurement-induced phase transition* (MIPT) and has been subject to intense research in the very last few years (we cite here a few of the earliest works on this subject [LCF18, SRN19, BCA19, GH19, LF21, FVVY21, BCA20, JYVL19, LCLF20, ZGW$^+$20] as well as recent reviews [PV22, LRP22, FKNV23]).

There are multiple reasons why studying such transition may be of relevance. From the theory side, the entanglement transition for the case of Haar random circuits with random measurements in $(1+1)$-d has been connected to a (classical) percolation phase transition in 2D, described by a nonunitary conformal field theory with central carge $c = 0$. These types of conformal field theories are poorly understood. Understanding such random quantum circuits better may bring further insight into the nature of these conformal field theories. Still on the theory side, but from a more practical perspective, studying such random quantum circuits and their entanglement transitions may be of particular relevance in the context of *noisy intermediate scale quantum* (NISQ) devices. The minimal requirements needed to observe the MIPT, namely any set of unitary gates that is sufficiently entangling and randomly located mid-circuit measurements, makes the MIPT suitable to be probed in NISQ circuits, and this is indeed the case as has been done in works [4] [NNZ$^+$22, KSMM22, HIA$^+$23].

While RUCs provide a natural setup where to study such entanglement phase transitions, one can consider instead more abstract setups where the same minimal ingredients of locality and a tuning parameter driving the transition between area-law and volume-law entangled phases, are present. One such setup is *random tensor networks* which was studied even earlier than RUCs in Ref. [VPYL19]. In the next Section we describe a particular random tensor network where the entanglement tran-

[4] We remark that while the MIPT set-up is suitable for NISQ devices, it comes at a price of requiring post-selection, which forbids the scalability to a large number of qubits, and therefore, strictly speaking, fundamentally challenging to observe.

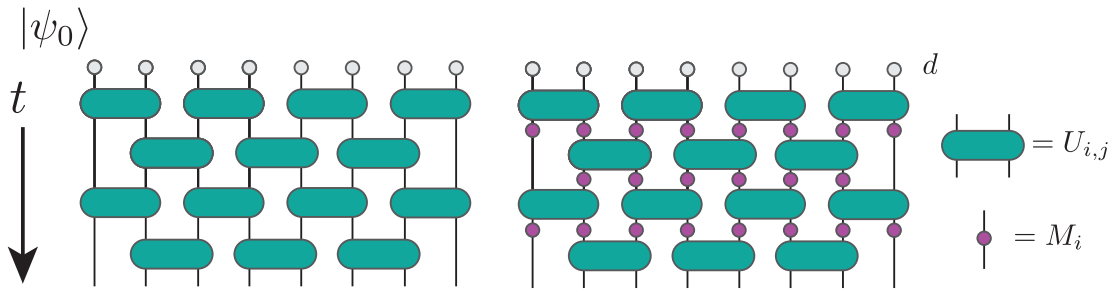

Figure 1.1. Random Unitary Circuit. Left: The gates U are drawn from the Haar ensemble of $d \times d$ matrices, where d is the local Hilbert space dimension ($d = 2$ for qubits), and act on a pair of neighbor qudits (gray dots for the initial state $|\psi_0\rangle$). Right: same but with interspersed random measurements.

sition can be accurately characterized. First, however we give a brief outline of the theory behind tensor networks.

1.2.1 Interlude: Tensor Network Basics

Consider any quantum state $|\psi\rangle$ with L degrees of freedom (dof) each of which carries a local Hilbert space dimension of size d. An exact representation of this state requires d^L complex numbers, a task which in the simplest instances of qubits with $d = 2$, permits even the most powerful computers to work with at most $L = \mathcal{O}(10)$ qubits.

Tensor networks are representations of wavefunctions in terms of tensors connected by bonds, representing the amount of entanglement shared between the different tensors. In many circumstances of interest, they provide efficient representations of wavefunctions, by exploiting locality and the structure of entanglement in the wavefunction. Tensors in general will have two types of indices. One type characterizing the physical dimension of the local Hilbert space, d, plus a set of l indices, one for each of the l neighbors this tensor is connected to. We shall label such tensors with one upper index for the physical dimension, and l subindices, e.g. $T^i_{j_1,..,j_l}$, with $i = 1, ..., d$. The dimension of each of these l indices is the *bond dimension* (which is in principle

different for different bond indices), and characterizes the strength of entanglement between that tensor and each of its neighbors. The physical link is not connected to any other tensor.

Consider now a one dimensional wavefunction representing L qudits. As mentioned, a naive description of such wavefunction would require d^L complex numbers. A representation of the same wavefunction as a tensor network, which for this particular scenario of $1D$ it is named *matrix product state* (MPS), requires instead $\mathcal{O}(L\chi^2 d)$, where χ is the maximum bond dimension between any pair of tensors, see Fig. 1.2. The core of the success of tensor network methods lies in the realization that for many quantum states of physical relevance, only a finite amount of entanglement is shared between physical tensors (representing qudits). In particular, ground states of local, gapped Hamiltonians obey area-law for their entanglement [Has06, WVHC08], which means the bond dimension for such states should be a constant independent of the system size L in 1D, allowing for a very efficient description of such states using tensor networks. The key step that allows to represent any arbitrary wavefunction in terms of a tensor network is the *singular value decomposition* (SVD), which permits to decompose any tensor such as the one in Fig. 1.2 in terms of the matrix S containing its singular values. These singular values are nothing else than the Schmidt eigenvalues separating the two parts of the wavefunction at that link. If we know a priori the structure of entanglement in the system, we can exploit this to our advantage, by restricting the maximum bond dimension at each link, which amounts to truncating the matrix S at each link to be of only size $\chi_L \times \chi_R$, where χ_L is the bond dimension to the *left* side of S and χ_R is the bond dimension to the *right* of S.

While tensor networks provide an efficient representation of generic ground states, one may wonder what happens with excited states, and in particular, with nonequilibrium states such as the ones generated by evolving an initial trivial state with RUCs. Studying the dynamics of MPSs can be done as well using the language of

Figure 1.2. Tensor network decomposition. Left: description of a one dimensional wavefunction of 5 qudits in terms of an MPS with tensors $T^{\alpha_i}_{\beta_{i-1}\beta_i}$ in the presence of open boundary conditions (obc). Right: decomposition of an arbitrary rank-4 tensor using SVD.

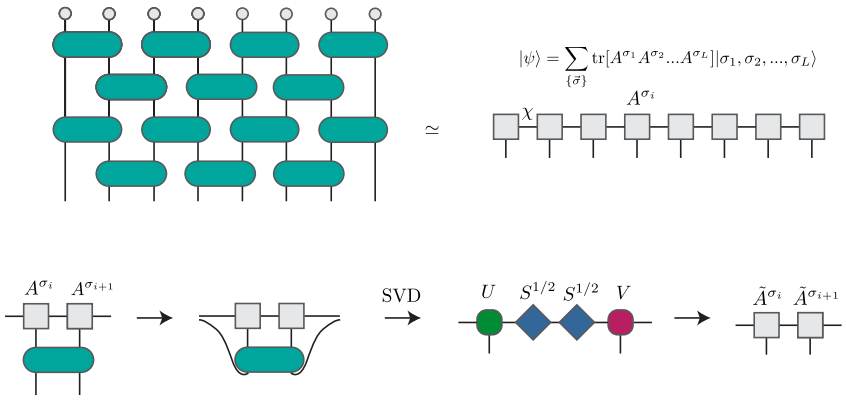

Figure 1.3. Mapping between quantum circuits and tensor networks: basics of the TEBD algorithm. Top: Any state evolved via a quantum circuit can be expressed in terms of a tensor network. Bottom: This requires contracting the gates with pairs of MPS blocks (tensors) A^{σ_i}, $A^{\sigma_{i+1}}$ followed by SVDs, identifying the new blocks $\tilde{A}^{\sigma_i} = US^{1/2}$, $\tilde{A}^{\sigma_{i+1}} = S^{1/2}V$.

tensor networks. In this case however the rapid growth of entanglement over time limits the efficiency of the method to short-to-intermediate time scales. The particular way tensors get updated upon time evolution is captured by the *time evolving block decimation* (TEBD) algorithm [Vid03, ZV04, Sch11b] (see Fig. 1.3), which is routinely used to study the dynamics of 1D quantum many-body systems in many contexts (in fact, we shall use this method in pretty much all the Chapters that follow when studying dynamical correlators).

Having constructed a tensor network it remains to compute observables and correlators. In this context it is useful to introduce the second kind of tensor network that

will be used a lot throughout, the *matrix product operator* (MPO). This is simply a generalization of the MPS tensor network to describe arbitrary operators, including density matrices. Its shape is very similar to that of an MPS except that each block of the tensor network has now an added physical index, thus MPOs have local tensors of the form $T^{\alpha_i,\bar{\alpha}_i}_{\beta_i\beta_{i+1}}$, where the second, dangling index $\bar{\alpha}_i$, refers to the *bra* in the density matrix description, i.e. $\rho = |\phi\rangle\langle\phi|$ [5]. Computing expectation values w.r.t. to mixed or pure states corresponds to contracting two tensor networks with each other in such a way so as to get a scalar. This amounts to contracting the physical, dangling bonds of the two tensor networks. For instance, the simplest example consists in contracting two MPS, e.g. $\langle\psi|\phi\rangle$.

There exists multiple ways to describe the same state using tensor networks. In other words, tensor networks have a redundancy in their description. There are two kinds of redundancies or degrees of freedom. The first one is *blocking* which we have discussed in passing. It is the idea that one can contract any virtual bonds in the network at the expense of getting a tensor with more indices (for instance in Fig. 1.2, the two tensors on both sides of the equality correspond to the same state). The second one, yet more important, is a *gauge* degree of freedom [PGSGG$^+$10]. This is a consequence of the fact we can always insert a resolution of identity between any pair of tensors, in such a way that each tensor gets redefined as $A \to M^{-1}AM$ (ommiting labels for the sake of exposition). This has very important consequences in the computation of physical (local) observables for one dimensional systems. The reason being is that, by exploiting this gauge dof, we can always bring an MPS into *canonical* form, which means any local observable between any two pairs of states can be computed by simply contracting the tensors at around the support of the operator

[5] In fact, any MPO can be mapped to a corresponding MPS by vectorizing a given density matrix, $\rho \to |\rho\rangle\!\rangle \equiv |\phi\rangle \otimes |\phi\rangle$. This vectorization procedure is used routinely when computing tensor network contractions involving density matrices, see in particular Sec. 4.1.2 of Chapter 4

corresponding to that observable, which is much more computationally efficient than contracting the entire tensor network.

1.3 Mean Field Entanglement Transitions in Random Tree Tensor Networks

We have seen that any state can be represented as a tensor network. Studying entanglement phase transitions in such setups may thus provide universal insights into the nature of the transition, not only applicable within the context of RUCs but other physical systems of relevance as well, of which the many-body localization transition is a prime example. The main object of study in these transitions is the entanglement entropy. In all such instances the entanglement entropy close to the transition and in the scaling limit takes the universal form $S - S_c = F((g - g_c)L^{1/\nu})$, with g the parameter driving the transition – either the bond dimension D in the case of random tensor networks, or the measurement rate p for random quantum circuits – and S_c the entanglement entropy at criticality.

While previous works had identified the presence of such entanglement transition in random quantum circuits subject to random measurement from numerical simulations [LCF18, SRN19, BCA19, GH19], it had not been clear whether such transition indeed existed, and if so what the critical properties of the transition should be (i.e. exact critical point, critical exponents, and exact scaling form of the entanglement at the transition). Ref. [JYVL19, BCA19] showed that there is indeed a phase transition at the critical point in Haar random circuits subject to random projective measurements using a replica approach (which we describe a bit more below). The notorious difficulty of the problem, in particular, the fact that the transition is described by a certain nonunitary conformal field teory with central charge $c = 0$ for which little is known about, hindered the analytical computation of the critical exponents.

Because of the innherent difficulty of the replicated statistical mechanics model, in particular the 2D topology of the resulting model, in Ref. [LPWV20] we studied a version of the same model but on a tree. The absence of loops in this setup should in principle make the extraction of critical exponents (and other critical properties) easier, but not necessarily trivial. We found that random tree tensor networks have indeed an entanglement phase transition, for which the critical properties can be extracted analytically (assuming the validity of the replica approach). In a sense, this is similar to the mean-field universality class familiar from standard condensed matter physics, albeit in a new setup.

The setup— We consider one-dimensional quantum wavefunctions $|\psi\rangle$ given by tree tensor networks (Fig. 1.4). The physical degrees of freedom are qudits of dimension d, which live at the boundary of the tree tensor network. Let q be the coordination number of the tree, and D the bond dimension of the tensor network. We choose the tensors to be random [HNQ$^+$16], obtained by drawing the tensor for each node of the tree independently from a featureless Gaussian distribution characterized by zero mean and unit variance. Because of the tree geometry, such wavefunctions can have logarithmic entanglement scaling, contrary to matrix-product states for example.

Our main goal is to study the entanglement properties of wavefunctions generated from this random ensemble. This approach is inspired in spirit by RMT, but it allows us to include some locality structure in the geometry of the "bulk" tensor network, controlling the entanglement of the boundary physical system. We will focus on the tensor-averaged Renyi entropies

$$S_A^{(n)} = \frac{1}{1-n}\overline{\log \frac{\mathrm{tr}\rho_A^n}{(\mathrm{tr}\rho)^n}}, \tag{1.3}$$

where $\overline{(\dots)}$ refers to averaging over random tensors, and ρ_A is the reduced density matrix in some contiguous interval A of size L_A obtained from tracing out the complement of A in $\rho = |\psi\rangle\langle\psi|$ (Fig. 1.4).

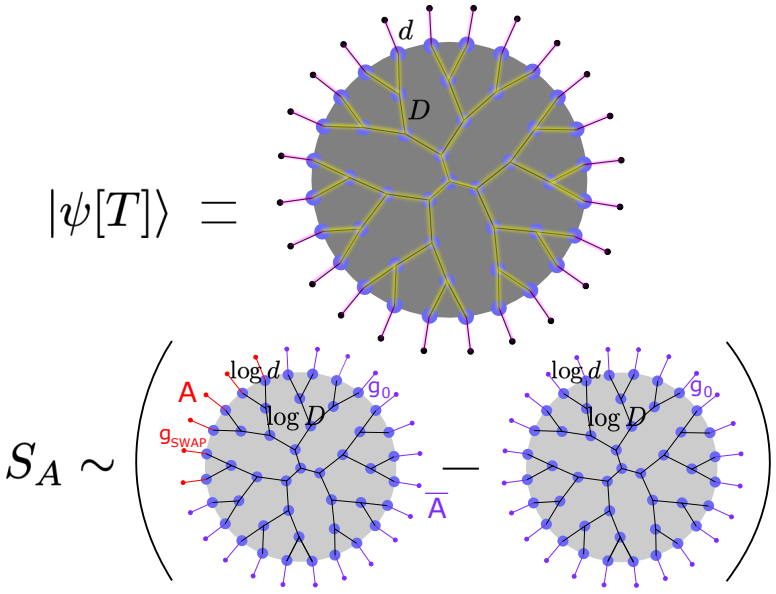

Figure 1.4. Random tree tensor networks. Top: tree tensor network geometry: the physical quantum degrees of freedom live at the boundary ("leaves") of the tree. Bottom: the entanglement entropy of a region A at the boundary can be expressed as the free energy cost of a domain wall of a classical statistical mechanics model defined on the Cayley tree.

Statistical Mechanics model — In order to compute these Renyi entropies, we follow Refs. [ZN19b, VPYL19, BCA19, JYVL19] and use a replica trick $\log \mathrm{tr}\rho_A^n = \lim_{m\to 0}((\mathrm{tr}\rho_A^n)^m - 1)/m$. This allows us to express (1.3) as

$$S_A^{(n)} = \frac{1}{n-1} \lim_{m\to 0} \frac{1}{m} \left(\mathcal{F}_A - \mathcal{F}_0\right), \tag{1.4}$$

with $\mathcal{F}_{A,0} = -\log \mathcal{Z}_{A,0}$ and $\mathcal{Z}_0 \equiv \overline{(\mathrm{tr}\rho^n)^m}$, $\mathcal{Z}_A \equiv \overline{(\mathrm{tr}\rho_A^n)^m}$. Using this exact identity, the calculation of the Renyi entropies reduces to computing $\mathcal{Z}_0$ and $\mathcal{Z}_A$, and to evaluate the replica limit (1.4). When m and n are integers, the averages in $\mathcal{Z}_0$ and $\mathcal{Z}_A$ can be evaluated analytically using Wick's theorem. One can then express the partition functions $\mathcal{Z}_A$ and $\mathcal{Z}_0$ in terms of a classical statistical mechanics model, whose degrees of freedom are *permutations* $g_i \in S_{Q=nm}$ labelling different Wick contractions at each vertex of the tensor networks. Since the degrees of freedom of this statistical mechanics model live on the nodes of the tree tensor network, they form a *Cayley tree*, and $\mathcal{Z}_A$ and $\mathcal{Z}_0$ differ only in their boundary conditions. Using the results of Ref. [VPYL19], we find that $\mathcal{Z}_0 = \sum_{\{g_i\}} \mathrm{e}^{-\mathcal{H}}$, with the following nearest-neighbor Hamiltonian

$$\mathcal{H} = -\sum_{\langle i,j\rangle} J_{\langle i,j\rangle} C(g_i^{-1} g_j), \tag{1.5}$$

where $C(g)$ counts the number of cycles in the permutation g, $J_{\langle i,j\rangle} = \log D$ with D the bond dimension for links connecting bulk tensors, and $J_{\langle i,j\rangle} = \log d$ (with d the dimension of the Hilbert space of the boundary physical qudits) for boundary couplings involving physical degrees of freedom. This Hamiltonian is invariant under global left/right multiplication of the degrees of freedom g_i by any permutation $h \in S_Q$, so it has a $S_Q \times S_Q$ symmetry. In this mapping, the trace over physical degrees of freedom in $\mathcal{Z}_0 = \overline{(\mathrm{tr}\rho^n)^m}$ forces the permutations on the boundary sites corresponding to the physical qudits to be fixed to the identity permutation $g_\partial = g_0 = ()$ in $\mathcal{Z}_0$. Meanwhile, boundary permutations in $\mathcal{Z}_A$ are fixed to identity if

they belong to $\overline{A}$ (the complement of A), whereas they are fixed to a different permutation $g_{\rm SWAP} = (12\dots n)^{\otimes m}$ if they belong to A. The permutation $g_{\rm SWAP}$ arises from enforcing the partial trace in $\mathcal{Z}_A \equiv \overline{({\rm tr}\rho_A^n)^m}$. Note that $C(g)$ is maximum for the identity permutation, so that the Hamiltonian (1.5) corresponds to ferromagnetic interactions.

In the language of this statistical mechanics model, the Renyi entropies (1.4) can be computed from the free energy cost of inserting a *domain wall* between the boundary permutations g_0 and $g_{\rm SWAP}$ at the entanglement interval. This provides a very simple picture of the scaling of the entanglement entropy as a function [6] of bond dimension D. If D is small (near 1), we expect the statistical mechanics model (1.5) to be disordered (paramagnetic), and the free energy cost in (1.4) will not scale with L_A: this corresponds to an area-law phase. If on the other hand D is large, the statistical mechanics model is in an ordered (ferromagnetic) phase with all bulk permutations aligned and equal to g_0, and the free energy cost in (1.4) will be given by the energy penalty of the bonds frustrated by the domain wall minimizing this energy ("minimal cut" through the network). For large L_A and generic intervals A, this minimal domain wall cuts $\sim \log L_A$ bonds of the tensor network (Cayley tree) corresponding to logarithmic entanglement scaling $S_A \sim (\log D) \log L_A$. This implies that the ordering transition of (1.5) at a critical coupling $J_c = \log D_c$ corresponds to an area- to logarithmic scaling of the Renyi entropies of the random tree tensor networks.

$Q = 2$ replicas and cavity method — In order to gain some insight into the scaling of the entanglement entropy, we start by analyzing the simpler case of $Q = 2$ replicas. As we will argue below, the mean-field nature of the statistical mechanics model on

[6] While the bond dimension D is in principle an integer, it is possible to construct tensor networks using projected entangled pairs that correspond to arbitrary D. In the following, we will assume $D > 1$ to be a real number.

the Cayley tree will make critical properties mostly independent of Q, allowing us to generalize this insight to the replica limit $Q \to 0$. For $Q = 2$, eq. (1.5) is simply an Ising model. If we let $g_i = \pm 1$ be the two elements of $S_2 \cong \mathbb{Z}_2$, (1.5) reads $\mathcal{H} = -\sum_{\langle i,j \rangle} J_{\langle i,j \rangle}(3 + g_i g_j)/2$, which up to an irrelevant additive constant, is an Ising model with coupling $K = J/2 = (\log D)/2$. To proceed, we use the so-called *Cavity Method* [MPV87, MMM09, DGM08] which is a standard approach for solving statistical mechanics problems on tree-like graphs. We start from an Ising model with coupling K, and generic boundary fields h_i acting on the boundary sites of the Cayley tree. It is straightforward to show that all boundary spins can be decimated, at the price of introducing new effective fields acting on the next layer of the tree, which now forms the new boundary. This process can then be iterated, and the resulting recursion ("cavity") equations for uniform boundary fields are then given by $\left[\sum_{\sigma_i = \pm 1} \exp(K \sigma_i \sigma_j + h^{(k+1)} \sigma_i)\right]^{q-1} = \mathcal{C} \exp(h^{(k)} \sigma_j)$, for some constant $\mathcal{C}$. Here we have assumed that we are working with $\mathcal{Z}_0$ for simplicity so that the boundary fields are uniform, but this approach can be readily extended to arbitrary inhomogeneous boundary fields.The critical behavior of this model is then easily deduced from solving for the cavity fields recursively. Approaching the transition from the paramagnetic phase, we find that the magnetization at the root of the tree decays exponentially with the number of layers N, $\langle \sigma_0 \rangle \sim \exp(-N/\xi)$ with a correlation length $\xi = -1/\log((q-1)\tanh K)$ that diverges at the critical coupling $K_c = \operatorname{arctanh}(1/(q-1))$, which is finite for coordination number $q > 1$. Expanding near the critical point yields $\xi \sim |K - K_c|^{-\nu}$, with $\nu = 1$. On the ferromagnetic side, we have $\langle \sigma_0 \rangle \sim h \sim (K - K_c)^{\beta}$, with $\beta = 1/2$. (A procedure to access this exponent was proposed in Ref. [GH19] in the context of random circuits.) The order parameter exponent $\beta = 1/2$ takes the mean-field value for a transition in the Ising universality class, a general feature of statistical mechanics on the Cayley tree [KT74]. On the other hand, the correlation

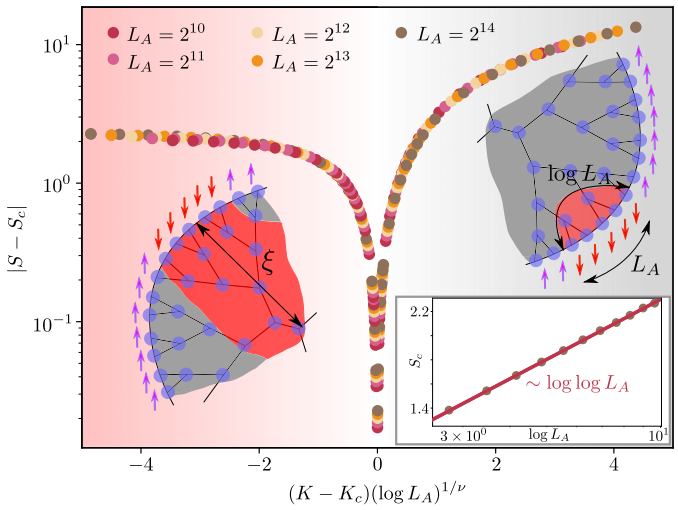

Figure 1.5. Entanglement scaling. Collapse of the boundary domain wall free energy cost for $Q = 2$ replicas, as a proxy for the entanglement entropy in the replica limit $Q \to 0$. For $K = (\log D)/2 > K_c$ the domain wall mostly follows a minimal cut through the bulk, so its energy scales logarithmically with the interval size L_A. For $K < K_c$, the domain wall fluctuates through the bulk over a number of layers given by the correlation length, which diverges as $\xi \sim |K - K_c|^{-\nu}$ with $\nu = 1$. Inset: at criticality, the entanglement scales as $S \sim \log\log L_A$.

length exponent $\nu = 1$ is inherited from quasi-one-dimensional physics, as has been noted previously [HI98].

Entanglement Scaling — The cavity method above can readily be applied to arbitrary configurations of the boundary fields, and can be used to evaluate eq. (1.4) in the case of $Q = 2$ replicas. We denote the averaged free energy cost of a domain wall $S(L_A) = \mathcal{F}_A - \mathcal{F}_0$, which is the quantity which becomes entanglement entropy in the limit $Q \to 0$ from eq. (1.4). On the paramagnetic side of the transition (small $K = (\log D)/2$), the Ising order decays ξ layers into the bulk, so we expect the entanglement to saturate to a constant value $S(L_A \to \infty) \propto \log \xi$, corresponding to area law scaling. This is consistent with our numerical results, which indicate a divergence $S(L_A \to \infty) \sim -\alpha \log(K_c - K)$ as $K \to K_c^-$. The saturation to this area law value occurs for $L_A \gg \xi_\star$ with the crossover scale $\xi_\star = \mathrm{e}^{\xi} = \mathrm{e}^{C/|K-K_c|}$. Therefore, while $\nu = 1$ in the bulk, in terms of the entanglement scaling the relevant diverging length

scale diverges exponentially near the transition, due to the tree geometry. On the ordered side of the transition ($K > K_c$), $S(L_A)$ is proportional to the energy cost of the domain wall which scales as the number of layers into the bulk $\sim \log L_A$. As expected from general scaling arguments, the prefactor is set by ξ, and we find $S(L_A) \sim \frac{\log L_A}{\xi}$. Finally, scaling at the critical point is required to be $S(L_A) \sim \alpha \log\log L_A$ by general scaling considerations from the behavior in the phases, in good agreement with our numerical solution to the cavity equations for the system sizes we can access (Fig. 1.5). In summary, we have

$$S \sim \begin{cases} \frac{\log L_A}{\xi} + \alpha \log\log L_A, & K \to K_c^+, \\ \alpha \log\log L_A, & K = K_c, \\ \alpha \log \xi, & K \to K_c^-. \end{cases} \tag{1.6}$$

We find that our results are consistent with the entanglement scaling at entanglement transitions in quantum chaotic systems subject to projective measurements or in wavefunctions given by square random tensor networks upon replacing $\log L_A \to L_A$ [SRN19, VPYL19, LCF19]. This is because geodesics (minimal cut minimizing the domain wall energy at large bond dimension) in flat 2D Euclidean space are given by straight lines, whereas they scale with the logarithm of the size of region A on the Cayley tree. These different regimes can be summarized by the universal scaling form $S - S_c = F((K - K_c)(\log L_A)^{1/\nu})$ with $\nu = 1$ shown in Fig. 1.5.

Replica limit — So far our results for the bulk critical exponent and for the entanglement scaling (1.6) were inferred from the case of $Q = 2$ replicas for simplicity. We now discuss how one can obtain the critical properties in the replica limit $Q \to 0$ of eq. (1.4). It is possible to apply the cavity method to the model (1.5), but the number of cavity fields is then given by the number of irreducible representations of S_Q. As a result, the replica limit $Q \to 0$ is still out of reach on the Cayley tree. To proceed, we use the following trick based on universality: we modify the Boltzmann weights of

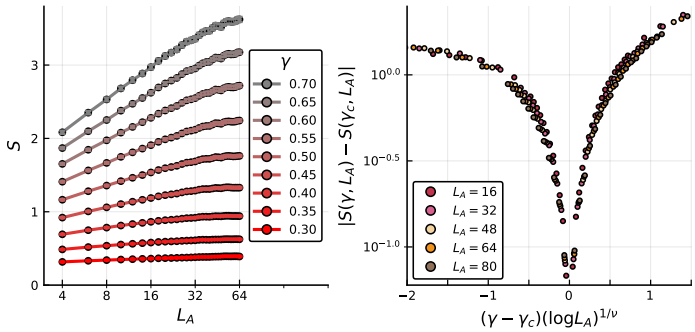

Figure 1.6. Numerical results. Left panel: averaged von Neumann entropy for random tree tensor network states of size $L = 256$ as a function of the subsystem size L_A for various values of γ, where $\gamma \in [0, 1]$ is a parameter tuning continuously the bond dimension between $D = 1$ and $D = 3$ (see text). Right panel: collapse of the data with $\gamma_c = 0.47$ and $\nu = 1$.

the model eq. (1.5) while preserving the $S_Q \times S_Q$ symmetry of the Hamiltonian (1.5). Therefore, we introduce a different statistical mechanics model

$$\mathcal{H}_{\text{modified}} = -\sum_{\langle i,j \rangle} \log\left(1 + K\bar{\chi}(g_i^{-1} g_j)\right), \tag{1.7}$$

where $\bar{\chi}(g) = \frac{Q-1}{Q!}\chi(g)$ with χ the character of the *standard* representation of the symmetric group S_Q. This model is still invariant under left/right multiplication by elements of S_Q, and since the standard representation is faithful and well-defined for any Q, we do not expect this modified model to have an enlarged symmetry. (This is inspired by the $O(N)$ model, whose critical behavior in 2D was understood by Nienhuis [Nie82] by introducing a different model with the same symmetry group.)

Remarkably, for uniform boundary conditions $g_\partial = g_0 = ()$ (corresponding to $\mathcal{Z}_0$), the modified model (1.7) is still solvable on the Cayley tree with coordination number $q = 3$ using a single cavity equation for any Q. The cavity equation reads $\sum_{g_i}(1 + h^{(k)}\bar{\chi}(g_i))^2(1+K\bar{\chi}(g_i^{-1}g_j)) = C(1+h^{(k-1)}\bar{\chi}(g_j))$. Using standard representation theory results, we find the following recursion relation for the boundary cavity fields

$$h^{(k-1)} = \frac{K}{Q!} \frac{2h^{(k)} + (h^{(k)})^2 \frac{Q-1}{Q!}}{1 + (h^{(k)})^2 \left(\frac{Q-1}{Q!}\right)^2}. \tag{1.8}$$

We can now analytically continue Q in this equation, and study the critical behavior as a function of Q. We analyzed the fixed points of this recursion relation and their stability as a function of Q. For $Q > 1$, we find first order transitions (with $Q = 2$ being special), while for $Q < 1$ there is a second order transition for $K_c = Q!/2$. For $K < K_c$, the correlation length reads $\xi^{-1} = \log \frac{K_c}{K}$ so we find $\nu = 1$ as in the Ising ($Q = 2$) case. For $K > K_c$, the cavity fields flow to a non-zero value which scales as $\sim (K - K_c)$, so we find $\beta = 1$ which is the mean-field magnetization exponent of the n-state Potts model with $n < 2$. In the replica limit, we thus find $\nu = \beta = 1$, which coincide with the critical exponents of the n-state Potts model on the Cayley tree (for $n < 2$). Those exponents *do not* depend on the replica number Q, as expected from mean-field critical behavior in general — the only exception is the exponent β which happens to be different for $Q = 2$ for symmetry reasons. We expect these exponents to control the critical behavior of our model (1.5) in the replica limit $Q \to 0$, and while we unfortunately cannot solve the modified model (1.8) with inhomogeneous boundary conditions, we also expect the general scaling (1.6) with $\nu = 1$ to hold for $Q \to 0$.

Numerical results — We verify our predictions by generating tree tensor network states and computing their entanglement properties numerically. Each state consists of random, gaussian-distributed tensors of dimension D on each node of the Cayley tree. By tuning the bond dimension we find a phase transition from area-law to logarithmic scaling of the entanglement entropy, with $D = 1$ (trivially) showing area-law scaling and $D = 3$ showing clear logarithmic scaling. As the dimension of tensors must be integer, we augment these states with additional tensors on each bond of the tree to interpolate between integer bond dimensions $D = 1$ and $D = 3$. With the size of the tensors on the nodes fixed at $D = 3$, we insert on each bond diagonal

tensors with elements $(1, \gamma, \gamma^2)$, with the parameter γ tuned continuously from $\gamma = 0$, corresponding to $D = 1$, to $\gamma = 1$, corresponding to $D = 3$. Upon tuning γ, we find a phase transition from area-law to logarithmic scaling of the entanglement entropy (Fig. 1.6), consistent with the mean-field theory results detailed above. We estimate the location of the critical point γ_c to be in the interval $[0.4, 0.6]$ and the critical exponent ν to take a value in $[1, 1.5]$. The precision is limited due to the rather small depth of the Cayley tree that is accessible numerically; however, we find that the quality of the collapse improves with system size and is comparable to our results for the Ising model on equally small Cayley trees.

CHAPTER 2

HYDRODYNAMICS OF INTEGRABLE SYSTEMS

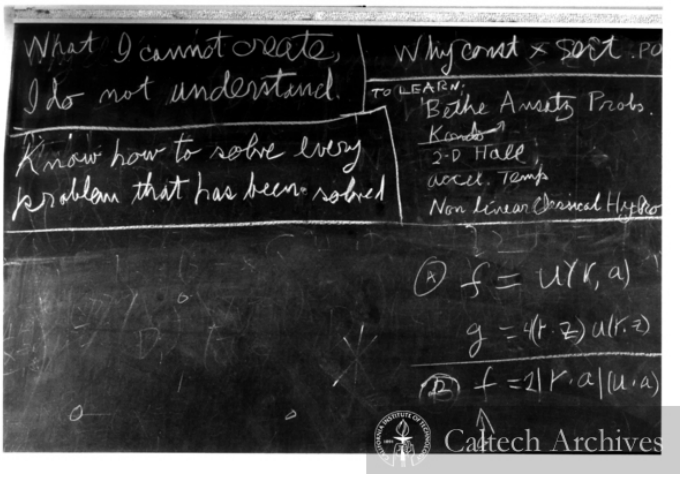

Figure 2.1. Feynman's last blackboard. In Feynman's last blackboard we can appreciate his interest in learning more about Bethe solvable models (that is, integrable systems), and hydrodynamics, the main topics of this Chapter. In Feynman's own words: *"I got really fascinated by these (1 + 1)-dimensional models that are solved by the Bethe ansatz and how mysteriously they jump out at you and work and you don't know why. I am trying to understand all this better."* Richard Feynman extracted from [Bat].

In this Chapter we discuss the thermodynamics and hydrodynamics of integrable systems. Integrable systems are many-body systems where scattering among particles is *nondiffractive*, in the sense that scattering events can be factored onto two-body scattering processes [Tak99] (this in turn is very much connected with the often used alternative definition that states that an integrable system is any many-body quantum system with an extensive or *complete* set of local conserved charges [Pol77, Sut04] [1]).

[1] To make things yet more confusing, integrability has a very different meaning within the context of classical dynamical systems governed by Hamilton's equation of motion. The common feature

This implies that all information about the momentum distribution in a generic initial state is preserved. While according to this definition of integrability, nothing prevents from considering two or three dimensional systems (see e.g. [Zam80, BB92]), we will focus our attention on one dimensional systems. There are various reasons for focusing on one dimensional integrable systems: *(i)* They are simpler to solve than their higher dimensional counterparts – indeed one cannot determine the outcome of a two-body scattering event in two and higher dimensions based solely on conservation of energy and momentum. At variance, in one dimension, scattering events are head on which means particles just suffer time delays – for classical particles, or phase shifts – for quantum particles. *(ii)* They are strongly interacting. The reduced dimensionality makes it more likely for particles to be closer to each other in one dimension than in higher dimensions. Stronger interactions in turn mean more room for exciting phenomena to occur. *(iii)* Last but not least, integrable systems in one dimension allow for various intriguing types of transport, a subject that will be the focus of Sec. 2.4.

In the first part of this Chapter we discuss the basics of integrability, with an emphasis on the Bethe equations and Thermodynamic Bethe Ansatz (TBA). We then discuss some basics of conventional hydrodynamics, making special emphasis on the method of hydrodynamic projections. We then extend this hydrodynamic framework to the realm of integrable systems, a framework now known as generalized hydrodynamics, or GHD. Then we present explicit expressions for transport coefficients obtained using this hydrodynamic framework. In the last section of this Chapter we present one of the simplest integrable models, the Rule 54 cellular automaton. This is a cellular automaton featuring two species of solitons. The particular simplicity of

---

among these classes of systems is the *exact solvability* of the model, in the sense that the equations of motion can be integrated, so that given the state of the system at $t = 0$, one can find the state at any later time t. This feature has deep consequences on the ergodic properties of integrable systems.

the model allows us to provide, for the first time, a sound numerical benchmark of the various predictions of GHD for the transport coefficients in an integrable system.

2.1 Basics of Integrability

The theory of integrability as we know it today starts with H. Bethe's Ansatz for solving a model of a "one dimensional metal" [Bet31]. This method was later further developed by other architects of the theory of integrability, including Yang and Yang, Lieb, Baxter, Gaudin, and others [Gau83, LM13, KBI97]. The basic ingredients of any integrable system living on a ring in $1D$ are the set of rapidities $\{\theta_i\}$, $i = 1, ..., N$ specifying the eigenstates (or quasiparticles) of the Hamiltonian in question, and the scattering matrix $S = S(\theta, \alpha)$ [2]. In the thermodynamic limit $L \to \infty$ at fixed density N/L, the set of rapidities becomes densely ordered on the real line (rapidities can be complex too, but for the sake of simplicity we restrict ourselves to real rapidities). In this case it is more convenient to speak of densities of rapidities, viz

$$\rho(\theta) = \lim_{L\to\infty} L^{-1} \sum_k \delta(\theta - \theta_k), \tag{2.1}$$

where the different rapidities θ_k are obtained for fixed L and ordered as $\theta_k < \theta_{k+1}$ for any k [3]. The quantity $\rho(\theta)$ is also referred to as root or quasiparticle density. This function determines completely the set of conserved charges, which read

$$\langle \hat{Q}_i \rangle = \int d\theta \rho(\theta) h_i(\theta), \tag{2.2}$$

---

[2]For certain Hamiltonians, including the XXZ, an eigenstate is specified not only by the set of rapidities, but also by its quasiparticle type, or color. For the moment we will assume that there is just one quasiparticle type. In Sec. 2.4 we shall see how to incorporate quasiparticle types when discussing transport in integrable systems. In this sense, it is helpful to think of the systems considered at this level of introduction as being spinless Bose gases (where no internal degree of freedom is present).

[3]It is known that in integrable models the quasiparticles fill levels like fermions, which means there cannot be any two quasiparticles with the same rapidity. This is a consequence of the Yang-Baxter equation which in turn follows from the requirement of the S matrix being factorizable [ARS01].

where h_i are the one particle eigenvalues of the conserved charges $\hat{Q}_i|\theta\rangle = h_i|\theta\rangle$. The functions h_i should form a complete basis of functions. One such basis is the set of polynomials $h_i = \theta^i$. Two charges are of special relevance, corresponding to the single particle energy $e(\theta) \sim \theta^2$, and momentum $p(\theta) \sim \theta$. The Bethe equations read

$$e^{i\theta_k L} = \prod_{l=1, l\neq k}^{N} S(\theta_k, \theta_l). \tag{2.3}$$

This formula comes from winding a quasiparticle around the ring, and using the fact that the S matrix is factorizable. Let us define the scattering kernel

$$T(\theta, \alpha) \equiv \frac{1}{i}\frac{\partial}{\partial\theta} S(\theta, \alpha). \tag{2.4}$$

Taking the logarithm on both sides of the Bethe equation and taking the continuum limit yields the standard form of the Bethe equations

$$\rho^{\text{tot}}(\theta) = \frac{p'(\theta)}{2\pi} + \int d\alpha T(\theta, \alpha)\rho(\alpha), \tag{2.5}$$

where we have introduced the density of states ρ^{tot}, which gives us the amount of available states per rapidity, and the derivative of the momentum w.r.t. the rapidity $p' = dp/d\theta$. Related to the density of states is the density of holes, given by $\rho^{\text{h}} = \rho^{\text{tot}} - \rho$.

Our formulas so far are a direct consequence of the integrability condition. Nothing has been said about the thermodynamics of integrable models. Thermodynamics tells us that for a system with a set $\{\hat{Q}_i\}$ of conserved charges, there corresponds a set of Lagrange multipliers or generalized chemical potentials $\{\beta_i\}$, so that the state of the system be described by a (generalized) Gibbs state $\sim \exp(-\sum_i \beta_i \hat{Q}_i)$. We would like to find the link between the thermodynamics described by such Gibbs state and the density of quasiparticles (2.1) which also fully characterizes the state of an integrable

system, i.e. $\rho(\theta) \overset{?}{\leftrightarrow} \exp(-\sum_i \beta_i \hat{Q}_i)$. Such link is given by the Thermodynamic Bethe Ansatz (TBA) [YY69]

$$\varepsilon(\theta) = \sum_i \beta_i h_i(\theta) + \int d\alpha T(\theta, \alpha) F(\varepsilon(\alpha)), \tag{2.6}$$

where the function $F(\varepsilon)$ is the free energy density of a free particle of energy ε. The quantity ε should be viewed as a *pseudoenergy* that, a part from receiving contributions from all nonzero chemical potentials β_i, it has corrections due to interactions [Doy20]. The function $F(\varepsilon)$ depends solely on the statistics of the particles present. For classical particles it reads $F = -e^{-\varepsilon}$, for classical radiation $F = \log \varepsilon$, for fermions $F = -\log(1 + e^{-\varepsilon})$, and for bosons $F = \log(1 - e^{-\varepsilon})$. Related to this is the Fermi factor defined as $n \equiv dF/d\varepsilon$. Eq. (2.6), together with the Bethe equation (2.5) fully specify the thermodynamics of the system and permit us to work with any of the various thermodynamic variables discussed. For instance, from these two sets of equations it follows one can rewrite the Fermi factor as $n = \rho/\rho^{\text{tot}}$.

2.2 Basics of Hydrodynamics

This section follows greatly from Ref. [Doy20]. Hydrodynamics is a general physical theory that describes many particle systems with conservation laws at a scale somewhere between the microscopic scale following the motion of each particle, where the dynamics is reversible, and the thermodynamic scale, where the state is homogeneous and stationary. Hydrodynamics postulates local thermodynamic equilibrium. That is, at a coarse grained scale l, where $l \gg a$ with a a microscopic scale, but such that $l \ll L$ with L the spatial scale of the entire system, the system at that scale may be characterized by a set of local charges $\{q_i(x,t)\}$ that may depend on time, but that are nevertheless conserved over the entire system, i.e. $\partial_t Q_i = 0$, with

$Q_i = \int dx q_i(x,t)$. Furthermore, hydrodynamics posits that the set of these charges satisfy a set of conservation laws of the form

$$\partial_t q_i(x,t) + \partial_x j_i(x,t) = 0, \tag{2.7}$$

where crucially the current densities $j_i(x,t)$ depend in turn on (in principle all) the conserved charge densities through the equations of state $j_i = j_i(\{q_i(x,t)\})$. A consequence of the maximum entropy principle dictates that not just the current, but any observable $\hat{\mathcal{O}}(x,t)$ upon averaging over maximum entropy locally stationary states, i.e. Gibbs states of the form $\hat{\rho} \propto e^{-\sum_i \sum_x \beta_i(x)\hat{q}_i(x)}$, are functions of the conserved charges, i.e. $\mathcal{O}(x,t) \equiv \langle \hat{\mathcal{O}}(x,t) \rangle = \mathcal{O}(\{q_i(x,t)\})$. We will thus reserve the "hat" for (classical or quantum) observables to distinguish them from their corresponding hydrodynamic variables. The equation of state thus provides the link between the exact microscopic dynamics in terms of observables (i.e. Eq. (2.7) putting hats on top of the variables and replacing when necessary the partial derivatives by discrete ones), and the local thermodynamics – this is the basis of hydrodynamics. In this way, when applicable, one can view the theory of hydrodynamics as describing the simplest nonequilibrium setup, one where a set of local conservation laws exist and local thermodynamic equilibrium is present, describing the transition from *local* equilibrium to *global* equilibrium. The different *classes* of hydrodynamic theories are only distinguished by the type of equation of state, i.e. the kind of functionality the currents have on the charges. We shall come to this in the next section.

It is quite remarkable that a system comprised of $\approx 10^{23}$ particles may be effectively described by a (small) set of equations of the form (2.7). Preparing the system in an initial state, we expect it to reach equilibrium after a long time, that is, to thermalize. This equilibrium state may be global, in the sense that the final state will only depend on the parameters of the bath (such as temperature, pressure, etc) or *local*, in the sense that equilibrium is reached accross a finite region of space, in

which case the rest of the system acts as a reservoir. According to the maximum entropy production principle, we expect the system to maximize entropy subject to constraints given by the conserved charges Q_i. As a consequence, after a long time the system is expected to approach a Gibbs state of the form $\propto \exp(-\sum_i \sum_x \beta_i(x) q_i(x))$, where the Lagrange parameters $\{\beta_i\}$ are in one-to-one relationship with the charge densities via $\beta_i = \delta f / \delta q_i$, with f the free energy density [Doy20].

2.2.1 Transport in conventional hydrodynamics

The theory of transport is concerned with the sort of functionality the currents may have with time. The standard setup to study transport is to subject the system to a small imbalance in one of the conserved charges, and see how it spreads according to (2.7). This is the basis of linear response (LR) theory. Despite the apparent simplicity of Eq. (2.7), systems can display rich transport phenomenology. Such rich phenomenology is indeed encoded in the equation of state $j_i = j_i(\{q_i(x,t)\})$, which ultimately dictates the sort of dynamics one may observe in experiments. Following the logic behind LR, we let the charges take the form $q_i(x,t) = q_i^* + \delta q_i(x,t)$, where q_i^* is some homogeneous background charge and δq_i is a small perturbation on top of this charge. Then we may carry out a *gradient* expansion in the charge imbalance δq_i in the equation state to give $j_i = \sum_j A_{i,j} \delta q_j + \sum_j \mathcal{D}_{i,j} \partial_x \delta q_j + ...$, where we have dropped out an irrelevant constant term and the $\cdots$ represent higher-order terms. The matrix $\mathbf{A}$ sometimes receives the name of *flux Jacobian* and it is responsible for ballistic transport, provided the rest of the terms in the expansion can be disregarded. In this case one speaks of hydrodynamics at the Euler scale or Euler hydrodynamics. Many systems however display diffusive behavior, in which case the matrix $\mathcal{D}$ cannot be ignored. These corrections to the Euler hydrodynamics are sometimes termed Navier-Stokes corrections. Ballistic and diffusive behavior comprise perhaps the two

most common types of transport found in nature. However, more exotic behavior may be found, a discussion of which is postponed for later.

Euler scale terms.– To get a handle on the transport coefficients one resorts to the framework of hydrodynamic projections. First, we introduce the inner product

$$\langle\!\langle \hat{\mathcal{O}}_1 | \hat{\mathcal{O}}_2 \rangle\!\rangle_{\vec{\beta}} \equiv \frac{1}{\mathrm{tr}[e^{-\sum_i \beta_i \hat{Q}_i}]} \mathrm{tr}[\hat{\mathcal{O}}_1^\dagger \hat{\mathcal{O}}_2 e^{-\sum_i \beta_i \hat{Q}_i}] \tag{2.8}$$

as well as the product (which strictly speaking is not inner)

$$\langle\!\langle \hat{\mathcal{O}}_1 | \hat{\mathcal{O}}_2 \rangle\!\rangle^c_{\vec{\beta}} \equiv \frac{1}{\mathrm{tr}[e^{-\sum_i \beta_i \hat{Q}_i}]} (\mathrm{tr}[\hat{\mathcal{O}}_1^\dagger \hat{\mathcal{O}}_2 e^{-\sum_i \beta_i \hat{Q}_i}] - \mathrm{tr}[\hat{\mathcal{O}}_1^\dagger e^{-\sum_i \beta_i \hat{Q}_i}] \mathrm{tr}[\hat{\mathcal{O}}_2 e^{-\sum_i \beta_i \hat{Q}_i}]) \tag{2.9}$$

Then, the susceptibility matrix (a.k.a. static covariance matrix) $\mathbf{C}$ reads

$$\begin{aligned} C_{i,j} &= \frac{1}{L} \langle\!\langle \hat{Q}_i | \hat{Q}_j \rangle\!\rangle^c_{\vec{\beta}} \\ &= \int dx \langle\!\langle \hat{q}_i(x) | \hat{q}_j(0) \rangle\!\rangle^c_{\vec{\beta}}. \end{aligned} \tag{2.10}$$

The last equality follows from translation invariance. It is easy to see that the same matrix can be obtained via $C_{i,j} = -\delta q_i / \delta \beta_j$ or as $C_{i,j} = -\delta^2 f / \delta \beta_i \delta \beta_j$, the latter being the familiar expression found in basic thermodynamics textbooks. Similarly we can define other hydrodynamic matrices. Of particular relevance is the Drude matrix given by

$$D_{i,j} = \lim_{t \to \infty} \frac{1}{2tL} \int_{-t}^{t} ds \langle\!\langle \hat{J}_i(s) | \hat{J}_j(0) \rangle\!\rangle^c_{\vec{\beta}}. \tag{2.11}$$

The Drude matrix gives the singular contribution to the d.c. conductivity (which we define precisely below) and its name comes as one may expect from the Drude model describing charged particles in the presence of an external electric field and in the presence of a damping force proportional to their velocity. By ergodicity [Doy20]

we expect that the time evolved currents should belong to the subspace of conserved charges. Denote the projection operator onto the subspace of conserved charges as

$$\mathcal{P}\hat{\mathcal{O}} = \frac{1}{L}\sum_{j,k} \hat{Q}_j (\mathbf{C}^{-1})_{j,k} \langle\!\langle \hat{Q}_k | \hat{O} \rangle\!\rangle^c_{\vec{\beta}}. \tag{2.12}$$

According to the ergodic theorem [Doy20], the Drude matrix may be expressed as

$$D_{i,j} = \frac{1}{L}\langle\!\langle \hat{J}_i | \mathcal{P}\hat{J}_j \rangle\!\rangle^c_{\vec{\beta}} = \frac{1}{L}\langle\!\langle \mathcal{P}\hat{J}_i | \hat{J}_j \rangle\!\rangle^c_{\vec{\beta}} = \frac{1}{L}\langle\!\langle \mathcal{P}\hat{J}_i | \mathcal{P}\hat{J}_j \rangle\!\rangle^c_{\vec{\beta}}. \tag{2.13}$$

In other words,

$$D_{i,j} = \frac{1}{L^2}\sum_{k,l} \langle\!\langle \hat{J}_i | \hat{Q}_k \rangle\!\rangle^c_{\vec{\beta}} (\mathbf{C})^{-1}_{k,l} \langle\!\langle \hat{Q}_l | \hat{J}_j \rangle\!\rangle^c_{\vec{\beta}}. \tag{2.14}$$

Eqs. (2.13, 2.14) reveal that despite the fact that the Drude matrix involves a temporal correlator, as per (2.11), this can be expressed solely in terms of thermodynamic data, involving products of conserved charges and their currents. This will be of key importance when studying transport in integrable systems. We mention also that (2.14) affords as well a more compact representation in terms of the matrix $\mathbf{B}$ [Doy20] with components

$$B_{i,j} \equiv \frac{1}{L}\langle\!\langle \hat{J}_i | \hat{Q}_j \rangle\!\rangle^c_{\vec{\beta}} = \sum_k A_{i,k} C_{k,j}. \tag{2.15}$$

So that

$$\mathbf{D} = \mathbf{B}\mathbf{C}^{-1}\mathbf{B}^T = \mathbf{A}\mathbf{C}\mathbf{A}^T. \tag{2.16}$$

Navier-Stokes terms.– The hydrodynamic matrices discussed so far contain only information about the thermodynamics of the model, and they appear at the Euler scale of hydrodynamics. Going beyond this requires analyzing the diffusive or Navier-Stokes corrections, which are encoded in the diffusion matrix $\mathcal{D}$ discussed earlier. At variance with the other matrices, this matrix goes beyond thermodynamics in that it

is not solely determined by maximum entropy states, and instead it is encoded in the hydrodynamics of the specific model [Doy20]. These are the terms that give rise to an "arrow of time", i.e. produce entropy. Related to the diffusion matrix is the Onsager matrix $\mathbf{L}$ which is simply the product of the diffusion matrix and the covariance matrix, $\mathbf{L} = \mathcal{D}\mathbf{C}$. This essentially gives the regular part of the d.c. conductivity which one can measure in transport experiments. Recall that the conductivity σ relates the response of currents in the presence of an external field $\hat{E}$ as $\hat{J}_a(\omega) = \sum_b \sigma_{a,b}(\omega)\hat{E}_b(\omega)$, where $\hat{J}_a(\omega) = \int_{-\infty}^{\infty} \hat{J}_a(t)e^{i\omega t}dt$ (here $\hat{E}$ is often taken as an observable coupling to one of the charges, e.g. $\hat{E} = h\hat{Q}_i$). The Green-Kubo formula tells us that the conductivity tensor is determined by the current-current autocorrelation function [Kub57, BHMK$^+$21]

$$\sigma_{a,b}(\omega) = \beta \lim_{t\to\infty} \lim_{L\to\infty} \frac{1}{L} \int_0^t e^{i\omega\tau} K_{a,b}(\tau) d\tau, \tag{2.17}$$

$$K_{a,b}(t) \equiv \frac{1}{\beta} \int_0^\beta \langle\!\langle \hat{J}_b(0) | \hat{J}_a(t + i\lambda) \rangle\!\rangle_\beta^c d\lambda, \tag{2.18}$$

where crucially the correlation function above is evaluated at fixed temperature (we will see later on how to compute transport coefficients in a Floquet system where energy is not conserved). The real part of the conductivity tensor then decomposes into a sum of a divergent and a regular component

$$\mathrm{Re}\sigma_{a,b}(\omega) = \beta\pi D_{a,b}\delta(\omega) + \sigma_{a,b}^{\mathrm{reg}}(\omega), \tag{2.19}$$

where the divergent part is proportional to the Drude matrix $\mathbf{D}$ and if nonzero indicates the presence of ballistic transport. The Onsager matrix is then given by [NDMP22]

$$\mathbf{L}_{a,b} = \lim_{t\to\infty} \int_{-t}^{t} ds \left(\langle\!\langle \hat{J}_a(s) | \hat{J}_b(0) \rangle\!\rangle_\beta^c - D_{a,b} \right). \tag{2.20}$$

Knowledge of the Onsager matrix gives us access to the diffusion matrix, as $\mathcal{D} = \mathbf{L}\mathbf{C}^{-1}$.

2.3 Generalized Hydrodynamics

The equations of hydrodynamics *generalize* to the case when the system possesses an infinite number of conserved charges, that is, when the system is integrable. The particular hydrodynamic framework that enables the study of such integrable systems goes under the name of *generalized hydrodynamics* (or GHD for short). One may wonder why such a framework is even needed, for integrable systems are known to be *exactly solvable* in the first place. The reason is that while integrability has provided a remarkably powerful framework to study thermodynamics in detail [vAvEW$^+$08, YY69], studying correlation functions and the dynamics of integrable systems has been only possible in very few setups. At variance with conventional hydrodynamics, GHD exploits the quasiparticle picture of integrable systems, which permits finding explicit formulas for transport coefficients as we will discuss below. Before that however we discuss the hydrodynamics of integrable systems at the Euler scale. The basic assumption of GHD is that at each hydrodynamic cell, the system is in local thermodynamic equilibrium and one may thus define a local density of quasiparticles $\rho(\theta; x, t)$. The charge and current densities may be expressed as

$$q_i(x,t) = \int d\theta \rho(\theta; x, t) h_i(\theta), \tag{2.21}$$

$$j_i(x,t) = \int d\theta v^{\text{eff}}(\theta; x, t) \rho(\theta; x, t) h_i(\theta), \tag{2.22}$$

where the effective velocities are given by

$$v^{\text{eff}}(\theta; x, t) = \frac{(e')^{\text{dr}}(\theta; x, t)}{(p')^{\text{dr}}(\theta; x, t)}, \tag{2.23}$$

with $e' = de/d\theta$. Here the superscript dr stands for *dressed*. It accounts for the effects of interactions. Any dressed function g obeys

$$g^{\text{dr}}(\theta; x, t) = g(\theta; x, t) + \int d\theta' T(\theta, \theta') n(\theta'; x, t) g^{\text{dr}}(\theta'; x, t). \tag{2.24}$$

Eq. (2.21) is the direct generalization of (2.2) under the hydrodynamic assumption stated above. Eq. (2.22) instead is nontrivial, and was only proven for integrable field theories in [CADY16a] and extended to generic integrable models years later in [VY19]. The continuity equations at the Euler scale (a.k.a. GHD equations) thus read

$$\partial_t \rho(\theta; x, t) + \partial_x [v^{\text{eff}}(\theta; x, t)\rho(\theta; x, t)] = 0, \tag{2.25}$$

where completeness of the charges $\{h_i\}$ has been used. The interpretation of this equation is quite clear: it is an advection equation where the velocities get renormalized as a result of interactions. At this point we can ommit the space-time dependence and write our expressions more compactly in terms of operators and vectors with support on rapidity space. This means the kernel of the integrable model in question is represented as an operator acting on vectors as the convolution

$$\mathbf{T}\vec{h}|_\theta = (T * h)|_\theta = \int d\theta' T_{\theta,\theta'} h_{\theta'}, \tag{2.26}$$

while any other operator will be represented as a diagonal operator, in particular, for the Fermi factor acting on a vector this means $\mathbf{n}\vec{h}|_\theta = n_\theta h_\theta$. With this notation the dressing operation (2.24) thus reads

$$\vec{g}^{\text{dr}} = (\mathbb{1} - \mathbf{T}\mathbf{n})^{-1}\vec{g}. \tag{2.27}$$

Likewise, the GHD equations in this notation read $\partial_t \vec{\rho} + \partial_x(\mathbf{v}^{\text{eff}}\vec{\rho}) = 0$. It is possible to rewrite the GHD equations in a yet simpler way in terms of the Fermi factors. First note that using the Bethe equations one has $\mathbf{v}^{\text{eff}}\vec{\rho} = \frac{1}{2\pi}\mathbf{n}\vec{e}'^{\text{dr}}$. Using this we find using some simple algebra

$$\partial_t \vec{\rho} = \frac{1}{2\pi}\left(\mathbb{1} + \mathbf{n}\mathbf{T}^{\text{dr}}\right)\partial_t \mathbf{n}\vec{p}'^{\text{dr}}, \tag{2.28}$$

$$\partial_x(\mathbf{v}^{\text{eff}}\vec{\rho}) = \frac{1}{2\pi}\left(\mathbb{1} + \mathbf{n}\mathbf{T}^{\text{dr}}\right)\partial_x \mathbf{n}\vec{e}'^{\text{dr}}, \tag{2.29}$$

where we have defined the dressed kernel $\mathbf{T}^{\mathrm{dr}} = (\mathbb{1} - \mathbf{Tn})^{-1}\mathbf{T}$. Combining these relations with the GHD equations immediately gives us

$$(\partial_t + \mathbf{v}^{\mathrm{eff}}\partial_x)\vec{n} = 0. \tag{2.30}$$

Let us note that within this notation, it is easy to extend our discussion to integrable systems where states are characterized not only by a given rapidity, but also by a color or type. This extension requires minimal modifications within this language. We define the parity [DNBD19]

$$\sigma = \mathrm{sgn}(\mathrm{p}'(\theta)). \tag{2.31}$$

The scattering kernel depends now on rapidity as well as on quasiparticle type, $T_{a,b}(\theta, \alpha)$, with the indices a, b taking on discrete values characterizing the various quasiparticle types. The scattering kernel acting on an arbitrary vector $\vec{h}$ (which depends on both rapidity and quasiparticle type) takes on a very similar expression to that in (2.26), except now the convolution is generalized so that $\int d\theta \to \sum_a \int d\theta$, with the sum running over the quasipartile types (similar considerations hold for diagonal matrices acting on vectors). The dressing operation is modified now and reads $\vec{g}^{\mathrm{dr}} = (\mathbb{1} - \mathbf{Tn}\sigma)^{-1}\vec{g}$, where the matrix $\mathbf{n}$ acts again diagonally on both rapidity as well as on quasiparticle type.

2.4 Transport in Integrable Systems

So far we have discussed GHD at the Euler scale. Going beyond the Euler scale, the next leading order term in the hydrodynamic expansion is of Navier-Stokes type. One may wonder how integrable systems, whose defining feature is the presence of stable, ballistically propagating quasiparticles (solitons), can incorporate diffusive terms in the hydrodynamic equations. The answer to this is best illustrated using a kinetic

picture [GHKV18a]: as quasiparticles move they exert random time delays on each other as a result of collisions, effectively causing diffusion. Hence, integrable systems obey hydrodynamic equations where to leading order, both Euler and Navier-Stokes terms are present, and hence the general formulas for calculating various transport coefficients valid within conventional hydrodynamics (see Sec. 2.2.1) are still valid here. A remarkable difference however between conventional hydrodynamics and generalized hydrodynamics is that the rather rigid structure of integrability present in the latter allows for explicit formulas of the various hydrodynamic matrices and transport coefficients in terms of quasiparticle data. At the Euler scale the only matrices present are the static covariance $\mathbf{C}$, the Jacobian flux $\mathbf{A}$, and the Drude weight $\mathbf{D}$. These were found for the Lieb-Liniger model within GHD in [DS17a] and later generalized to arbitrary integrable models using low momentum single particle-hole form-factors in [DNBD19]. They are expressed as [Doy20]

$$\mathbf{A} = (\mathbb{1} + \mathbf{nT})^{-1}\mathbf{v}^{\text{eff}}(\mathbb{1} + \mathbf{nT}), \tag{2.32}$$

$$\mathbf{B} = (\mathbb{1} + \mathbf{nT})^{-1}\mathbf{v}^{\text{eff}}\rho\mathbf{f}(\mathbb{1} + \mathbf{Tn})^{-1}, \tag{2.33}$$

$$\mathbf{C} = (\mathbb{1} + \mathbf{nT})^{-1}\rho\mathbf{f}(\mathbb{1} + \mathbf{Tn})^{-1}, \tag{2.34}$$

$$\mathbf{D} = (\mathbb{1} + \mathbf{nT})^{-1}(\mathbf{v}^{\text{eff}})^2\rho\mathbf{f}(\mathbb{1} + \mathbf{Tn})^{-1}, \tag{2.35}$$

where $\mathbf{f}$ is a thermodynamic factor which takes account of the specific statistics of the bare particles and is related to the free energy appearing in (2.6) through $f = -\frac{d^2F/d\varepsilon^2}{dF/d\varepsilon}$ [Doy20]. Explicitly: $\mathbf{f} = \mathbf{1}$ for classical particles, $\mathbf{f} = \mathbf{n}$ for classical radiation, $\mathbf{f} = \mathbf{1} - \mathbf{n}$ for fermions, and $\mathbf{f} = \mathbf{1} + \mathbf{n}$ for bosons. The diffusive corrections to the Euler scale GHD were found in [GHKV18a, DNBD18]. The hydrodynamic matrices involved in this case are determined by the low momentum two particle-hole form factors [DNBD18], or alternatively, using a kinetic picture [GHKV18a]. First, the diffusion matrix can be expressed as

$$\mathcal{D} = (\mathbb{1} - \mathbf{nT})^{-1}\rho^{\mathrm{tot}}\tilde{\mathcal{D}}(\rho^{\mathrm{tot}})^{-1}(\mathbb{1} - \mathbf{nT}), \tag{2.36}$$

where $\tilde{\mathcal{D}}$ is the *diffusion kernel* whose components are given as [DNBD19]

$$\tilde{\mathcal{D}}_{a,b}(\theta,\alpha) = \delta_{a,b}\delta(\theta-\alpha)\tilde{w}_a(\theta) - \tilde{W}_{a,b}(\theta,\alpha). \tag{2.37}$$

The off-diagonal components of the diffusion kernel are the result of interparticle scatterings between quasiparticles of different velocities and are given by

$$\tilde{W}_{a,b}(\theta,\alpha) = \frac{1}{2}\rho_a(\theta)f_a(\theta)\frac{T^{\mathrm{dr}}_{a,b}(\theta,\alpha)T^{\mathrm{dr}}_{b,a}(\alpha,\theta)}{\rho^{\mathrm{tot}}_a(\theta)^2}|v^{\mathrm{eff}}_a(\theta) - v^{\mathrm{eff}}_b(\alpha)|, \tag{2.38}$$

while the diagonal components, determined by $\tilde{w}(\theta)$, are the result of quasiparticle fluctuations of rapidity θ as a result of random scattering processes. Its explicit expression given by

$$\tilde{w}_a(\theta) = \frac{1}{2}\sum_b \int d\alpha \rho_b(\alpha)(1-n_b(\alpha))\left(\frac{T^{\mathrm{dr}}_{a,b}(\theta,\alpha)}{\rho^{\mathrm{tot}}_a(\alpha)}\right)^2 |v^{\mathrm{eff}}_a(\theta) - v^{\mathrm{eff}}_b(\alpha)|. \tag{2.39}$$

2.5 A toy model for an integrable system: Rule 54

Having discussed GHD in quite general terms, we will now discuss a remarkably simple model, the Rule 54 cellular automaton (CA), where all the formulas discussed above take on a very simple form. Our goal here is to numerically show the formulas relating transport coefficients presented in the previous section valid for integrable systems. This model bears particular importance in the context of integrable systems. It is one of the simplest integrable models known, displaying just two kinds of solitons (ballistically moving modes). This model has proved to be a remarkable testbed where to explore many ideas of integrability, ranging from exact expressions of nonequilibrium steady states [PMM16, KMPV18, KVGP20, KB21b], operator and

entanglement spreading [Gop18a, GHKV18a, KB21a], hydrodynamics within the context of GHD [BKP21], and thermalization properties [KB21c]. Our contribution here is a numerical confirmation of the GHD formulas for transport coefficients (in particular, up to date no numerical evidence of the formulas for the d.c. conductivity in an integrable system has been given). Most of the analytical results presented here can be found in Refs. [GHKV18a, FGV19, BKP21].

2.5.1 The model

A state in the Rule 54 CA is specified by $2L$ sites each taking elements in the Boolean set $\mathcal{F} = \{\square, \blacksquare\}$, with the prescription $\square \cong 1$ and $\blacksquare \cong 0$. We label sites $i \in \mathbb{Z}/2$ and distinguish sites being A type if $i \in \mathbb{Z}$, and B otherwise. A unit cell consists of an adjacent pair of A and B sites. Given some seed or initial state, the Rule 54 flips an element at site i ($\square \leftrightarrow \blacksquare$) if any of its two adjacent sites is in the state $\square$. An illustrative snapshot of the resulting dynamics is shown in Fig. 3.4. This *classical* dynamical rule admits a representation in terms of the Floquet map $\hat{W}_j = \hat{\sigma}^x_j(\mathbb{1} - \underset{j-\frac{1}{2}\,j+\frac{1}{2}}{\blacksquare\,\blacksquare}) + \underset{j-\frac{1}{2}\,j+\frac{1}{2}}{\blacksquare\,\blacksquare}$, $j \in \mathbb{Z}/2$, where $\blacksquare$ denotes the projector onto state $|\blacksquare\rangle$, i.e. $\blacksquare\,|\blacksquare\rangle \equiv |\blacksquare\rangle$, and $\hat{\sigma}^x_j = \hat{\sigma}^+_j + \hat{\sigma}^-_j$, where $\hat{\sigma}^+_j = |\square\rangle\langle\blacksquare|_j$, $\hat{\sigma}^-_j = |\blacksquare\rangle\langle\square|_j$ Each time step is then given by a two step cycle as $\hat{F} = \hat{W}_B\hat{W}_A$, $\hat{W}_{A/B} = \bigotimes_{j\in A/B}\hat{W}_j$. From now and for ease of notation we indicate the location of the unit cell by labeling the i'th site of A type, e.g. for a state involving 6 sites $|\psi\rangle = |\cdots \underset{j-1\;\;j\;\;j+1}{\square\blacksquare\square\square\blacksquare\square}\cdots\rangle$, where also for clarity of notation we separate adjacent unit cells. From now on we only label the necessary unit cells.

2.5.2 Thermodynamics and hydrodynamics

Equilibrium states in Rule 54 are expressed in terms of the classical partition function $Z = \mathrm{tr}[e^{-\mu_R\hat{N}_R - \mu_L\hat{N}_L}]$ which can be computed using the transfer matrix

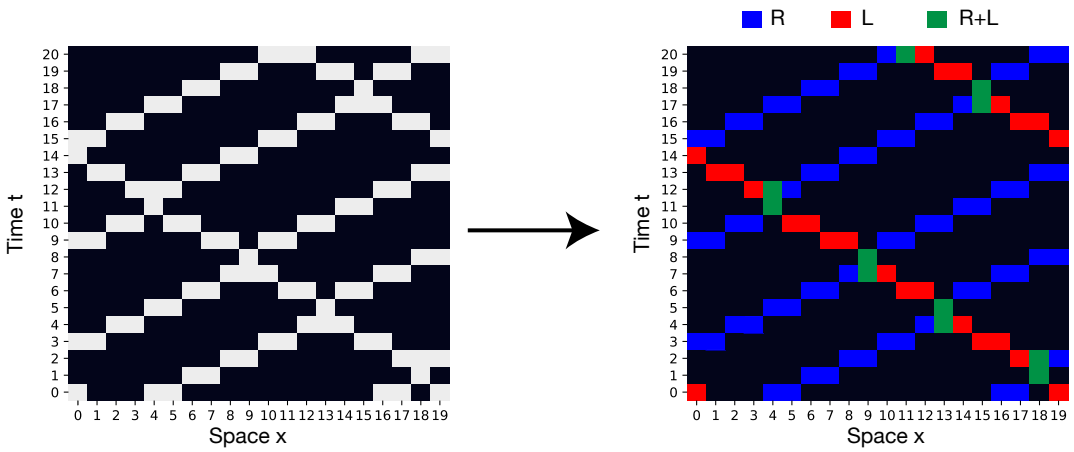

Figure 2.2. Snapshot of the Rule 54. Right: each soliton occupies a cell of two sites. Blue sites correspond to right moving solitons, red sites correspond to left moving solitons, and green sites correspond to a pair of right and left moving soliton colliding.

$$T = \begin{pmatrix} 1 & 1 & e^{-\mu_R-\mu_L} & e^{-\mu_R/2} \\ e^{-\mu_R-\mu_L} & e^{-\mu_R-\mu_L} & e^{-\mu_L} & e^{-\mu_R/2-\mu_L} \\ 1 & 1 & e^{-\mu_R-\mu_L} & e^{-\mu_R/2} \\ e^{-\mu_R/2} & e^{-\mu_R/2} & e^{-\mu_R/2-\mu_L} & e^{-\mu_R-\mu_L} \end{pmatrix}, \tag{2.40}$$

written in the $\{\blacksquare\blacksquare, \square\blacksquare, \blacksquare\square, \square\square\}$ basis. Knowledge of the transfer matrix allows us to compute expected values and fluctuations of any observable in equilibrium. At the root in the development of the GHD framework is the assumption of *local quasistationarity* whereby observables are evaluated w.r.t. some arbitrary background state locally in thermodynamic equilibrium

$$\langle \hat{\mathcal{O}}_x^{(t)} \rangle_{\mu_R,\mu_L} \equiv \frac{1}{Z} \mathrm{tr}[\hat{\mathcal{O}}_x^{(t)} e^{-\sum_x \mu_R(x)\hat{\rho}_{R,x}+\mu_L(x)\hat{\rho}_{L,x}}]. \tag{2.41}$$

To avoid clutter we may simply denote such expectation values as $\mathcal{O}_x^{(t)} \equiv \langle \hat{\mathcal{O}}_x^{(t)} \rangle_{\mu_R,\mu_L}$ making implicit assumption that such quantities are evaluated w.r.t. an arbitrary background state. Focusing on the right movers first note that $\hat{\rho}_{R,x}^{(1)} - \hat{\rho}_{R,x} = -\hat{j}_{R,x+1/2} +$

$\hat{j}_{R,x-1/2}$, where $\hat{j}_{R,x+1/2} =$  (a word on notation: sometimes observables will be written either as $\hat{\mathcal{O}}^{(0)}$ or as $\hat{\mathcal{O}}$ interchangeably, depending on the context). This implies

$$\hat{\rho}^{(t+1)}_{R,x} - \hat{\rho}^{(t)}_{R,x} = \hat{j}^{(t)}_{R,x-1/2} - \hat{j}^{(t)}_{R,x+1/2}. \tag{2.42}$$

Proceeding identically for the left movers we get

$$\hat{\rho}^{(t+1)}_{L,x+1/2} - \hat{\rho}^{(t)}_{L,x+1/2} + \hat{j}^{(t)}_{L,x+1} - \hat{j}^{(t)}_{L,x} = 0, \tag{2.43}$$

with the local current $\hat{j}_{L,x} = -$  . Note that there exists some freedom on the way we choose the local currents as we can always add a local gradient term in (2.42,2.43) that would still give rise to the conservation of $N_{R/L}$. These exact relations give rise to the following hydrodynamic equations upon coarse graining

$$\partial_t \rho_{+/-} + \partial_x j_{+/-} = 0, \tag{2.44}$$

where for convenience we have rotated to basis of positive and negative movers, $\rho_{+/-} = \rho_R \pm \rho_L$. We will alternatively refer to these modes as density and imbalance of particles, respectively. The currents here are given by $j_{+/-} = \rho_R v_R \pm \rho_L v_L$. To find the velocities $v_{R/L}$ we proceed as in [GHKV18a]: consider a right mover starting at $(x^0, t^0) = (0, 0)$ and ending at (x, t). As it travels to the right with a bare velocity $v^0_R = +1$ it will encounter left movers that started closer than $x - v_L t$ causing time-delays so that after t time steps $t = x + \rho_L(x - v_L t)$. This gives $v_R = x/t = (1 + \rho_L v_L)/(1 + \rho_L)$. Similar arguments for a left mover leads to $v_L = (-1 + \rho_R v_R)/(1 + \rho_R)$. Solving these two equations gives

$$v_{R/L} = \pm 1 \mp \frac{2\rho_{L/R}}{1 + \rho_R + \rho_L}. \tag{2.45}$$

As a result, we have in particular $j_+ = \rho_-$. This equation holds microscopically, which means that this Euler relation is exact – we do not have higher order (diffusive)

corrections. The current for ρ_- is more complicated and includes diffusive corrections. The GHD formalism takes advantage of the integrability of the model through the Bethe and TBA equations. The simplicity of the model permits us to write down a closed form for these [FGV19]. We can either work in the R, L or the $+, -$ basis, being both related via $\vec{\rho} = \begin{pmatrix} \rho_R, & \rho_L \end{pmatrix} = \frac{1}{2}\mathbf{O}\begin{pmatrix} \rho_+, & \rho_- \end{pmatrix}$ with

$$\mathbf{O} = \begin{pmatrix} 1 & 1 \\ 1 & -1 \end{pmatrix}. \tag{2.46}$$

The scattering kernel, written in the R, L basis reads

$$\mathbf{K} = \begin{pmatrix} 1 & -1 \\ -1 & 1 \end{pmatrix}. \tag{2.47}$$

Note that the scattering kernel in the $\{+, -\}$ basis is diagonal with 0 in the $+, +$ component. That is, ρ_+ is a zero mode of $\mathbf{K}$ and as such it will spread purely ballistically as alluded above. As before, we denote the *dressing* operation $\vec{h}^{dr} = (\mathbb{1} + \mathbf{Kn})^{-1}\vec{h}$ for any vector $\vec{h} \in \mathbb{R}^2$. The Bethe equation (expressing $\vec{\rho} = \begin{pmatrix} \rho_R, & \rho_L \end{pmatrix}$) reads

$$\vec{\rho} = \mathbf{n}\vec{1}^{dr}, \tag{2.48}$$

where $\vec{1} = \begin{pmatrix} 1, & 1 \end{pmatrix}$, and the Fermi factors in matrix form read $\mathbf{n} = \text{diag}\begin{pmatrix} n_R, & n_L \end{pmatrix}$. Solving the Bethe equation yields

$$n_{R/L} = \frac{\rho_{R/L}}{\rho^{tot}_{R/L}}, \tag{2.49}$$

where the total density of states reads

$$\rho^{tot}_{R/L} = 1 + \rho_{L/R} - \rho_{R/L}. \tag{2.50}$$

The Bethe equation also implies

$$\rho\vec{v} = \mathbf{n}\bar{v}^{dr}, \tag{2.51}$$

where $\vec{v} = \begin{pmatrix} v_R, & v_L \end{pmatrix}$. Differentiating w.r.t. t and x eqs. (2.48) and (2.51) and after some straightforward algebra gives the following advection equation written in terms of Fermi factors

$$\partial_t\vec{n} + \mathbf{v}\partial_x\vec{n} = 0. \tag{2.52}$$

In a GGE with chemical potentials μ_R and μ_L, the Fermi factors are given by $n_{R/L} = 1/(1 + \exp(\epsilon_{R/L}))$, where the quantities $\epsilon_{R/L}$ are solutions of the TBA equations [FGV19]

$$\epsilon_{R/L} = \mu_{R/L} + \log\frac{1 + e^{-\epsilon_{R/L}}}{1 + e^{-\epsilon_{L/R}}}. \tag{2.53}$$

Eqs. (2.48) and (2.53) fully determine the thermodynamics of Rule 54 as indicated by the following diagram

$$\{\rho_R, \rho_L\} \underset{(2.48)}{\leftrightarrow} \{n_R, n_L\} \leftrightarrow \{\epsilon_R, \epsilon_L\} \underset{(2.53)}{\leftrightarrow} \{\mu_R, \mu_L\}. \tag{2.54}$$

2.5.3 Transport coefficients

The continuity equations (2.44) admit diffusive corrections and they give rise to nonzero transport coefficients. Here we are only interested in the d.c. conductivity and Drude weights. The conductivity tensor reads [MKP17]

$$\sigma_{a,b}(\omega) = \frac{1}{2}G_{a,b}(0) + \sum_{t=1}^{\infty} G_{a,b}(t)e^{i\omega t}, \tag{2.55}$$

with the connected current-current correlation function $G_{a,b}(t) = 1/L\langle\hat{J}_a^{(t)}\hat{J}_b^{(0)}\rangle^c \equiv 1/L(\langle\hat{J}_a^{(t)}\hat{J}_b^{(0)}\rangle - \langle\hat{J}_a^{(t)}\rangle\langle\hat{J}_b^{(0)}\rangle)$ where in our case we will choose for convenience the

basis of density and imbalance of particles, i.e. $a, b \in \{+, -\}$. Sending $t \to \infty$ in $G_{a,b}(t)$ we obtain the Drude weight

$$D_{a,b} = \lim_{t\to\infty} G_{a,b}(t). \tag{2.56}$$

Taking instead the zero-frequency (long-wavelength) limit of (2.55) we obtain the d.c. conductivity

$$\sigma^{d.c.}_{a,b} = \frac{1}{2}G_{a,b}(0) + \sum_{t>0} G_{a,b}(t) \geq 0, \tag{2.57}$$

where the last inequality follows from the known fact that the integrated autocorrelation function is always nonnegative. Of course, for integrable systems this diverges. It is then customary to split the d.c. conductivity in terms of a regular and a divergent component, the latter being proportional to the Drude weight. From now on we will refer to this regular part as the genuine d.c. conductivity, i.e.

$$\sigma^{d.c.}_{a,b} = \frac{1}{2}\tilde{G}_{a,b}(0) + \sum_{t>0} \tilde{G}_{a,b}(t), \tag{2.58}$$

with $\tilde{G}_{a,b}(t) \equiv G_{a,b}(t) - D_{a,b}$. To compute these two quantities we resort to the GHD matrices discussed in the previous section. The Drude matrix reads

$$\mathbf{D} = (\mathbb{1} + \mathbf{nK})^{-1}\rho(\mathbb{1} - \mathbf{n})\mathbf{v}^2(\mathbb{1} + \mathbf{Kn})^{-1} \tag{2.59}$$

from where we extract $D_{a,b}$ for a given equilibrium state determined by $\mu_{R,L}$. To simplify the expressions of the Drude matrix let us consider $\mu_R = \mu_L$. The Drude matrix has components

$$D_{+,+} = 2\frac{\rho_L(1-\rho_L)}{(1+2\rho_L)^2}, \quad D_{-,-} = 2\frac{\rho_L(1-\rho_L)}{(1+2\rho_L)^4}, \tag{2.60}$$

the others vanishing. To get the d.c. conductivity matrix we first need the susceptibility matrix

$$\mathbf{C} = (\mathbb{1} + \mathbf{nK})^{-1}\rho(\mathbb{1} - \mathbf{n})(\mathbb{1} + \mathbf{Kn})^{-1}. \tag{2.61}$$

We will also need the diffusion kernel, whose components are

$$\tilde{\mathcal{D}}_{a,a} = \frac{1}{2}\rho_b(1 - n_b)\left(\frac{K^{\rm dr}_{a,b}}{\rho^{\rm tot}_a}\right)^2 |v_a - v_b|, \tag{2.62}$$

$$\tilde{\mathcal{D}}_{a,b\neq a} = \frac{1}{2}\rho_a(1 - n_a)\left(\frac{K^{\rm dr}_{a,b}}{\rho^{\rm tot}_a}\right)^2 |v_a - v_b| = \left(\frac{\rho^{\rm tot}_b}{\rho^{\rm tot}_a}\right)^2 \tilde{\mathcal{D}}_{b,b}. \tag{2.63}$$

From here we obtain the diffusion matrix

$$\mathcal{D} = (\mathbb{1} + \mathbf{nK})^{-1}\rho^{\rm tot}\tilde{\mathcal{D}}(\rho^{\rm tot})^{-1}(\mathbb{1} + \mathbf{nK}). \tag{2.64}$$

The diffusion matrix gives us the diffusive corrections (Navier-Stokes term) to the continuity equation (2.44)

$$\partial_t\vec{\rho} + \partial_x(\mathbf{v}[\rho]\vec{\rho}) = \partial_x(\mathcal{D}[\rho]\partial_x\vec{\rho}). \tag{2.65}$$

Written explicitly in terms of Fermi factors in the R, L basis we get

$$\begin{aligned}
\partial_t n_R + \frac{1}{1+2n_L}\partial_x n_R &= \frac{n_L(1-n_L)}{(1+2n_L)^3}\partial_x^2 n_R - \frac{n_R(n_R-1)}{(1+2n_R)(1+2n_L)^2}\partial_x^2 n_L, \\
\partial_t n_L + \frac{1}{1+2n_R}\partial_x n_L &= \frac{n_R(1-n_R)}{(1+2n_R)^3}\partial_x^2 n_L - \frac{n_L(n_L-1)}{(1+2n_L)(1+2n_R)^2}\partial_x^2 n_R.
\end{aligned} \tag{2.66}$$

One can also check that indeed $\mathcal{D}_{+,+} = \mathcal{D}_{+,-} = 0$, so that diffusive corrections for the positive movers vanish, as argued earlier. The d.c. conductivity matrix then reads

$$\sigma^{d.c.} = \mathcal{D}\mathcal{C}. \tag{2.67}$$

We will test the prediction

$$\sigma^{d.c.}_{-,-} = 4\frac{n_L(1-n_L)n_R(1-n_R)}{(1+2n_L)^2(1+n_R+n_L)(1+2n_R)^2}, \tag{2.68}$$

(which is valid for any $\mu_{R,L}$) the other components being zero.

2.5.4 Numerical results

We verify the GHD predictions against first-principle numerical simulations. We use a matrix product operator (MPO) purification scheme to compute expectation values as well as correlation functions of operators evolved under Heisenberg dynamics w.r.t. mixed initial states.

In Fig. 2.3 we compare the GHD predictions solving (2.44) and the MPO based numerical results using a maximum bond dimension $\chi = 32$. We choose a system size of $L = 200$ to allow for smooth initial conditions, which in this case we choose to be a superposition of gaussians in $\mu_R(x)$ and $\mu_L(x)$. For the GHD equations, we first solve the TBA and Bethe equations. This fixes the initial conditions $\rho_R(0,x)$ and $\rho_L(0,x)$. We then feed these initial conditions into (2.65) to solve using the Crank-Nicholson algorithm. We remark that the diffusive corrections in (2.65) are so small that to the naked eye solving these eqs. with or without these corrections do not seem to make any visible difference. However, as we shall see such diffusive corrections can be better captured when studying instead transport via current-current correlation functions. We remark that the simplicity of the set-up allows for very fast computation times, both for the GHD and MPO results (of the order of seconds for solving the GHD equations and of minutes for the MPO time evolution on a regular laptop).

In Fig. 2.4 we show the results of computing (connected) current-current correlation functions $\langle J_a(t)J_b(0)\rangle^c$ using MPO time evolution when the background state is $\mu_R = \mu_L = 0$. Again, we find perfect agreement between our numerical results and the GHD predictions (2.60). Using (2.58) we verify as well the GHD predictions

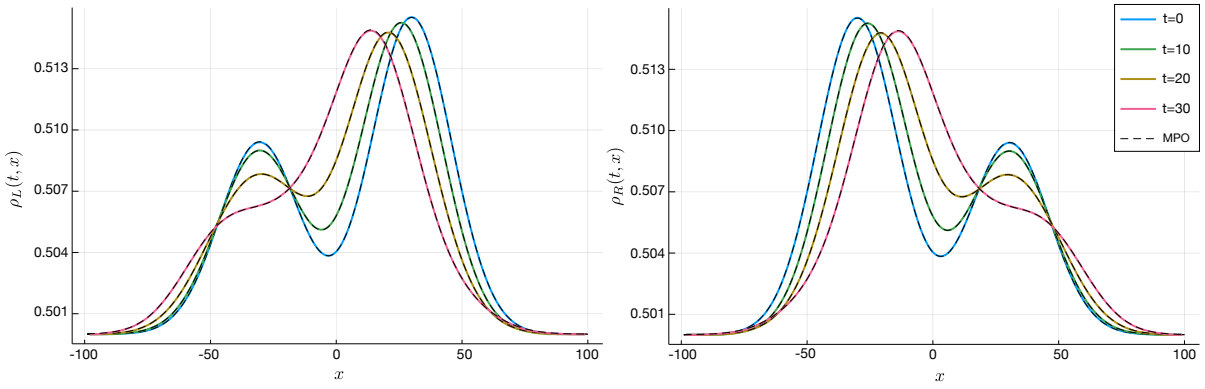

Figure 2.3. GHD predictions vs MPO results I. Left (right): left (right) movers density profiles as a function of space-time for an initial state given by $\mu_R(x) = \alpha \exp(-\beta(x+30)^2)$ and $\mu_L(x) = \alpha \exp(-\beta(x-30)^2)$ with $\alpha = 0.1$ and $\beta = 0.002$. MPO results using $\chi = 32$.

for the d.c. conductivity which in this case takes the value $\sigma^{d.c.} = 1/128$. The case $\mu = 0$ is special for the following reason. Any string operator $\hat{\mathcal{O}}$ has e.v. for fixed μ of $\langle \hat{\mathcal{O}} \rangle_\mu = \frac{e^{a\mu}}{(1+e^\mu)^b(3+e^\mu)}$, with $a, b \in \mathbb{Z}_0^+$. This implies that at $\mu = 0$, $\hat{j}_{-,j}$ evolves onto a linear combination of such string operators with integer weight, i.e. $\hat{j}_{-,j}^{(t)} = \sum_i n_i \hat{\mathcal{O}}_i$, with n_i some integer, and so it follows $\langle \hat{J}_-^{(t)} \hat{J}_-^{(0)} \rangle_{\mu=0} = \sum_i m_i/2^{b_i}$, with m_i, b_i some positive integers. In fact it is easy to realize that $\langle \hat{J}_-^{(t)} \hat{J}_-^{(0)} \rangle_{\mu=0} = n(t)/2^{2t+1}$ for $t > 0$, where $n(t)$ is again a positive integer. The denominator in this expression comes from the fact that at any given time $t > 0$, the longest string cannot have greater length than $2t+1$. With this information and the numerical results (which are exact at least for big enough χ) we can extract easily the values of $n(t)$ (a priori any floating point number from the numerical results could be interpreted as being either rational or irrational; this analysis discards the latter possibility). It is quite remarkable that, despite the fact that $n(t)$ seems at plain sight growing odd numbers (e.g. $n(3) = 5$, $n(5) = 121$, $n(10) = 68667$, $n(12) = 1045967$), they conspire to add to something very simple, as reflected in the value of the d.c. conductivity $\sigma_{-,-}^{d.c.} = 1/128$.

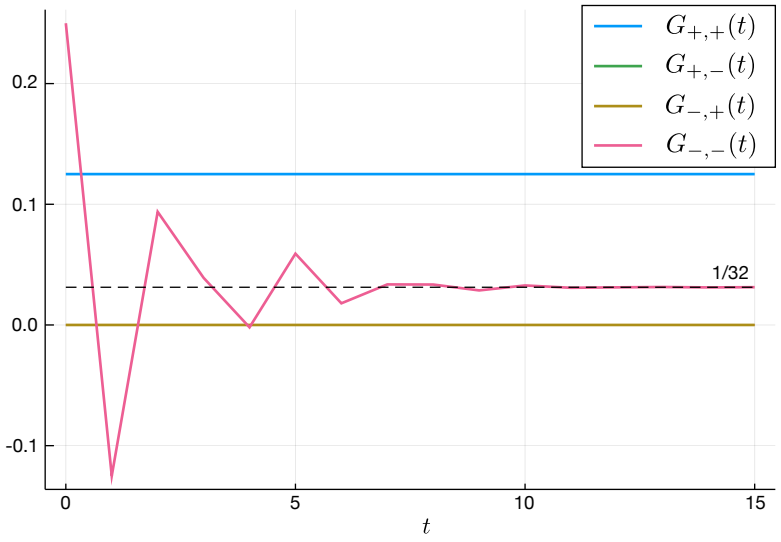

Figure 2.4. GHD predictions vs MPO results II. Current-current correlation function $\langle J_a(t)J_b(0)\rangle^c$ for $a, b \in \{+, -\}$ at $\mu_R = \mu_L = 0$ using MPOs of $\chi = 128$ and predicted Drude weight $D(\mu = 0) = 1/32$.

We conclude this section by benchmarking the GHD predictions for $D(\mu)$ and $\sigma^{d.c.}(\mu)$ in Fig. 2.5 finding again spectacular agreement between predictions and MPO results. We remark that the $\sigma^{d.c.}$ values are not particularly small and yet there is no appreciable discrepancy between the *coarse-grained* results based on GHD and those using first-principle, *microscopic* calculations based on MPO techniques. We extend the benchmarks of $\sigma^{d.c.}$ to arbitrary $\mu_{R/L}$ in Fig. 2.6.

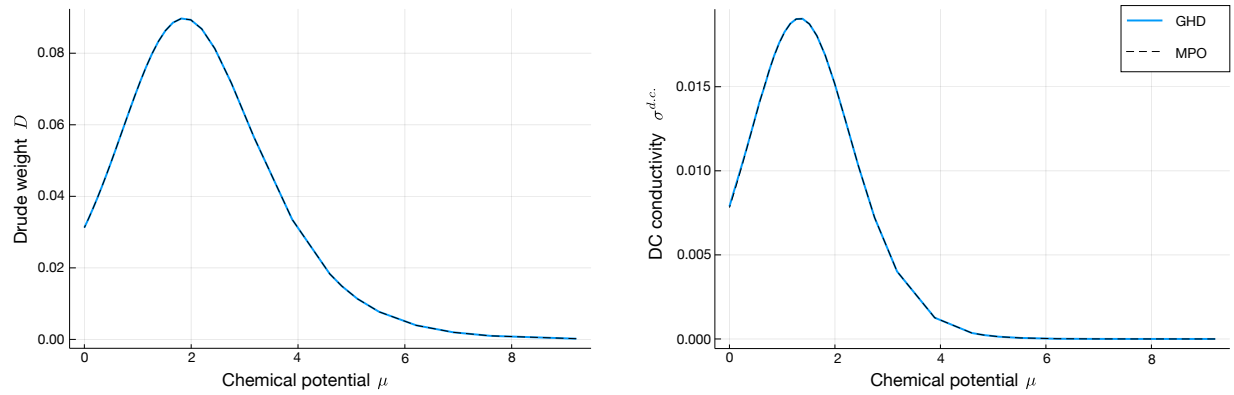

Figure 2.5. GHD predictions vs MPO results III. Transport coefficients Drude weight (left) and d.c. conductivity (right) as a function of chemical potential $\mu_R = \mu_L = \mu$. MPO results using $\chi = 128$.

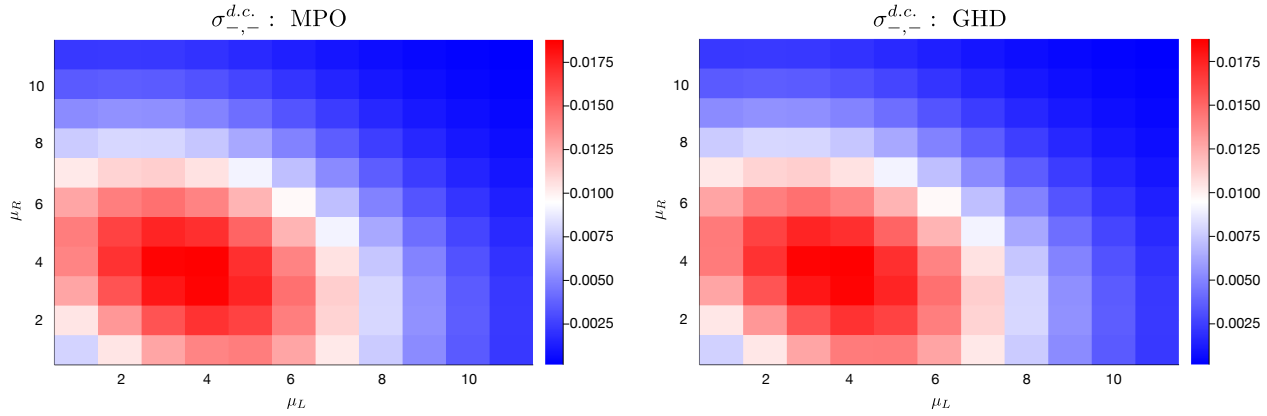

Figure 2.6. GHD predictions vs MPO results IV. Left (right): d.c. conductivity tensor $\sigma^{d.c.}_{a,b}$ vs. $\mu_{R/L}$ via MPO (GHD).

CHAPTER 3

CHAOS BY BREAKING INTEGRABILITY

This Chapter discusses the core of the Thesis. The first Chapter dealt with the dynamics of quantum chaotic systems, while the second one dealt with the hydrodynamics of integrable systems. Most systems in Nature however are neither perfectly chaotic nor completely solvable. Our aim in this Chapter is to develop a kinetic framework that aims to link these two classes of systems.

The first part of this chapter, Sec. 3.1, discusses Ref. [LPWGV21a], which describes our effort to describe nonequilibrium transport in physically meaningful setups (i.e. away from strict integrability). Our starting point is any integrable model of choice, described by GHD, and which is perturbed when adding the simplest rhs on the GHD equations (2.25) corresponding to a single decay rate determined phenomenologically and that in turn preserves a few charges. This decay rate governs the decay of the slowest decaying modes of the theory. We validate the predictions of our approximation against matrix product operator calculations on chaotic quantum spin chains, finding surprisingly good agreement. We show that despite its simplicity, our framework can capture phenomena distinctive of strongly interacting systems, such as widely separated charge and energy diffusion constants.

The previous framework, being phenomenological in nature, does not offer enough insights into the nature of transport in weakly perturbed integrable systems. With the aim of understanding such transport better, in the next section, Sec. 3.2, we study a particular realization of integrability breaking in Rule 54, an integrable cellular automaton that was already discussed in great detail in the last Chapter. Integrability

breaking is induced by forcing movers to change direction at random, effectively preserving the density of movers, while breaking the conservation of the *imbalance* of movers (i.e. the difference in the number of right *vs.* left movers). While simple to state, the particular mechanism that realizes backscattering in Rule 54 is constrained to a certain subspace so as to preserve the density of movers, which leads to some intriguing transport that we fail to understand in detail. In spite of this, we manage to understand analytically dynamics at the level of *tagged* quasiparticles. The results of this section are based on Ref. [LPGV22].

In the last section, Sec. 3.3, we step back and consider a simpler integrable model to that of Rule 54, the hard-rod gas, which is a model similar to Rule 54 but in the space-time continuum and with in principle arbitrary velocities for the bare particles of the model. As in Rule 54, we shall consider backscattering as the source of noise. The simplicity of dealing with backscattering noise in the hard-rod gas model as compared to Rule 54 arises from the fact that noise and interactions in the former are decoupled from each other. This allows us to compute transport analytically away from integrability in this setup, providing a rare example of fully analytically tractable dynamics away from the integrable point. The results of this section are based on Ref. [LPV23].

3.1 Generalized relaxation time approximation

Motivation — As discussed in Chapter 2, GHD allows to compute transport in integrable systems, a surprising feature given the infinitely many conservation laws in these systems. Realistic systems, however, are only *approximately* integrable. On short timescales they obey GHD, but on the longest timescales they cross over to conventional hydrodynamics. A general theory of this crossover has remained elusive, despite recent progress [LLP81, MMGS13, HKM13, EKMR14, JHR06, LMMR14, LGS16a, BCK15, BEGR15, BEGR16, CDD$^+$19, SR10, MR18, MMGS16, AF17, SVO18,

MR19, BCR+19, CBM18, FGV20a, DBD20, DNMKI20, BDNDL20a, PCC+20, BLGR20, BGR20]. In principle one can write a collisional Boltzmann equation for weak integrability breaking [FGV20a, DBD20]. However, in general the collision integral is intractable, as it depends on *all* the matrix elements of the integrability-breaking perturbation. In special cases, such as long-range interactions, slowly fluctuating noise, or weakly interacting systems, the integrability-breaking perturbation can itself be expressed in terms of GHD data [FGV20a, DBD20]. More generally, however, integrability-breaking perturbations lie outside of GHD: for example, Umklapp scattering involves large momentum transfer, and thus cannot be captured by a long-wavelength theory such as GHD. In the absence of the GHD framework, evaluating the collision integral is an intractable task.

This work addresses the question of integrability breaking from a fundamentally different perspective. Instead of microscopically deriving the collision integral, we adopt a simple but general approximation, which we call the "generalized relaxation time approximation" (GRTA), by analogy with the conventional relaxation time approximation (RTA) for weakly interacting electrons [Bre99]. The GRTA assumes that there is a single dominant relaxation time that controls the onset of chaos. This assumption allows us to efficiently simulate dynamics away from the integrable limit. Although our approach resembles the conventional RTA in positing a unique relaxation time, its implementation and physical consequences are completely different. The RTA deals with nearly free particles, so their scattering kinematics is simple. By contrast, in an interacting integrable system, the momentum carried by each quasiparticle is a nonlinear functional of the full quasiparticle distribution function. Thus, when one describes a scattering process in an integrable system, not only the matrix elements but also the delta functions conserving momentum and energy are nontrivial to evaluate.

Instead, we implement the GRTA as follows. In GHD, one regards a system as locally being in a generalized Gibbs ensemble (GGE) [RDO08b, LEG$^+$15, VR16a], with chemical potentials for each conservation law [VR16a]. The key step in our approach is to replace the local GGE with a *local* thermal Gibbs state, subject to the residual conservation laws, at some finite rate $1/\tau$ (where τ is the generalized relaxation time). The main assumption is that there is a unique *local* relaxation rate for the quasiparticle distribution function. This is justified under certain assumptions, and (as we discuss below) fails sometimes; however, we find that it is remarkably accurate at reproducing numerical time evolution, even when the integrability-breaking perturbations are not especially small. For initial states far from equilibrium, the GRTA (unlike the RTA) gives rise to nontrivial relaxation dynamics, as the local equilibrium state is a nontrivial functional of the local quasiparticle distribution. Moreover, contrary to the simplest implementation of the RTA, GRTA preserves conservation laws and is suitable to study hydrodynamics. Thus, we argue the GRTA captures the "generic" crossover from generalized to conventional hydrodynamics.

Boltzmann equation — Let us imagine perturbing an integrable system with Hamiltonian $\hat{H}_0$ by a small, nonintegrable perturbation $\hat{V}$ of order g that destroys all but a few conservation laws. We assume that the expressions for charges and currents are unchanged – neglecting $\mathcal{O}(g)$ corrections to these quantities, and force terms that are treated elsewhere [BAC19]. The leading effect of the nonintegrable perturbation is to thermalize quasiparticle distributions at long times $t \gg \mathcal{O}(g^{-2})$. Integrability breaking endows the GHD equation with a collision integral

$$\partial_t \rho_\lambda + \partial_x \left(v_\lambda^{\text{eff}}[\rho] \rho_\lambda \right) = \mathcal{I}_\lambda[\rho]. \tag{3.1}$$

that mixes quasiparticle sectors, where the index λ labels both rapidities, as well as any possible quasiparticle colors. This collision integral $\mathcal{I}_\lambda$ can in principle be derived perturbatively using Fermi's Golden Rule (FGR), and is $\mathcal{O}(g^2)$ [FGV20a,

DBD20, BDNDL20a]. It involves the matrix elements (form factors) of the integrability breaking perturbations, which can be expressed in terms of hydrodynamical data only for noninteracting systems, and for perturbations involving low momentum transfer such as slowly varying noisy potentials or long-range interactions [FGV20a]. Eq. (3.1) was analyzed within linear response in Ref. [FGV20a], and was shown to lead to diffusive hydrodynamics in general.

Generalized relaxation-time approximation — For most physical integrability-breaking perturbations, the matrix elements of the perturbation cannot be expressed in terms of hydrodynamic data. In the few cases where the collision integrals can be written down explicitly, they are impractical to implement numerically, even for simple physical processes like particle loss in a Bose gas [BDD20]. For context, we remark that even for weakly-interacting fermions, collision integrals are often approximated by using the relaxation-time approximation (RTA), which suffices to capture most of the relaxation physics and to describe experiments. Here, we introduce a generalized relaxation-time approximation (GRTA), which amounts to choosing a simple form for the collision integral:

$$\partial_t \rho_\lambda + \partial_x \left(v_\lambda^{\rm eff}[\rho] \rho_\lambda \right) = -(\rho_\lambda - \rho_\lambda^{\rm Gibbs}[\rho])/\tau. \tag{3.2}$$

This right-hand side enforces local thermalization on a typical relaxation timescale τ as follows: $\rho_\lambda^{\rm Gibbs}[\rho]$ is a nonlinear functional of the state ρ_λ, defined as the distribution of quasiparticles of a Gibbs state with the same value of the conserved quantities q_α ($\alpha = 1, \ldots, N$ corresponding to the charges preserved by the integrability breaking perturbation) as the state ρ_λ. For example, consider a Bose gas where the integrability breaking perturbation preserves energy E, particle number N and momentum P. Then the distribution $\rho_\lambda^{\rm Gibbs}[\rho]$ corresponds to the (boosted) Gibbs ensemble density matrix $\hat{\rho}_{\rm Gibbs} = \frac{1}{Z} {\rm e}^{-\beta(\hat{H} - \mu \hat{N} - \nu \hat{P})}$ where β, μ and ν are chosen so that the average

particle number, energy and momentum are the same as in the state ρ_λ. By definition, we have $\int d\lambda(\rho_\lambda - \rho_\lambda^{\text{Gibbs}})h_\alpha(\lambda) = 0$, ensuring the conservation of the charges $\hat{Q}_\alpha$.

Physically, the GRTA assumes that local relaxation is controlled by a single relaxation rate. Of course, realistic FGR collision integrals have a lot more structure, involving a hierarchy of relaxation rates. However, we expect this approximation to capture the key physics of integrability breaking. One can formalize this intuition as follows. The relaxation of charges in the presence of weak integrability-breaking is captured by the equation $\partial_t Q_i = -\sum_j \Gamma_{ij} Q_j$, where $\mathbf{\Gamma}$ is a matrix that is itself a functional of the equilibrium state [FGV20a, DBD20]. The spectrum of the matrix $\mathbf{\Gamma}$ contains zero modes corresponding to the residual conserved charges, as well as other eigenmodes that capture the characteristic decay rates. If there is a gap between the zero modes and the decaying modes, one can identify this gap with $1/\tau$, and replace the matrix $\mathbf{\Gamma}$ with a projector onto modes that decay at rate $\sim 1/\tau$, which is justified at long enough times where $\mathrm{e}^{-t/\tau}$ will dominate exponentials decaying with faster rates. The GRTA corresponds to replacing $\mathbf{\Gamma}^{-1} \approx \tau$ for all decaying charges, which approximately coincides with the projection approach, provided that all residual conserved currents have approximately similar overlaps with the slowest-decaying modes of $\mathbf{\Gamma}$. (This construction indicates that the GRTA will fail whenever there are arbitrarily slowly relaxing modes, as we expect on physical grounds, and also when the currents of residual charges have very different overlaps with the slowest-relaxing modes of $\mathbf{\Gamma}$.)

We evaluate the right-hand side of eq. (3.2) as follows. We compute the (density of) conserved charges q_α (say particle number, momentum and energy) in the state $\rho_\lambda(x,t)$, and invert the equation of states of the model – known from the equilibrium thermodynamic Bethe ansatz (TBA) [Tak99] – to find the Lagrange multipliers (in our example, β, μ and ν) of the Gibbs state corresponding to those values. Using TBA, we then compute the density of quasiparticles $\rho_\lambda^{\text{Gibbs}}[\rho]$ corresponding to those

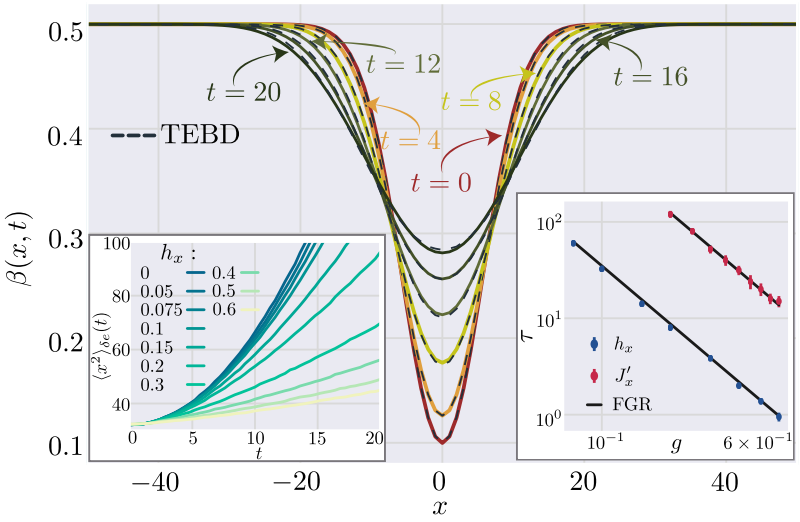

Figure 3.1. Energy transport in nonintegrable spin chains: inverse temperature profiles $\beta(x,t) = 1/T(x,t)$ in an XXZ spin chain with a staggered transverse field h_x breaking integrability. The TEBD data for $h_x = 0.2$ is described very well by eq. (3.3) and GRTA with $\tau \simeq 8$. *Left inset:* Variances of the energy profiles *vs* time from TEBD, for various values of h_x, showing a crossover between ballistic and diffusive transport. *Right inset:* The fitted values of τ agree with the FGR scaling (3.5) for both $g = h_x$ (staggered x-fields) and $g = J'_x$ (staggered xx-couplings).

Lagrange multipliers and thus I_λ. Note that we use the equation of states of the *unperturbed* (integrable) model. This is justified perturbatively by the fact that the integrability breaking perturbation smoothly modifies thermodynamic quantities and the equation of states (with small changes if the perturbation is weak), while it dramatically affects the dynamics at long times. We take τ to be an unknown constant, a single phenomenological parameter to be determined by comparing the solution of eq. (3.2) to numerics or experiments.

Numerical solution— To implement this GRTA scheme numerically, we develop a general numerical scheme to solve (3.1), which can be used both near and far from equilibrium. Following the numerical methods of Ref. [BVKM17, BAC19, MS20] in the integrable case, we find it convenient to work with the "normal modes" of GHD, which are given by the occupation ratios (Fermi factors) $n_\lambda = \rho_\lambda / \rho_\lambda^{\text{tot}}$, where

$\rho_\lambda^{\rm tot} = \rho_\lambda + \rho_\lambda^h$ is the total density of states at rapidity λ and ρ_λ^h the density of holes. There is a one-to-one correspondence between the density of quasiparticles ρ_λ and the occupation ratios n_λ, provided by the Bethe equations. In terms of n_λ, the Boltzmann equation (3.1) takes the *advection* form

$$\partial_t n_\lambda + v_\lambda^{\rm eff}[n]\partial_x n_\lambda = I_\lambda[n], \tag{3.3}$$

where I_λ is simply related to $\mathcal{I}_\lambda[\rho]$. We then solve this equation by finite elements, discretizing space, time, and rapidity. We use a backward first order scheme $n_\lambda(x,t) = n_\lambda(x - v_\lambda^{\rm eff}[n(x,t)]\Delta t, t - \Delta t) + \Delta t I_\lambda[n(x,t)]$, where crucially, the velocity and collision integrals in the right-hand side are evaluated at time t to improve stability. We solve this equation by iteration, and check convergence with respect to the small parameters Δt, Δx and $\Delta\lambda$.

Energy transport in spin chains— The GRTA approach has the advantage of being very general, and can be applied to chaotic spin chains near integrability. To illustrate this, we consider the spin-$\frac{1}{2}$ XXZ spin chain with integrability breaking perturbations

$$\hat{H} = \sum_i (\hat{S}_i^x \hat{S}_{i+1}^x + \hat{S}_i^y \hat{S}_{i+1}^y + \Delta \hat{S}_i^z \hat{S}_{i+1}^z) + \hat{V}, \tag{3.4}$$

with anisotropy $\Delta = \frac{1}{2}$, and $\hat{V} = h_x \sum_i (-1)^i \hat{S}_i^x$ or $\hat{V} = J_x' \sum_i (-1)^i \hat{S}_i^x \hat{S}_{i+1}^x$. When $\hat{V} = 0$, this model is integrable, and energy transport is purely ballistic as the total energy current is a conserved quantity. As higher-order corrections vanish exactly, energy transport can be captured extremely well by GHD [BVKM17]. The staggered perturbation $\hat{V}$ breaks integrability and the $U(1)$ symmetry of the XXZ model.

We consider energy transport in the Hamiltonian (3.4) by preparing a local region with temperature $T = 10$ embedded in a uniform equilibrium background with

temperature $T = 2$ [1]. We simulate the dynamics of this system up to time $t = 20$ by evolving the density matrix using time-evolving block decimation (TEBD) and compare with the GRTA (3.2) for various values of τ. We compare the local temperature profiles $T(x, t)$ between the two approaches, using the equilibrium equation of state of Eq. (3.4) to convert energy density to temperature. (This accounts for the shift in the equilibrium energy density due to the perturbation $\hat{V}$, which can readily be captured using perturbation theory). We find a best fit for the single parameter τ by matching the full temperature profiles from the TEBD simulations and the GRTA.

We find that GRTA is able to describe the nonintegrable dynamics of (3.4) remarkably well with a single parameter τ for each $\hat{V}$, for various values of h_x or J'_x ranging from 0.05 to 0.6, corresponding to almost two decades in τ. Moreover, the fitted values of τ all agree very well with the simple FGR scaling

$$\tau \simeq C g^{-2}, \tag{3.5}$$

with $C \approx 0.32(5)$ for $g = h_x$ (staggered x-fields), and $C \approx 4.95(5)$ for $g = J'_x$ (staggered xx-couplings). This is remarkable, as in general we expect that relaxation times should depend on temperature, and the initial state considered has a wide range of temperatures. Allowing for limited dependence of τ on the state ρ – such as through the local temperature — might be necessary to capture strongly nonequilibrium setups with even wider temperature ranges. While the variance of the profiles of the local perturbation in energy grows quadratically (indicating ballistic transport) in the integrable case, it crosses over to linear (diffusive) growth for times $t \gg \tau$.

[1] We have chosen energy transport in this model because GHD accurately describes energy transport in the integrable limit even at relatively short times. For other quantities like spin, GHD remains asymptotically valid, but there are larger corrections at short times; these are corrections to GHD, rather than to GRTA.

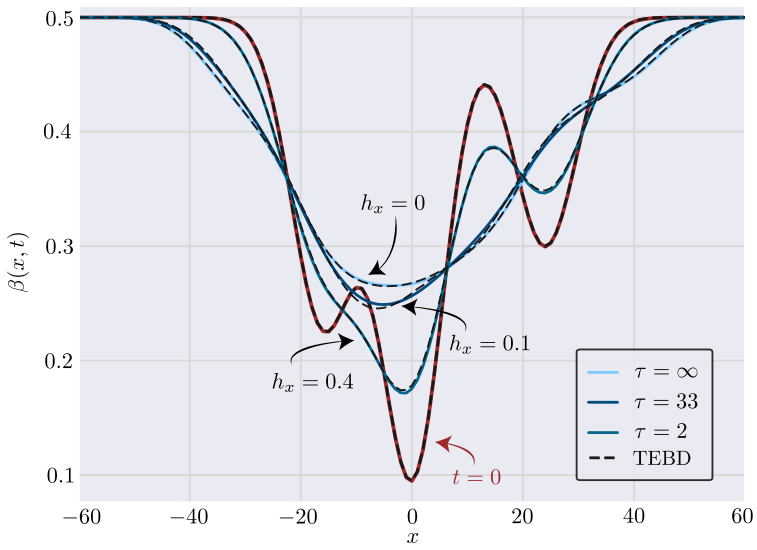

Figure 3.2. Generic energy transport in chaotic spin chains: inverse temperature profiles $\beta(x,t) = 1/T(x,t)$ at time $t = 20$ in an XXZ spin chain with a staggered transverse field h_x breaking integrability, comparing TEBD and GRTA starting from a non-trivial inhomogeneous initial state. The values of τ in GRTA for each h_x were determined from Fig. 3.1.

This scaling implies that the whole time evolution for all values of g we consider can be described quite accurately using a single free parameter C. While we obviously expect corrections to this GRTA approach, combined with the expected FGR scaling (3.5), it clearly captures most of the physics of integrability breaking. Surprisingly GRTA is able to describe energy transport even for strongly chaotic chains for which the relaxation time τ is $\mathcal{O}(1)$.

To illustrate the predictive power of GRTA, we study energy transport for a more complicated inhomogeneous initial state, for various values of the staggered field h_x, comparing GRTA to TEBD (Fig 3.2). Note that there is no free parameter here, as the values of the relaxation time $\tau(h_x)$ are fixed from the analysis of Gaussian initial states in Fig. 3.1, and follow approximately eq. (3.5). The agreement is remarkable, and illustrates that GRTA captures energy transport in this generic nonintegrable spin chain not only qualitatively, but also to a large extent quantitatively (the error between GRTA and TEBD is at most 2%).

Hydrodynamics of nonintegrable Bose gases— We study now the crossover from generalized to conventional hydrodynamics in one-dimensional Bose gases, governed by the Lieb-Liniger Hamiltonian

$$\hat{H}_0 = \int dx\, \hat{\Psi}^\dagger \left(-\frac{\nabla^2}{2m} - \mu \right) \hat{\Psi} + c\hat{\Psi}^\dagger \hat{\Psi}^\dagger \hat{\Psi} \hat{\Psi}, \tag{3.6}$$

with $m = 1/2$ and $c = 1$ hereafter. We first consider integrability-breaking perturbations that relax momentum: in this case, the conserved quantities in the Gibbs state of the GRTA are particle number and energy. We implement both far from equilibrium free expansions into vacuum of a cloud of atoms which models experiments on ultracold Bose gases (Fig. 3.3a) [KWW06, LHMG$^+$09, LHMHM11, RSB$^+$13, KMHM14, BHML$^+$12, LSM$^+$12, VLM$^+$13, SJS$^+$17, KPHM17, SBDD19, TKL$^+$18a], and linear response setups where the initial state is a small local perturbation on top of an equilibrium Gibbs state (Fig. 3.3b). We confirm that the conservation of both energy and particle number are satisfied to a very good accuracy for all plotted time scales ($< 0.5\%$). We find that while the variance of the profiles of the local perturbation in both energy and particle density grow quadratically (indicating ballistic transport) in the integrable case, they crossover to linear (diffusive) growth for times $t \gg \tau$. Diffusive hydrodynamics is expected as momentum is not conserved, and we see that energy and particle number have different diffusion constants, inherited from the different Drude weights of the integrable limit.

We have also solved the hydrodynamic evolution of a Bose gas (3.6) with a perturbation that preserves particle number, energy, and momentum. Our scheme fully preserves Galilean invariance, so the particle current is momentum and is therefore conserved: we observe "sound modes" propagating ballistically in the nonintegrable case, which broaden diffusively on the time scales simulated. We also observe a small heat mode near the origin. This is consistent with what is expected from conventional, Navier-Stokes hydrodynamics in one dimension. We note that conventional

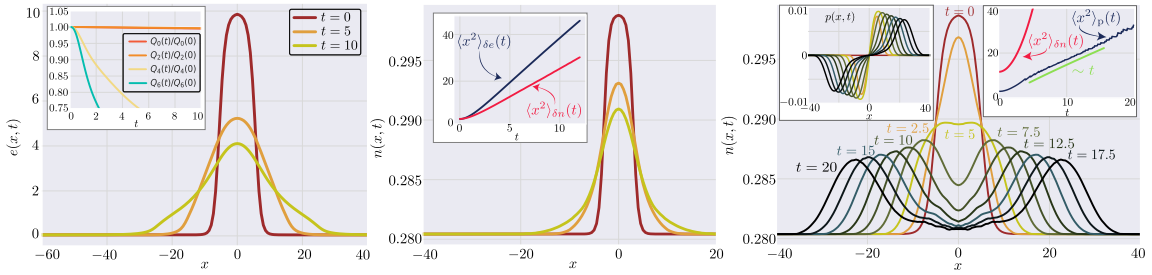

Figure 3.3. Crossover from generalized to conventional hydrodynamics in 1d Bose gases using GRTA with $\tau = 1$. *Left*: Energy density *vs* time for free expansion of a cloud into vacuum, for a GRTA perturbation conserving energy and particle number. *Inset*: evolution of the charges Q_n of the Lieb-Liniger model, showing conservation of particle number $Q_0 = N$ and energy $Q_2 = E$. *Middle*: Particle density after a linear-response perturbation to a thermal state with $T = 1$ and $\mu = 0$, for a GRTA perturbation conserving energy and particle number. *Inset*: variances of the energy and particle density profiles, showing diffusive behavior. *Right*: Linear-response initial state for a GRTA perturbation conserving energy, particle number and momentum. *Left inset*: Momentum profiles. *Right inset*: Variance of the particle number profiles showing ballistic transport (red), and diffusive broadening of the sound peaks in the momentum profiles (blue).

hydrodynamics is generically anomalous in one dimension, and adding noise to our equations is expected to broaden the sound peaks in a superdiffusive way (dynamical exponent $z = 3/2$) – instead of diffusive – as predicted by the theory of nonlinear fluctuating hydrodynamics [NR02, vB12, Spo14]. It would be interesting to include noise in our framework to check this.

3.2 Backscattering in Rule 54

While the *generalized* relaxation-time approximation method discussed in the previous section proves very effective at computing transport away from integrability, understanding better this dynamics from first-principles seems out-of-reach in general. The main bottleneck for a full understanding of the physics of integrability breaking is a lack of tools to compute the various decay rates governing the relaxation of nonconserved charges, which should be controlled by Fermi Golden's Rule (FGR).

Our relaxation-time approximation scheme assumes a single, dominant time scale that governs relaxation. The associated effective decay rate, extracted phenomenologically, can be used to compute transport. Here we aim at extracting this effective decay rate *ab-initio*, and more generally compute transport coefficients, by considering backscattering noise in Rule 54 – the integrable cellular automaton already discussed in Chapter 2. Our main finding here is that, while such a single dominant time scale exists, given by the smallest decay rate, transport coefficients such as the diffusion constant are not determined by this parameter. Instead, one must take into account the transient dynamics as well as we will explain, rendering the problem analytically out-of-reach. However, some signatures of transport are still accessible analytically. These are the self-diffusion constants of the tracers and associated quantities.

3.2.1 Interlude: integrability breaking in Hamiltonian systems

Before embarking on breaking integrability in the Rule 54 model, it is worth taking a brief detour and discuss what we expect from the study of integrable Hamiltonian systems with at least one broken conservation law. This is a topic with a long history in the literature of integrable systems (see e.g. [MMGS13, KWE11, BEGR16, LGS16b, BK17, DKPR16, VR16b]), that has regained some interest recently in the context of GHD [FGV20b, DBD21, BLV21, BDNDL20b, LPWGV21a]. Our main goal is to review briefly the assumptions that go into this framework, as they appear to fail for Rule 54.

Consider a system described by an integrable Hamiltonian $\hat{H}_0$ and a perturbation $g\hat{V} = g\int dx\hat{v}(x)$ that breaks the conservation of charge $\hat{q}_i$, so that the total Hamiltonian is given by $\hat{H} = \hat{H}_0 + g\hat{V}$. A necessary requirement for $\hat{V}$ to break the conservation of $\hat{Q}_i = \int dx\hat{q}_i(x)$ is that $[\hat{Q}_i, \hat{V}] \neq 0$. The dynamics of the e.v. of the charge, $q_i = \langle\hat{q}_i\rangle$, up to $\mathcal{O}(g^3)$ is governed by

$$\partial_t q_i = g^2 \int_{-t}^{t} ds \langle [\hat{V}^0(s), \hat{Q}_i] v(0) \rangle^c + \mathcal{O}(g^3), \tag{3.7}$$

where as usual when dealing with perturbation theory, operators are evolved in the interaction picture, $\hat{O}^0(t) = e^{i\hat{H}_0 t}\hat{O}e^{-i\hat{H}_0 t}$ and the only assumption so far is a background homogeneous state with density matrix $\rho_0 = Z^{-1}\exp(-\sum_j \beta^j \hat{Q}_j)$ and $[\hat{Q}_j, \hat{Q}_k] = 0$ for any pair of charges. Note that neglecting $\mathcal{O}(g^3)$ terms and assuming a continuous spectrum of $\hat{H}_0$ we recover the Fermi Golden Rule (FGR) expression

$$\partial_t q_i = 4\pi^2 g^2 \sum_n \delta(\Delta\epsilon)\delta(\Delta p)\Delta q_i |\langle n|\hat{u}|\rho\rangle|^2, \tag{3.8}$$

where an insertion of the identity in terms of eigenstates of $\hat{H}_0$ has been made, and e.v.s have been expressed in terms of the quasiparticle density ρ. The rhs is sometimes referred to as the *drift*. The terms $\Delta\epsilon$, Δp, are the difference in energy (w.r.t. the unperturbed Hamiltonian) and momentum, between states $|n\rangle$, $|\rho\rangle$, and Δq_i is the difference in charge eigenvalue of $\hat{Q}_i$ in $|n\rangle$ vs. $|\rho\rangle$. Lastly, we have implicitly taken $t \to \infty$, $L \to \infty$, to bring down the $\delta(\cdot)$ terms. An analogous expression to (3.8) may be found if instead of an integrable Hamiltonian H_0, we started off from a Hamiltonian with at least one conserved charge $\hat{Q}_i$, so this result is rather universal. One key assumption for the validity of FGR in many-body systems, as pointed out in *e.g.* [MRDR19], is that the system should *(i) equilibrate quickly* and *(ii)* be *weakly-coupled*. The fast equilibration condition means that after a finite time τ^*, the system relaxes to the diagonal equilibrium ensemble of the unperturbed Hamiltonian – this ignores hydrodynamic tails effects. The weak coupling condition means $g\tau^* \ll 1$. (See [MRDR19] for precise meaning of these conditions).

3.2.2 Setup in the noisy Rule 54

When considering breaking the conservation of either of the two charges in Rule 54, we find it more natural to break the conservation in the imbalance of solitons. From a

physical standpoint this setup should mimic the physics of breaking the conservation of momentum in a Bose gas system in the presence of Galilean invariance (recall the imbalance corresponds to the current of density of solitons, $j_+ = \rho_-$). One way to implement this choice of integrability breaking is to convert a right mover into a left mover with probability p, and viceversa. Ultimately we seek a r.h.s. in (2.44) of the form $-\rho_-/\tau$ in the spirit of a relaxation time approximation [LP83], where the relaxation time $\tau \propto 1/p$. This would result in an exponential decay over time of the nonconserved charges ρ_-. Microscopically, the integrability breaking mechanism should be of the form $\underset{i}{\square\square} \rightleftarrows \underset{i}{\square\square}$ with probability p (collision terms appearing in $\hat{\rho}_{R/L,i/i+1/2}$ are left intact). One can show that in order for the perturbation to preserve the number of particles it must act on a specific subspace. There are various choices for such a subspace which we report in A.1, the simplest of which is given when applying the following projector

$$\hat{\Pi}_j = \hat{\Pi}_{R,j} + \hat{\Pi}_{L,j+1/2}, \tag{3.9}$$

where $\hat{\Pi}_{R,j} \equiv \underset{j}{\blacksquare\square\square\blacksquare\blacksquare}$, $\hat{\Pi}_{L,j+1/2} \equiv \underset{j}{\blacksquare\blacksquare\square\square\blacksquare}$. The dynamics is then given by a two step process: first, we evolve by one time step via the unitary map $\hat{F}$. Next, we apply the map $\underset{j}{\square\square} \leftrightarrow \underset{j}{\square\square}$ with probability p on those unit cells that belong to subspace (3.9). We repeat this procedure t times and average over both initial configurations and trajectories (which are now stochastic). An instance of such dynamics is shown in Fig. 3.4. While this dynamics can be implemented efficiently via a simple classical Monte Carlo (MC) algorithm, an alternative description can be given using the language of quantum channels. Quantum channels allow not only for unitary evolution within the system, but *generalized measurements* as well, the latter giving rise to dissipation. The basic ingredient is a set of Kraus operators $\{\hat{K}_i\}$ that *evolve* a given state described by a density matrix $\hat{\rho}(t) \to \hat{\rho}(t+1) = \sum_\mu \hat{K}_\mu \hat{\rho}(t) \hat{K}_\mu^\dagger$ and that satisfy the completeness condition $\sum_\mu \hat{K}_\mu^\dagger \hat{K}_\mu = \hat{\mathbb{1}}$. A well-known fact is that the choice of

these Kraus operators is not unique [NC02]. The specific choice of Kraus operators for our setup is delegated to A.1. The benefit of a purely quantum mechanical description of the dynamics in terms of Kraus operators is that such time evolution is *exact* and can be in principle simulated via time dependent matrix product operator (tMPO) techniques [Sch11a, Orú14]. We have ran these simulations finding agreement with MC where possible. In practice we have found that for the time scales involved away from integrability, there is little benefit in using tensor networks.

3.2.3 Tracer dynamics

To give some intuition of the transport properties away from integrability we consider the limit $\mu \to \infty$ (low density of particles). Here the dynamics becomes trivial – interactions are irrelevant and our system is effectively described as a single soliton undergoing a random walk with a mean free path set by the noise, a picture that remains true in general, see left panel of Fig. 3.4. The imbalance decays with a decay rate given by $\Gamma = 2p$ (in the continuous time case) and $\Gamma = -\log(1-2p)$ (in the discrete time case). The density of particles in turn spreads diffusively. Starting with an initial state $\rho_{+,x} = \delta_{x,0}$ the late time shape for ρ_+ is exactly given by the gaussian $\rho_{+,x} = \frac{1}{\sqrt{4\pi\mathcal{D}t}} e^{-\frac{x^2}{4\mathcal{D}t}}$, with a diffusion constant $\mathcal{D}$ given by $\mathcal{D} = 1/\Gamma$.

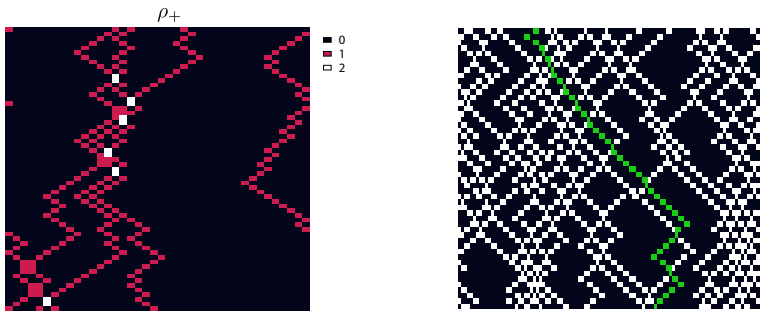

Figure 3.4. Snapshot of the noisy Rule 54.. Left: Snapshot of density of particles in the presence of noise in Rule 54 at low density $\mu \gg 1$. Right: dynamics of a tagged particle (in green) near half-filling $\mu = 0$.

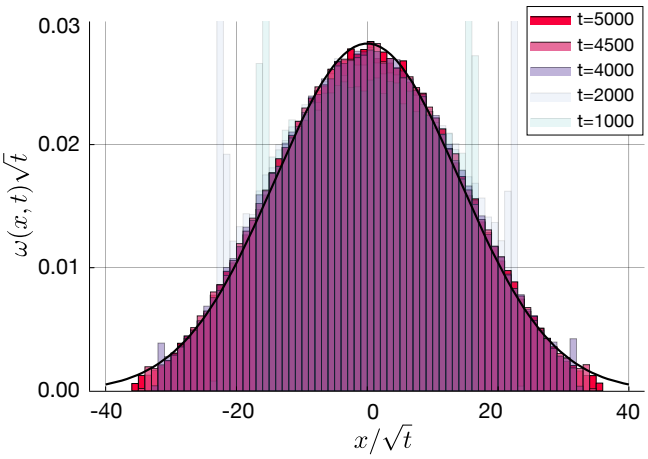

Figure 3.5. Tracer distribution profile at half-filling $\mu = 0$. The distribution follows a normal distribution at long enough times $\sim \mathcal{N}(0, 2D^*t)$ (black line) with D^* the self-diffusion constant extracted from (3.11). Results shown for $p = 0.02$ and $\mu = 0$ ($D^* = 100$). Results for a system size $L = 800$ using pbc.

Away from the trivial limit $\mu \to \infty$ the dynamics consists of a bunch of particles interacting with each other and subject to noise (a *Brownian hard-rod gas* in essence, with fixed bare velocity ± 1). As a proxy for transport we focus on the dynamics of a tracer. Studying tracer dynamics is arguably much simpler than *many-body* correlation functions, yet this has proved useful as a first step at determining the nature of transport in integrable systems by exploiting the quasiparticle picture [GHKV18b, GV19]. Studying fluctuations of quasiparticle trajectories essentially gives the diagonal components of the diffusion kernel (see Eq. 2.62), and as such cannot fully determine the diffusion constant (which requires knowledge of the off-diagonal components as well). A complete characterization of each tracer i in Rule 54 is given in terms of its *flavor* η_i which is a random variable taking the value $+1$ if the tracer is moving right, or -1 if it is moving left, and its coordinates (x, t). A snapshot of what the dynamics looks like for a tagged particle away from integrability is shown on the right panel in Fig. 3.4. We are interested in the dynamics over homogeneous equilibrium background states. The flavor η should average to zero, $\langle \eta(t) \rangle = 0$ (this

is because at equilibrium $\mu_R = \mu_L$ and at any given time, particles of both flavors are equally likely). As a result we study instead fluctuations $\langle \eta(t)\eta(0)\rangle$. From the theory of Brownian motion we expect this quantity to decay exponentially with a characteristic flavor decay rate Γ^* which we seek to determine. We imagine tagging a right tracer starting at coordinates $(0,0)$. Its ensemble survival probability (the probability for the tracer to turn left) should be proportional to $p \times \langle \hat{\Pi}_{R,x}\rangle$ (this is because the perturbation can only act within the subspace $\hat{\Pi}_{R,x}$). To fix the proportionality constant we need the constraint that in order for the perturbation to act at x, a right particle at x must exist in the first place, hence the survival probability of the tagged right particle should be $\Gamma^*_R = p \times \langle \hat{\Pi}_{R,x}|\hat{\rho}_{R,x}\rangle = p\frac{\langle \hat{\Pi}_{R,x}\rangle}{\langle \hat{\rho}_{R,x}\rangle} = p\frac{\langle \hat{\Pi}_{R}\rangle}{\langle \hat{\rho}_{R}\rangle}$, with $\langle\cdot|\cdot\rangle$ denoting conditional expectation value, and where in the last equality we have used the fact that we are considering homogeneous background states, so that $\langle \hat{\mathcal{O}}_x\rangle = \langle \hat{\mathcal{O}}\rangle$. An identical argument for the left movers would yield instead $\Gamma^*_L = p\frac{\langle \hat{\Pi}_{L}\rangle}{\langle \hat{\rho}_{L}\rangle}$. At equilibrium $\mu_R = \mu_L = \mu$ the two decay rates are equal and so the flavor decay rate is $\Gamma^* = 2p\gamma^*$, with $\gamma^* = \frac{\langle \hat{\Pi}_{R}\rangle}{\langle \hat{\rho}_{R}\rangle} = \frac{\langle \hat{\Pi}_{L}\rangle}{\langle \hat{\rho}_{L}\rangle}$ and whose expression can be found using the one dimensional transfer matrix of Rule 54 (2.40)

$$\gamma^* = \frac{e^{3\mu}}{(1+e^{\mu})^2(3+e^{\mu})}. \tag{3.10}$$

We find that our numerical results match perfectly this formula for small enough p, as shown in Fig. 3.6. We also note that in the limit of very low filling, this formula reproduces the decay rate expected for a free particle, $\gamma^* \to 1$. With this at hand we can also quantify how tracer particles diffuse. Each particle will be subject to collisions with other particles and backscattering events that happen at rate $p\gamma^*$. As a result each particle will diffuse with a characteristic self-diffusion constant $\mathcal{D}^*$ (which in general, is different from the *full* diffusion constant $\mathcal{D}$). In other words, the probability distribution $\omega(x,t)$ to find a tracer at coordinates (x,t) assuming it started at the origin, $(0,0)$, should become a Gaussian that broadens as

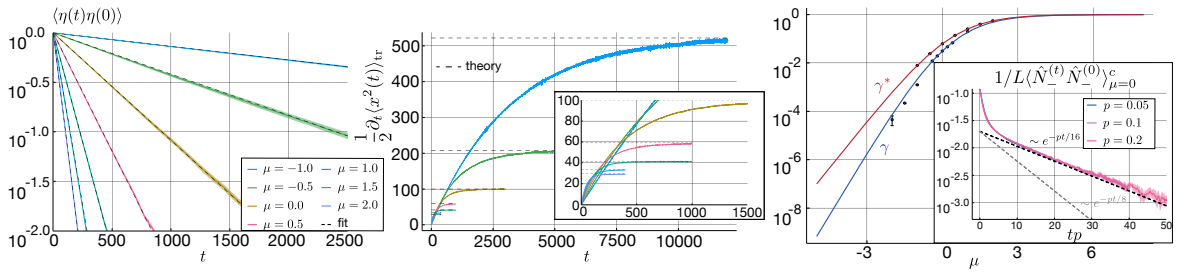

Figure 3.6. Tracer vs full dynamics. Left panel: flavor decay as a function of time for values of μ that range from $\mu = -1.0$ to $\mu = 2.0$ with steps of size $\Delta\mu = 0.5$ with $p = 0.02$. Black dashed lines correspond to best fits. Middle panel: derivative of tracer variance as a function of time along with theory predictions for the self-diffusion constant $\mathcal{D}^*$ shown in black dashed lines. Inset shows a zoom over the region of $\mu > 0$. Right panel: flavor decay rate γ^* and correlator decay rate (at the longest time scales) γ vs μ, including numerical data points extracted from a blind fit. Inset shows the scaling collapse in the large t limit at $\mu = 0$ along with a fit with the conjectured decay rate $\gamma = 1/16$. Also shown for comparision the corresponding flavor decay rate $\gamma^* = 1/8$.

$\langle x^2(t)\rangle_{\rm tr} \equiv \int x^2\omega(x,t) \asymp 2\mathcal{D}^* t$, where $\asymp$ denotes the scaling limit $p \to 0^+$, $t \to \infty$, pt fixed. To determine $\mathcal{D}^*$ we use the following standard formula for a Brownian particle $2\mathcal{D}^* = l^2/\tau^*$ with l the mean-free path and τ^* the tracer's lifetime. Plugging in $l = v\tau^*$, with v the tracer's velocity whose expression is $v = \frac{(1+e^{\mu})}{(3+e^{\mu})}$ [GHKV18b] and $\tau^* = 1/p\gamma^*$ we find

$$\mathcal{D}^* = \frac{1}{2}v^2\tau^* = \frac{(1+e^{\mu})^4}{e^{3\mu}(3+e^{\mu})}\frac{1}{2p}. \tag{3.11}$$

The results for the self-diffusion constant are shown in Fig. 3.5, and Fig. 3.6 indicating very good agreement with the formula (3.11).

3.2.4 Transport in the noisy Rule 54

Having argued the presence of diffusive dynamics at the level of tracer dynamics, we now briefly discuss transport properties. Using the Kubo formula, we are interested in the two-point function of currents $G_{+,+}(t) = 1/L\langle \hat{J}_+^{(t)}\hat{J}_+^{(0)}\rangle^c$. Recall that in the integrable limit the currents correspond just to the imbalance $\hat{N}_-$, and are thus

conserved. The effects of integrability breaking are already encoded in the temporal evolution of $\hat{N}_-$, which will be the main object of study in what follows [the full current is given locally as $\hat{j}_{+,x+1/2} = (\mathbb{1} - 2p\hat{\Pi}_x)\hat{\rho}_{-,x+1/2}$]. To study $G_{+,+}$ we time evolve the total imbalance by one time step, which gives us

$$\hat{N}_-^{(t+1)} - \hat{N}_-^{(t)} = -2p\hat{\Pi}_-^{(t)}, \tag{3.12}$$

where $\hat{\Pi}_- \equiv \sum_i \hat{\Pi}_{-,i}$ with $\hat{\Pi}_{-,i} \equiv \hat{\Pi}_i\hat{\rho}_{-,i}$. Already this equation of motion (e.o.m.) tells us that the imbalance should decay. On general grounds, nonconserved charges are expected to decay exponentially fast with a drift consistent with FGR [TKL+18b, MRDR19, FGV20b, DBD21, LPWGV21a]. To extract the drift from here we can evaluate this e.o.m. in an ensemble with slight imbalance, where we take $\mu_R = \mu + \delta$ and $\mu_L = \mu - \delta$ with $\delta \to 0$. Alternatively, we can simply study the correlator $\langle \hat{N}_-^{(t)} \hat{N}_-^{(0)} \rangle$ at fixed $\mu_R = \mu_L \equiv \mu$. To lowest order in p we find (see A.2 for details on the derivation)

$$\frac{1}{L}\partial_t \langle \hat{N}_-^{(t)} \hat{N}_-^{(0)} \rangle = -4p \frac{e^{3\mu}}{(1+e^{\mu})^3(3+e^{\mu})} + \mathcal{O}(p^2), \tag{3.13}$$

where the time derivative is taken to be discrete. Eq. (3.13) is exact up to leading order in p, and thus is analagous to FGR (3.8). However, for our noisy Rule 54 model the subleading terms $\mathcal{O}(p^2)$ cannot be disregarded, as shown in the Appendix of Ref. [LPGV22], thereby indicating a breakdown of perturbation theory in the noisy FFA, and ultimately implying a breakdown of FGR in our setup. More precisely, the terms $\mathcal{O}(p^2)$ involve sums over time of correlators which approach a constant at long times. The presence of such a "Drude weight" in those correlators imply that the higher-order terms actually scale with time, and cannot be neglected at long times even if $p \ll 1$. A possible way to interpret this result is that Rule 54 fails to equilibrate on its own. The lack of a dephasing mechanism in the model is what prevents from

truncating the series expansion to leading order in the perturbation coupling p. In the Appendix of Ref. [LPGV22] we indeed show by computing explicitly the second order corrections (as well as the third order corrections) that they grow in time as $\mathcal{O}(t^2)$ ($\mathcal{O}(t^3)$), thereby invalidating any perturbative analysis in the vein of FGR. One can show however that a proper resummation of the perturbative series reveals the following scaling form of the two-point function for the currents (see Ref. [LPGV22])

$$G_{+,+}(t) \asymp F(pt), \tag{3.14}$$

with F a function characterizing transport that would be interesting to characterize in future work. While the function F decays exponentially for $pt \gg 1$, we emphasize that the diffusion constant depends on the whole scaling function F, and not on a single decay rate. Properly characterizing this function would likely involve understanding the decay of all the other conserved quantities of Rule 54, even if those decouple from its hydrodynamics in the integrable case.

3.3 Backscattering in the hard-rod gas

The specific backscattering mechanism in Rule 54 made the analysis of transport very challenging. To simplify the analysis further, we consider here backscattering in the hard-rod gas model. As in the Rule 54, backscattering here reverts the momentum of particles. A further motivation for studying this model is that most integrable models we know of can be mapped to *generalized* hard-rod gases, so our conclusions directly generalize to other models [DYC18]. We remark that, just as in the Rule 54 model, backscattering – corresponding to large momentum transfer, is outside the types of integrability-breaking perturbations considered in the existing literature. This is because the current framework for dealing with integrability-breaking perturbations is built on the *form-factor* expansion formalism, which is a system-

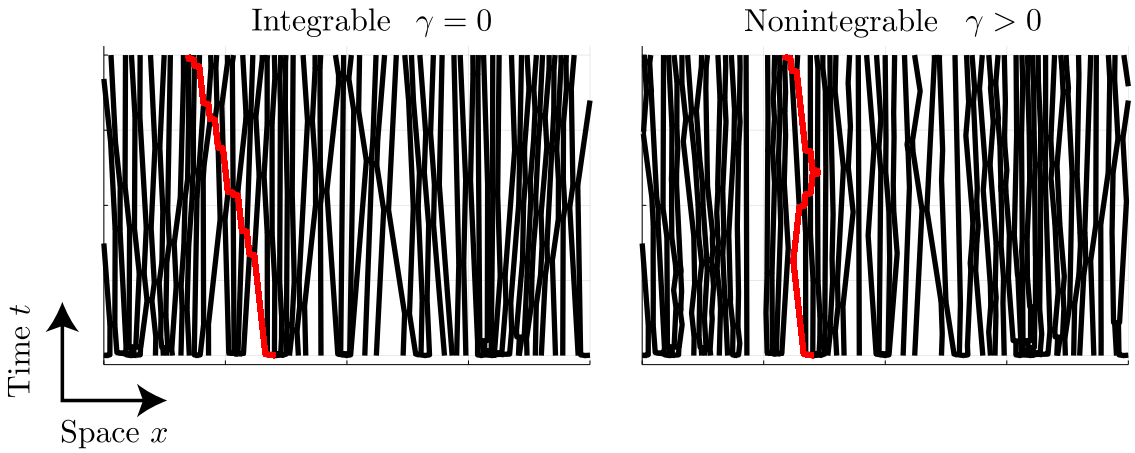

Figure 3.7. Snapshots of the dynamics of hard-rods. Left panel: integrable limit. Right panel: nonintegrable dynamics with backscattering at a rate $\gamma > 0$. In red, trajectories of quasiparticles. In the integrable limit, the velocity of quasiparticles gets renormalized as a result of collisions with other quasiparticles. Same initial conditions in both panels.

atic approach for dealing with perturbations that exert low-momenta transfer on the quasiparticles.

Stochastic backscattering leads to decay of infinitely many conserved charges, including momentum, but also preserves infinitely many residual conserved quantities corresponding to even moments of the velocity distribution of the gas. The resulting model thus displays features of both integrable and chaotic dynamics. In Fig. 3.7 we show snapshots of what the dynamics of the hard-rod gas looks like at the integrable point, as well as in the presence of noisy backscattering.

Hard-rod gas with stochastic backscattering — The one-dimensional hard-rod gas is an integrable model that can be best understood as a set of classical particles subject to a hard-core repulsive potential

$$\mathcal{H}_0 = \sum_{j=1}^{N} \frac{p_j^2}{2} + \sum_{j<k} U(x_j - x_k), \quad U(\delta x) = \begin{cases} 0, & |\delta x| > a, \\ \infty, & |\delta x| \leq a, \end{cases} \tag{3.15}$$

where a denotes the rods' length, and x_j and p_j denote positions and momenta (setting mass $m = 1$). Starting from a configuration with $x_{j+1} - x_j \geq a$, the rods evolve freely until they encounter another rod, $x_{j+1} - x_j = a$, at which point the two rods exchange velocity instantaneously. Because of the simple kinematics of such elastic collisions, the full distribution of velocities (or momenta) is conserved by the evolution and the model is thus integrable. Quasiparticles can be defined by tagging rods with fixed momenta (see Fig. 3.7). Quasiparticles are displaced by an amount a after each collision, so that they move with an effective velocity that depends on the density of all other rods with different momenta. The large-scale, coarse-grained dynamics of hard-rods is described by a Boltzmann-type equation for the phase-space density $\rho_k(x,t) = \frac{d^2N}{dxdk}$ given as [Per69, BDS83, DS17b]

$$\partial_t \rho + \partial_x (v^{\text{eff}} \rho) = 0, \; v_k^{\text{eff}}[\rho] = k + \frac{a \int_{k'} (k - k') \rho_{k'}(x,t)}{1 - a \int_{k'} \rho_{k'}(x,t)}. \tag{3.16}$$

This kinetic equation can also be interpreted as an Euler-scale GHD equation for the hard-rod gas [CADY16b, BCDNF16, DS17b]. There are diffusive corrections to this equation, due to the randomness of the scattering shifts arising from thermal fluctuations of the initial state [LPS68, Spo82, BS97, DS17b, DNBD18, GHKV18b, DNBD19]; in what follows we will ignore those as they are subleading in the limit of weak integrability breaking [FGV20b]. The integrability of the model can be seen from the infinite set of conservation laws (as $N \to \infty$) corresponding to the various moments w.r.t. the velocities, with charge densities $q_n = \int k^n \rho$.

We then introduce an integrability-breaking perturbation in the following way: with rate γ, we stochastically backscatter rods by flipping the sign of their velocity. This perturbation converts right-moving rods into left-moving ones, and *vice-versa*. Clearly, this perturbation leads to momentum relaxation, and breaks the conservation of all *odd* moments q_{2n+1} of the velocity distribution. On the other hand, all even charges q_{2n} remain conserved: in other words, the odd part of the velocity distribution

decays, while the even part remains conserved. Any even velocity distribution is an equilibrium steady-state under this perturbation.

Generalized Boltzmann equation — In the presence of an integrability breaking perturbation, such as backscattering noise, eq. (3.16) acquires a right hand side, captured by a collision integral $\mathcal{I}_k[\rho]$. In what follows we shall be interested in the linear response regime, so we write $\rho_k(x,t) \to \rho_k^* + \delta\rho_k(x,t)$, such that the stationary state, ρ^*, is an even function of momentum and uniform in space (the latter condition follows from eq. (3.16) subject to $\partial_t \rho^* = 0$), $\rho_k^* = nf(k)$, with n the density of particles and f an even function. In this regime the resulting linearized Boltzmann equation reads [FGV20b]

$$\partial_t \delta\rho + A\partial_x \delta\rho = -\Gamma\delta\rho, \tag{3.17}$$

where A and Γ are hydrodynamic matrices that act on velocity space, with $\Gamma_{k,q} \equiv -\delta\mathcal{I}_k/\delta\rho_q|_{\rho=\rho^*}$. The matrix A follows from linearizing (3.16), and reads [DS17b] $A = R^{-1}v^{\text{eff}}R$, with $v_k^{\text{eff}} = v_k^{\text{eff}}[\rho^*]$, $R = 1 - \theta^* T$ and $\theta^* = (1-an)^{-1}\rho^*$ an effective occupation number, and the kernel T acts as follows on a test velocity function $(T\psi)_k = -a\int dk' \psi_{k'}$. All matrix operations in those expressions act on velocity space. The operator Γ contains the decay rates of the different conserved modes in the original integrable model. Residual conserved quantities thus correspond to zero modes of Γ. In the case of backscattering noise, we have $(\Gamma\psi)_k = \gamma(\psi_k - \psi_{-k})$. As expected, this perturbation breaks the conservation of odd charges, while preserving the remaining ones. Thus the resulting model is of a new kind, where the system is neither fully chaotic nor integrable: in the following we will show that transport is entirely diffusive, despite the existence of infinitely-many conservation laws. The observable of interest will be the diffusion constant of conserved modes. Since the system under consideration has infinitely-many conserved charges, the resulting diffusion constant will be an infinite dimensional matrix. To derive an expression for this, one can project Eq. (3.17) onto decaying and conserved modes. The matrix

A will mix all modes, so the task is to solve the resulting system of equations. To leading order in a gradient expansion, one can show (see Sec. B) that the diffusion matrix reads (see also [FGV20b, DBD21])

$$\mathcal{D} = \bar{P}A(P\Gamma P)^{-1}A\bar{P}, \tag{3.18}$$

where P projects onto the subspace of nonconserved modes, and $\bar{P}$ onto its complementary, i.e. onto the subspace of conserved modes.

Non-interacting limit — To gain some intuition on the problem at hand, we first solve the simple limit of free rods (*i.e.* $a = 0$). Intuitively, in that limit each rod is simply undergoing a random walk with mean free path $v_k/(2\gamma)$. In that limit we have $A_{k,k'} = v_k\delta(k - k')$ with $v_k = k$, *i.e.* the velocity of rods in the absence of interactions. The linearized Boltzmann equation simply couples the $(k, -k)$ modes

$$\begin{pmatrix} \partial_t + v_k\partial_x + \gamma & -\gamma \\ -\gamma & \partial_t - v_k\partial_x + \gamma \end{pmatrix} \begin{pmatrix} \delta\rho_k \\ \delta\rho_{-k} \end{pmatrix} = \begin{pmatrix} 0 \\ 0 \end{pmatrix}. \tag{3.19}$$

Going to Fourier space (ω, q), this reveals two eigenvalues at low energy: $\omega_q = -i2\gamma + \mathcal{O}(q^2)$ corresponding to the decaying mode $\delta\rho_k^- \equiv \delta\rho_k - \delta\rho_{-k}$, and $\omega_q = -i\mathcal{D}q^2 + \mathcal{O}(q^4)$, with $\mathcal{D} = v_k^2/(2\gamma)$, corresponding to the diffusive mode $\delta\rho_k^+ \equiv \delta\rho_k + \delta\rho_{-k}$. Similar equations have been discussed, *e.g.*, in the context of the hydrodynamics of stochastic conformal field theories (CFTs) [BD17]. Away from the free particle limit, the diffusive modes no longer correspond to this particular combination, as the A matrix will connect modes of different velocities k. To solve the hard-rod problem with backscattering we take a step back and solve the limit when there are only a discrete number of velocities, in which case A becomes a finite dimensional matrix.

Discrete velocity distribution — To analyze the case of discrete number of particles it suffices to analyze the case of only two particle species (a more detailed

analysis may be found in the Appendix C). Consider a background state given by velocities in the set $\{\pm v_1, \pm v_2\}$, and their respective probabilities $\{\frac{p_1}{2}, \frac{p_2}{2}\}$ with $p_1 + p_2 = 1$. We can write down an exact expression for the discrete version of the hydrodynamic matrices above. These read $T = -aJ_4$, $\Gamma = \gamma\Gamma_1 \oplus \Gamma_2$, with J_4 the 4×4 matrix of all ones, and $\Gamma_i = \begin{pmatrix} 1 & -1 \\ -1 & 1 \end{pmatrix}$, where the subindex i refers to the subspace of velocities $\{\pm v_i\}$. The noise matrix Γ_i is diagonalized with the matrix $O_i = \begin{pmatrix} 1 & 1 \\ 1 & -1 \end{pmatrix}$ revealing a zero mode corresponding to $\delta\rho_i^+ = \delta\rho_i^R + \delta\rho_i^L$, with $\delta\rho_i^{R/L}$ denoting the density of particles (above the background state) moving with velocity $\pm v_i$, respectively. There is also a decaying mode, corresponding to $\delta\rho_i^- = \delta\rho_i^R - \delta\rho_i^L$. Note that contrary to the non-interacting case, these *are not* normal modes of the hydrodynamic equations, since they do not diagonalize the velocity matrix A. The diffusion matrix is thus given as

$$\mathcal{D}_{i,j} = \sum_k A_{(+,i),(-,k)} \Gamma^{-1}_{(-,k),(-,k)} A_{(-,k),(+,j)}, \tag{3.20}$$

where the different matrices are written in the basis of $\pm$ modes (i.e. the matrix A results from a rotation by $O = O_1 \oplus O_2$). The resulting diffusion matrix is off-diagonal, where some of these elements may be negative (see Appendix C). However, the matrix has strictly positive eigenvalues given by

$$\mathcal{D}_i = \frac{(v_i^{\text{eff}})^2}{2\gamma}, \; v_i^{\text{eff}} = \frac{v_i}{1 - an}, \; i = 1, 2. \tag{3.21}$$

Thus, the diffusion constant of the long-lived modes of the model, which are different from the conserved modes ρ_i^+ since the diffusion matrix is not diagonal (in contrast to the free particle case discussed above), is solely determined by the effective velocity of the original modes (in the integrable limit) and by the backscattering rate. This

formula is also consistent with previous findings in the Rule 54 cellular automaton [LPGV22], and is analogous to the free particle case discussed above when replacing the velocities by their renormalized counterparts. This result is fairly intuitive: backscattering acts simply on the effective quasiparticles of the interacting model, so the mean-free path is set by the *effective* velocity instead of the bare one; we will come back to this intuition below.

We focus now on the structure factor of the density of particles which is the observable of interest, giving us access to diffusion constant and a.c. conductivities. This reads $S(x,t) = \langle \delta\rho(x,t)\delta\rho(0,0)\rangle_c$, with $\delta\rho = \delta\rho_1^+ + \delta\rho_2^+$ and the label c refers to the connected part of the correlator. With the aid of the eigenvector matrix that diagonalizes $\mathcal{D}$ given by W with components $W_{i,i} = 1 - anp_i$, $W_{i,j\neq i} = -anp_i$, and the equilibrium charge fluctuation matrix $C = \langle \delta\rho\delta\rho\rangle = R^{-1}\rho^* R^T$ in the eigenmode basis, we can compute the structure factor matrix for the conserved modes $S_{i,j}(x,t) = \langle \delta\rho_i^+(x,t)\delta\rho_j^+(0,0)\rangle_c$. The exact expressions for these may be found in the Appendix C. The rod density structure factor is then given as $S(x,t) = \sum_{i,j} S_{i,j}(x,t)$, and we find the simple expression

$$S(x,t) = n(1-an)^2\langle g(x, 2\mathcal{D}_i t)\rangle, \tag{3.22}$$

where $\langle\cdot\rangle = \sum_i p_i \cdot$ and $g(x,\sigma^2) = \frac{e^{-\frac{x^2}{2\sigma^2}}}{\sqrt{2\pi\sigma^2}}$. This expression is also consistent with the sum rule $\int dx S(x,t) = \sum_{i,j} C_{i,j}$. In Fig. 3.8 we present the results from simulating numerically the hard-rod gas where rods take in velocities $v_1 = 1$, $v_2 = 1/2$ with probabilities $p_1 = p_2 = 1/2$. The parameters used in the simulation are: backscattering rate $\gamma = 0.005$, system size $2L = 20$, number of hard-rods $N = 400$, and hard-rod length $a = 0.01$. We use periodic boundary conditions (pbc), and subtract off initial fluctuations due to finite size effects. For comparison we also present the results from the free theory predictions, corresponding to the limit $a \to 0$, showing that the dynamics is both chaotic and interacting. The small discrepancies from the

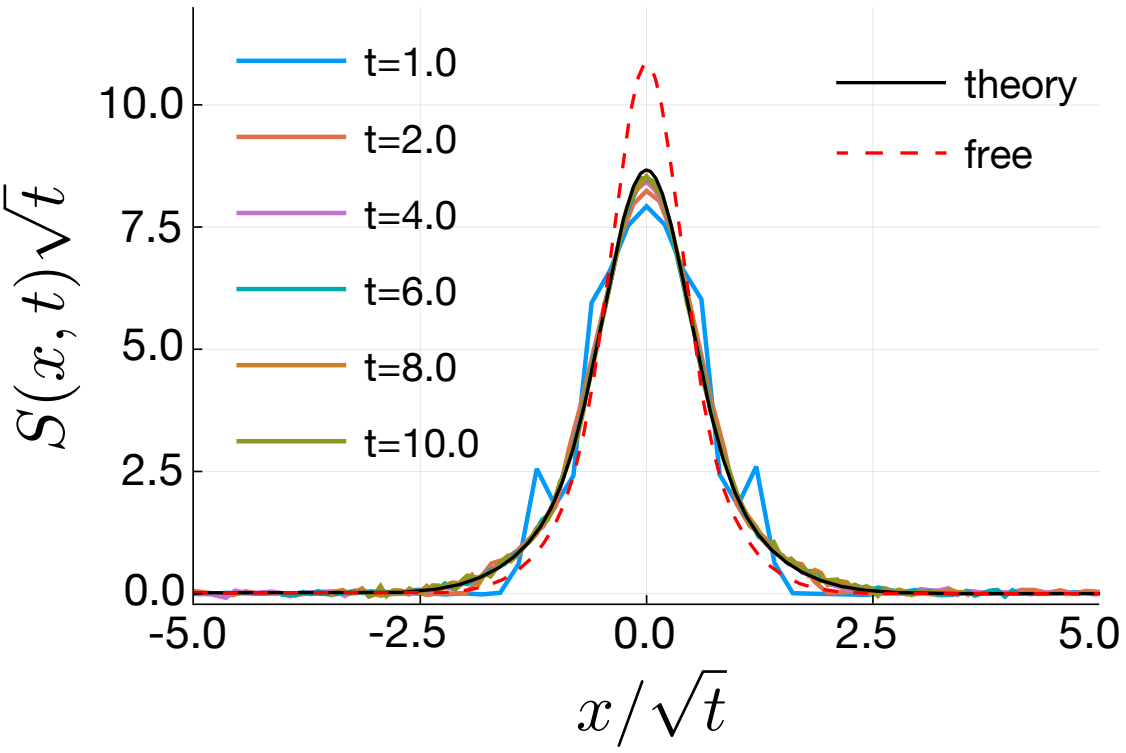

Figure 3.8. Structure factor(discrete case). The background state is given by a uniform superposition of states with velocities $v_1 = 1$, $v_2 = 1/2$ (and $p_1 = p_2 = 1/2$). The theory predictions follow Eq. (3.22) with the respective diffusion constants $\mathcal{D}_1$, $\mathcal{D}_2$. For comparison we also show the free theory results, corresponding to the $a \to 0$.

theory predictions are the result of the dynamics not having fully thermalized on the timescales of the simulation.

General case— When the spectrum of velocities is continuous, for instance, given by a Gaussian packet centered around $k = 0$, the approach taken for a discrete spectrum is still helpful. Indeed it is straightforward to extend the previous analysis to the case of an arbitrary discrete spectrum of velocities by induction from the studied case of two particle species – see Appendix C. In particular, the diffusion constant of each of the hydrodynamic modes in the presence of backscattering will be given by Eq. (3.21). This result still carries over to the continuum.

The tractability of this problem can be understood in terms of the simple action of the backscattering perturbation in terms of the normal modes of GHD, that is, the

modes $\delta\tilde{\rho} = R\delta\rho$ that diagonalize the matrix A. Formally, the problem is dramatically simplified by the fact that $[R, \Gamma] = 0$, where $R = 1 - \theta^* T$ is the matrix that diagonalizes A (whose eigenvalues correspond to the effective velocities). The physical meaning of this constraint is that effectively, backscattering noise acts simply on the quasiparticles dressed by interactions. In that basis, the Boltzmann equation (3.17) now reads

$$\partial_t \delta\tilde{\rho}_k + v_k^{\text{eff}} \delta\tilde{\rho}_k = -\gamma(\delta\tilde{\rho}_k - \delta\tilde{\rho}_{-k}), \tag{3.23}$$

where $\delta\tilde{\rho}_k \equiv (R\delta\rho)_k$ and $v_k^{\text{eff}} = v_k^{\text{eff}}[\rho^*]$. We note that this simplification occurs only if the backscattering rate is velocity independent, since $(T\gamma)_k \neq (\gamma T)_k$ in general. Further, the requirement that $(R\delta\rho)_{-k} = \delta\tilde{\rho}_{-k}$ follows from the equilibrium occupation number being an even function $\theta_k^* = \theta_{-k}^*$ (as it should in equilibrium), and from the symmetry of the scattering kernel $T_{k,-k'} = T_{-k,k'}$. The generalized Boltzmann equation (3.23) is a direct generalization of eq. (3.17) in the presence of interactions, where the effective velocities are now dressed by the effects of interactions. The problem therefore reduces to the non-interacting one (3.19): backscattering leads to a 2×2 problem in the $(k, -k)$ basis of GHD normal modes. The residual hydrodynamic modes $\delta\tilde{\rho}_k^+ \equiv \delta\tilde{\rho}_k + \delta\tilde{\rho}_{-k}$ satisfy

$$(\partial_t^2 + 2\gamma\partial_t - (v_k^{\text{eff}})^2 \partial_x^2)\delta\tilde{\rho}_k^+ = 0, \tag{3.24}$$

which exhibits a crossover from ballistic transport at short times ($\gamma t \ll 1$), to diffusive transport with diffusion constant $\mathcal{D}_k = (v_k^{\text{eff}})^2/2\gamma$ at long times ($\gamma t \gg 1$). Diffusion is induced by the decay of the nonconserved charges ('$-$' modes) with decay rate 2γ.

Anomalous structure factor— Focusing on in the long time limit of the conserved modes, the resulting structure factor follows from that in Eq. (3.22), with $np_i \to \rho_k^*$ the hard-rod phase space density at equilibrium. Taking $\rho_k^* = np(k)$ with

$p(k)$ a Gaussian (thermal) velocity distribution centered at 0 and with variance σ^2, the rod density structure factor reads

$$S(x,t) = \frac{n(1-an)^3}{\pi\sigma}\sqrt{\frac{\gamma}{t}}K_0\left(\frac{1-an}{\sigma}\sqrt{\frac{\gamma}{t}}|x|\right), \tag{3.25}$$

with $K_0(x) = \int_0^\infty \mathrm{e}^{-|x|\cosh t}dt$ the modified Bessel of second kind. In Fig. 3.9 we compare the theory predictions with the numerical results showing excellent agreement. We trace back this singular behavior to the presence of infinitely many conserved charges, each with a different diffusion constant, conspiring to produce a profile that is evidently nongaussian. In particular, the structure factor shows a singularity of logarithmic nature at the origin independently of the rods' length, following from $K_0(ax) \underset{x\to 0}{=} -\gamma_{\text{Euler}} - \log(ax/2) + \mathcal{O}(x^2\log x)$, $a > 0$, with γ_{Euler} Euler's constant. This implies that the *return probability* (structure factor near the origin) is *anomalous*, with a logarithmic correction to the expected diffusive behavior

$$S(x \approx 0, t) \sim \frac{\log t}{\sqrt{t}}, \tag{3.26}$$

which we also observe in numerical simulations (Fig. 3.9). The effective diffusion constant of hard-rods in this limit is found as $\mathcal{D} = \frac{1}{2t}\int dx x^2 S(x,t)$ which yields $\mathcal{D} = n\sigma^2/2\gamma$, independently of the rods' length.

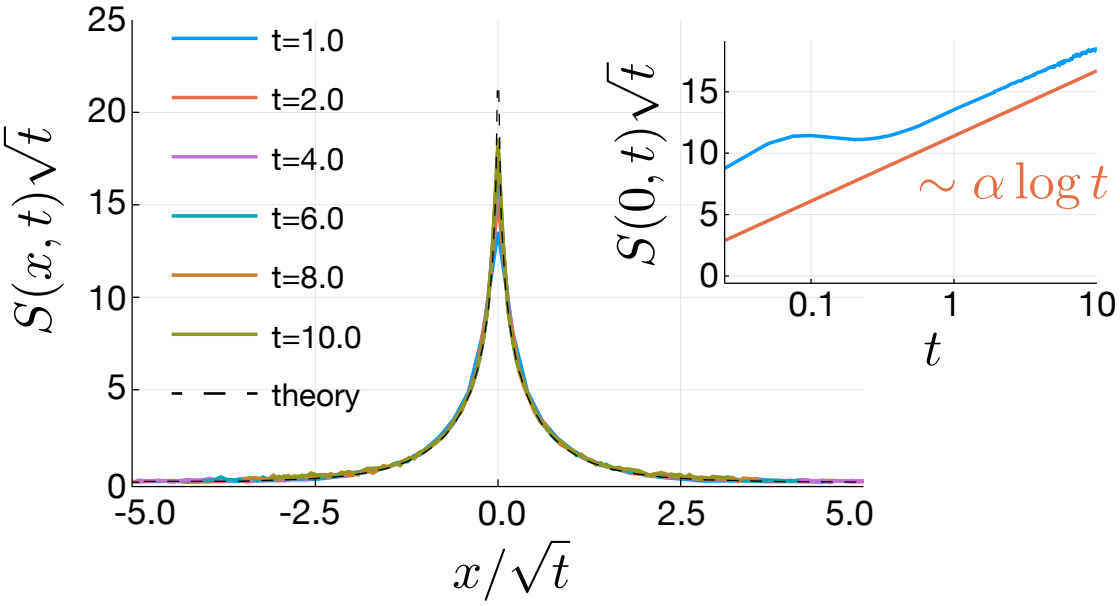

Figure 3.9. Anomalous structure factor. The background state is given by a a Gaussian (thermal) velocity distribution centered at 0 and variance σ^2. The theory predictions follow Eq. (3.25). Inset: scaling of structure factor at $x = 0$ (return probability) along with theory predictions (ignoring an offset for visual purposes), where $\alpha = n(1 - an)^3/2\pi\sigma$, follows also from Eq. (3.25).

CHAPTER 4

OPERATOR SPREADING IN CHAOTIC *VS.* INTEGRABLE MODELS

In this last Chapter we discuss operator spreading in both chaotic and integrable systems. Our aim here is to uncover any possible fingerprints that would allow us to distinguish these two classes of many-body systems. While both chaotic and integrable systems have operator operator fronts that broaden diffusively [1], albeit as a result of different mechanisms, as shown in [NVH18b, vKRPS18a, RPvK18a, KVH18a, GHKV18a] there are yet more subtle differences between the two. We find that while chaotic systems have purely gaussian operator fronts, the height of the operator front in integrable systems decays anomalously, at least within the times accessed by our matrix product based numerical simulations. This scaling is explained using a quasiparticle picture. Further, by fixing a *finite* bond dimension in our numerical simulations we find that chaotic systems are prone to dramatic numerical errors at and near the front, which makes these systems very hard to simulate. This is at variance with previous works that claimed chaotic systems may be easy to simulate near the front. We reconcile our numerical results with these works by a proper identification of the front. This work is based on Ref. [LPWGV21b].

[1] One can think of an operator front as follows: for any initially local operator $\mathcal{O}_0$, upon time evolution this operator becomes a complex superposition of Pauli strings (thinking of spin-1/2 systems for simplicity). The operator front measures the *weight* of the longest strings on this time evolved operator (see also Sec. 4.1.1).

4.1 Operator Right-weight, matrix product operators and truncation errors

In this Section, we introduce our main quantity of interest, the operator *right-weight*, and explain how it can be computed numerically using MPOs. We also address the effects of truncation errors.

4.1.1 Operator right-weight

Consider the spreading of an initially local operator $\mathcal{O}_0 \equiv \mathcal{O}(x=0)$ under Heisenberg time evolution. Under time evolution, this operator will grow into a more complicated one $\mathcal{O}(t) = [U(t)]^\dagger \mathcal{O}_0 U(t)$ being a superposition of many *strings* made of products of non-trivial local operators. A way to characterize the complexity of this object is by means of the OTOC. Consider another local operator at site x, $\mathcal{V}_x$. The OTOC is defined as the squared of the commutator between these two operators $\mathcal{C}(x,t) \equiv ||[\mathcal{O}(t), \mathcal{V}_x]||^2 = 2\left(1 - \mathrm{Re}(\mathrm{tr}[\mathcal{O}(t)^\dagger \mathcal{V}_x^\dagger \mathcal{O}(t) \mathcal{V}_x])\right)$. The shape of the OTOC shares universal features across generic systems including ballistic spreading of the wavefront, a rapid growth ahead of the wavefront and saturation behind the wavefront at late times. These features are showcased in Fig. 4.1 for the integrable XXZ model.

To characterize the size of an initially local operator $\mathcal{O}_0$ under Heisenberg evolution consider instead the decomposition

$$\mathcal{O}(t) = \sum_{\mathcal{S}} a_{\mathcal{S}}(t) \mathcal{S}, \tag{4.1}$$

where the sum above goes over all possible string operators (Pauli strings in the case of spin-1/2 operators). A complete understanding of operator spreading can be captured by the set of coefficients $\{a_{\mathcal{S}}(t)\}$, a task which is out of reach. Instead, we are

interested in coarse-grained quantities relating these coefficients. One such quantity is the *right-weight*. For a given operator $\mathcal{O}(t)$ it reads [NVH18b, VKRPS18b]:

$$\rho_R(j,t) = \sum_{\substack{\text{strings w/}\\ \text{rightmost}\\ \text{non-identity}\\ \text{on site j}}} |a_{\mathcal{S}}(t)|^2. \tag{4.2}$$

The coefficients $a_{\mathcal{S}}(t)$ appearing in the expression can be obtained exploiting the fact that these strings form an orthogonal basis in a Hilbert space of dimension $\mathcal{D}^2$: $a_{\mathcal{S}}(t) = \mathrm{tr}\left[\mathcal{S}^\dagger \mathcal{O}(t)\right]/\mathcal{D}$. (Here $\mathcal{D}$ is the Hilbert space dimension of states; i.e. $\mathcal{D} = 2^L$ for spin-1/2 chains). We require the initial operator to be normalized, i.e. $\mathrm{tr}\left[\mathcal{O}_0^\dagger \mathcal{O}_0\right]/\mathcal{D} = 1$, which implies (using unitarity) the sum rule: $\sum_{\mathcal{S}} |a_{\mathcal{S}}(t)|^2 = 1$. Note that by construction we also have $\sum_j \rho_R(j,t) = 1$. This conservation law has important consequences for the "hydrodynamics" of operator spreading in both integrable and non-integrable systems. On general grounds, we expect the associated current to behave as $j = v_B \rho_R - D\partial_x \rho_R + \ldots$, where v_B is the butterfly velocity characterizing the speed of the ballistically moving operator front, D is a diffusion constant that sets the generic diffusive broadening of the front, and the dots represent nonlinear and higher-derivative terms. In what follows we shall focus on spin-1/2 chains, both integrable and chaotic.

4.1.2 Matrix product operators

In order to measure the right-weight numerically, we use matrix product operator (MPO) techniques. For this purpose, we express Eq. (4.1) as a state in the Hilbert space of operators as is routinely done in the context of time evolution of MPOs [PKS+19], so that $\mathcal{O}(t) \to |\mathcal{O}(t)\rangle\!\rangle \equiv \sum_{\mathcal{S}} a_{\mathcal{S}}(t)|\mathcal{S}\rangle\!\rangle$. To evaluate the right-weight as a correlator, we introduce the projector onto the identity acting on site x, $\mathcal{P}_{\mathbb{1},x}$ (i.e. $\mathcal{P}_{\mathbb{1},x} \equiv |\mathbb{1}\rangle\!\rangle_x \langle\!\langle \mathbb{1}|_x)$, where $|\mathbb{1}\rangle\!\rangle \equiv \otimes_{x=1}^{L} \left(|00\rangle_x + |11\rangle_x\right)/\sqrt{2}$. We reserve odd entries of any MPS in this newly enlarged Hilbert space for the *physical* sites, and the even sites

for the *ancilla* sites[PKS+19]. It is then straightforward to show that the right-weight can be computed as follows

$$\rho_R(x,t) = \frac{\partial}{\partial x} \langle\langle \mathcal{O}(t)| \prod_{x' \geq x} \mathcal{P}_{\mathbb{1},x'} |\mathcal{O}(t)\rangle\rangle, \tag{4.3}$$

where ∂_x should be interpreted as a discrete spatial derivative.

We compute the right-hand side of eq. (4.3) using the TEBD algorithm (discussed in Sec. 1.2.1) applied to matrix product operators. We denote the maximum bond dimension as χ_{MAX}. Time evolution is implemented directly in operator space as $|\mathcal{O}(t)\rangle\rangle = e^{-it\mathcal{L}}|\mathcal{O}_0\rangle\rangle$ where $\mathcal{L} \equiv -H \otimes \mathbb{1} + \mathbb{1} \otimes H^T$, where the Kronecker product here is used to distinguish physical from ancilla space. In this language, standard two-point correlation functions can be computed as simple overlaps between states in this doubled Hilbert space.

In our numerical simulations, unless otherwise stated, we will be considering a system size of $L = 401$ sites, a fourth order Trotter decomposition of step size $dt = 0.1$ and a cutoff error of $\epsilon = 10^{-10}$. The system size was chosen so that the right-weight front never reaches the boundary of the system within the time scale of interest, which is $t_{\text{MAX}} \sim \mathcal{O}(10^2)$. These simulations are carried out using the C++ iTensor library [FWS20].

4.1.3 Operator front and truncation errors

In the remainder of this chapter, we will use this MPO approach to compute the right-weight in various interacting chaotic and integrable spin 1/2 chains. Before we address specific features of operator spreading in those different classes of systems, we address here the dramatic effects of truncation errors in the MPO approach. Representative plots of the right-weight and of OTOCs are shown in Fig. 4.1, for both a chaotic Ising chain, and for the integrable XXZ spin chain, using a finite bond dimension $\chi_{\text{MAX}} = 128$.

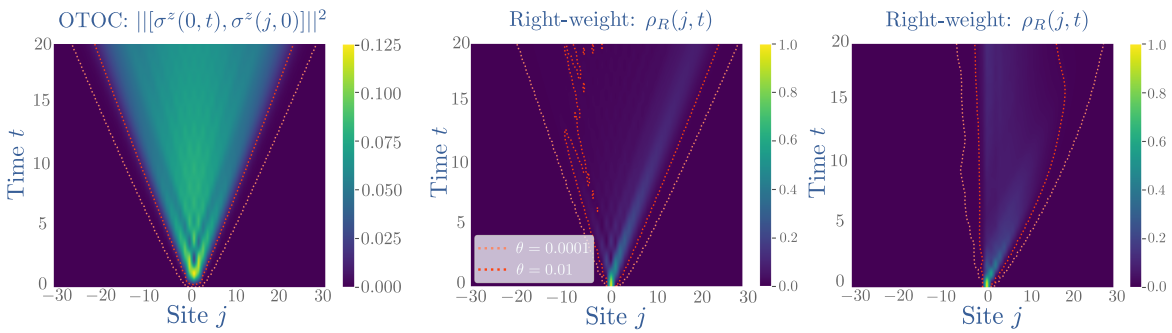

Figure 4.1. Operator spreading in integrable and chaotic spin chains starting from $\mathcal{O}_0 = \sigma_0^z$. Left panel: OTOC spatio-temporal profile in the integrable XXZ model for $\Delta = 0.5$ and $\mathcal{V}_x = \sigma_x^z$. Middle panel: right-weight profile still in the integrable XXZ model with $\Delta = 0.5$. Right panel: right-weight profile in the non-integrable *transverse-field Ising* model with $h_z = 0.9045$ and $h_x = 0.8090$. The dashed lines are contour lines following a given threshold θ. Data obtained with bond dimension $\chi_{\text{MAX}} = 128$. For integrable models, both the OTOC and the right-weight behave in a reasonable way, despite the relatively small bond dimension, but the front broadens subdiffusively because of truncation errors. In the chaotic case (right panel), the operator front disappears at finite time because of truncation errors.

For integrable chains, both the OTOC and the right-weight behave as expected, despite the finite bond dimension. However, as we will show below, some qualitative details end up being affected by the truncation errors. In particular, for finite bond dimension, we will see that the front broadens subdiffusively as t^α with $\alpha \approx 1/3$ for small bond dimensions, while we recover $\alpha = 1/2$ as $\chi_{\text{MAX}} \to \infty$. This explains the apparent $t^{1/3}$ broadening in the integrable Heisenberg chain observed in Ref.[XS20] using small bond dimension MPOs.

The effects of truncation errors on the operator front in chaotic chains are much more dramatic. As shown in the right panel of Fig. 4.1, the operator front (defined as the maximum of the right-weight, moving at the butterfly velocity v_B) fades away and disappears at short times. We will show below that this unphysical feature is entirely due to truncation errors, and can be deferred to longer times by increasing the bond dimension. Thus large bond dimensions are absolutely essential to describe the operator front correctly. In contrast, bond dimensions as low as $\chi_{\text{MAX}} = 4$ can be

enough to capture the exponentially-decaying tails of the operator front, as noted in Refs.[XS20, HPL19]. Our results are also consistent with contour lines for the OTOC being less than a given threshold ϵ being less sensitive to truncation errors for small ϵ (see dashed line in Fig. 4.1). However, as we show here, the small-ϵ contours *outside* the front are an unreliable guide to the location of the front itself (i.e., the maximum of the right-weight). In the case of integrable systems, using those tails to analyze the front broadening gives rise to incorrect results for low bond dimensions. In the following, we will carefully analyze the convergence of our results with respect to bond dimension; for practical purposes we restrict ourselves to maximal bond dimensions less than $\chi_{\mathrm{MAX}} = 512$ in most cases to access long enough times.

4.2 Operator front in integrable systems

Armed with this numerical tool, we analyze the operator front in integrable quantum systems. As in chaotic systems, we expect a ballistically moving front, broadening as $t^{1/3}$ in free systems [PK05, CDLV18, KHN18, XS20, LM18, Fag17], and $t^{1/2}$ in interacting integrable systems [GHKV18a]. In integrable systems, we expect the operator front to follow the fastest quasiparticle. For interacting integrable systems, quasiparticles behave as biased random walkers due to their random collisions with other quasiparticles [Gop18b, GHKV18a, DNBD18, GZ18, DNBD19]. In the following, we will confirm those predictions numerically, but also identify a key difference with chaotic systems. As we will show, the quasiparticle picture suggests that the peak height of the front decays anomalously as $t^{-3/4}$, at least at intermediate times, and scales with a non-Gaussian universal function that we compute exactly.

4.2.1 Free fermions

Before turning to *interacting* integrable quantum systems, we briefly recall how operators spread in spin chains dual to free fermions, following Ref.[LM18]. For

concreteness, we focus on the XX spin chain with Hamiltonian

$$H = J \sum_j S_j^x S_{j+1}^x + S_j^y S_{j+1}^y, \tag{4.4}$$

where S_j^α are spin-1/2 operators acting on site j, and $J = 1$ in the following. Let us consider the spreading of the Pauli operator σ^z of the XX model initially at site 0, that is $\mathcal{O}_0 = \sigma_0^z$. Since this Hamiltonian is Jordan-Wigner dual to free fermions, this reduces the possible Pauli strings participating in $\mathcal{O}_0(t)$. Out of the 4^L possible Pauli strings, only L^2 Pauli strings will contribute here. Indeed only the operators $\sigma_i^+ \left(\prod_{i<l<j} \sigma_l^z\right) \sigma_j^-$, σ_j^z, for general i, j, will contribute, as those are the only spin operators that map to quadratic fermions under a Jordan-Wigner transformation. The right-weight can thus be computed using standard free fermion techniques, and is given by

$$\rho_R(x,t) = [J_x(t)]^4 + 2[J_x(t)]^2 \sum_{y<x} [J_y(t)]^2, \tag{4.5}$$

were $J_x(t) \equiv 1/2\pi \int_{-\pi}^{\pi} \mathrm{e}^{-i(kx+\cos(k)t)} dk$ are Bessel functions of the first kind. As t and x become large, this yields the following scaling form for the right-weight [HRS04]

$$\rho_R(x,t) \sim \frac{1}{t^{2/3}} F\left(\frac{x-t}{t^{1/3}}\right), \tag{4.6}$$

where the butterfly velocity is $v_B = 1$, and F is some universal scaling function. This establishes that the operator front broadens subdiffusively as $t^{1/3}$ in free fermion systems.

4.2.2 Interacting integrable spin chains

We now turn our attention to operator spreading in *interacting* integrable systems. Our model of interest will be the paradigmatic spin-1/2 XXZ Hamiltonian

$$H = J \sum_j S_j^x S_{j+1}^x + S_j^y S_{j+1}^y + \Delta S_j^z S_{j+1}^z, \tag{4.7}$$

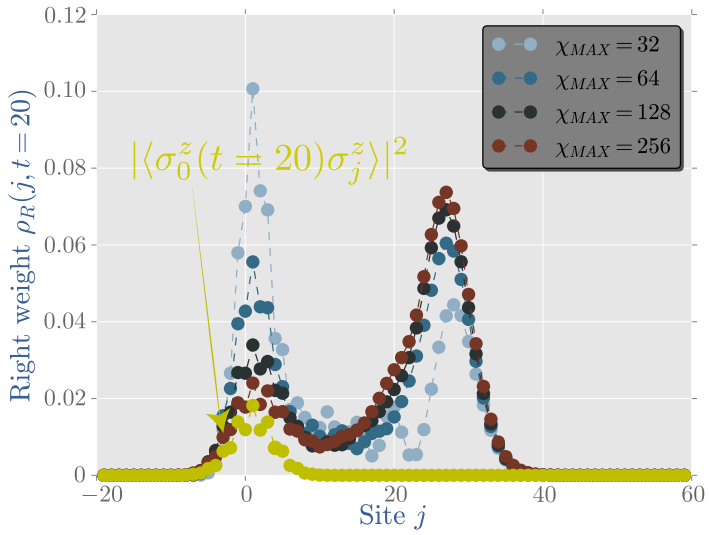

Figure 4.2. Right-weight spatial profile at $t = 20$ in the XXZ spin chain with $\Delta = 5$, and $\mathcal{O}_0 = \sigma_0^z$ for various maximum bond dimensions. The yellow data points correspond to the squared correlator $|\langle\sigma_0^z(t = 20)\sigma_j^z\rangle|^2$ at infinite temperature $\beta = 0$, which lower bounds the right-weight.

In what follows, we set $J = 1$. This model is integrable and in this sense "exactly solvable", though quantities such as OTOC or the right-weight are analytically out of reach, and have to be computed numerically.

We analyze numerically the right-weight $\rho_R(j, t)$ for various values of the anisotropy Δ. In what follows, we mostly focus on the initial operator σ_0^z, but we will also consider other operators. A typical plot of the right-weight at a given time (here $t = 20$), for $\Delta = 5$ is shown in Fig. 4.2, for different maximum bond dimensions. A few key features are worth noting. First, as already anticipated above, the operator front – corresponding to the right-moving peak in the right-weight – clearly requires large bond dimensions to be captured accurately. Second, the right-weight also shows a diffusively-spreading lump near the origin, lagging behind the operator front. This is a signature of the diffusive spin transport in this model [LŽP17]: the right-weight is lower bounded by the square of the infinite-temperature spin autocorrelation function $|\langle\sigma_j^z(t)\sigma_0^z\rangle|^2$, which is known to behave diffusively in the XXZ spin chain for

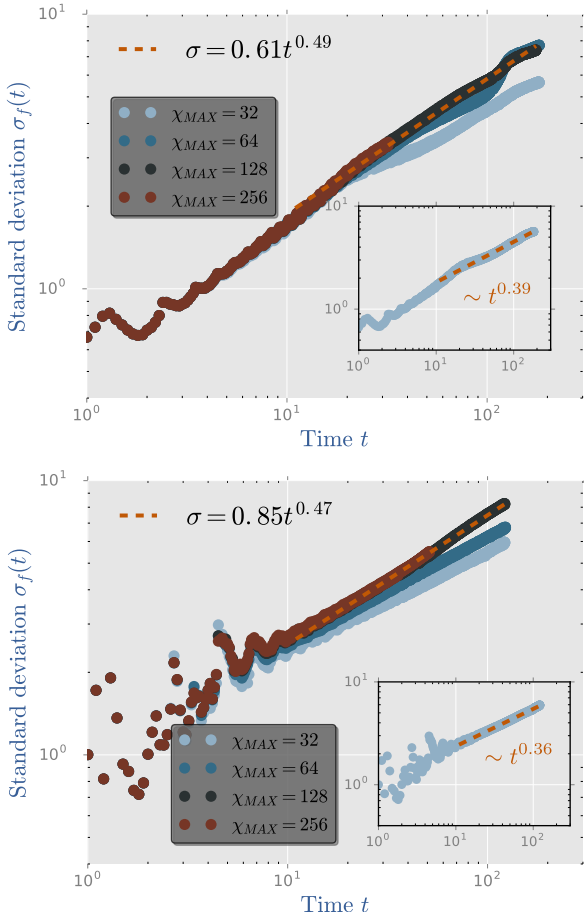

Figure 4.3. Standard deviation of the front of the right-weight versus time for various maximum bond dimensions plus a linear fit over the data for $\chi_{\mathrm{MAX}} = 128$ showing approximately diffusive spreading. Top panel: $\Delta = 1/2$ and $\mathcal{O}_0 = \sigma_0^z$. Bottom panel: $\Delta = 5$ and $\mathcal{O}_0 = \sigma_0^x$. Insets in both panels depict the standard deviation of the front for a small bond dimension $\chi_{\mathrm{MAX}} = 32$, showing that truncation errors lead to an operator front that broadens subdiffusively with an exponent close to $1/3$.

$\Delta > 1$ [LŽP17]. The effects of $U(1)$ conservation laws on operator spreading in chaotic systems was studied in Refs.[KVH18b, RPvK18b], and is qualitatively similar in the XXZ spin chain with $\Delta > 1$, as finite-temperature spin transport is diffusive in this regime [DNBD19] (see also Ref. [BHMK$^+$21]). In contrast, when $\Delta < 1$, spin transport in this system is known to be ballistic, and we do not observe a lump of right-weight near the origin (Fig. 4.1, left panel). The right-weight in this regime is still nontrivially lower-bounded by the dynamical correlation function; however, in this case the dynamical correlation function scales as $1/t$ all the way out to the light cone, so one does not expect a visible lump near the origin.

In integrable systems, we expect the operator front to coincide with the speed of the fastest quasiparticle [GHKV18a]. As a result, the butterfly velocity should depend on the density of all other quasiparticles, and thermal fluctuations naturally give rise to diffusive broadening of the front. To check this numerically, we compute the width of the operator front for an initially local operator as a function of time. By computing the standard deviation of the front of the right-weight for both $\Delta = 1/2$ and $\Delta = 5$ (Fig. 4.3), we find that the operator front does broaden as $\sigma_f \sim t^a$ with $a \sim 0.5$. As anticipated above, our results show that large bond dimensions are required to capture this diffusive broadening of the front (with bond dimensions larger than $\chi_{\text{MAX}} \sim 10^2$). Below that threshold, the results do not converge at intermediate to large times, and we find instead some apparent subdiffusive front broadening (see insets in Fig. 4.3).

An intuitive way to understand why one cannot restrict to low maximum bond dimension to study the *entire* operator front is to realize that finite bond dimension *truncations* are a non-local operation: while the tail is well-captured by a low maximum bond dimension (since this lies outside the lightcone, where the MPO is represented by lightly entangled blocks) at short enough times, the width of the front

	Free	Integrable	Chaotic
α	1/3	1/2	1/2
β	2/3	3/4	1/2

Table 4.1. Scaling exponents for generic operator fronts in quantum spin chains (for intermediate, accessible time scales). The width of the front scales as $w(t) \sim t^{\alpha}$, while the height scales as $h(t) \sim t^{-\beta}$.

is affected in a non-trivial way because of truncations deep in the light cone (see Fig. 4.2).

4.2.3 Scaling of the front and quasiparticle picture of operator spreading

At the moment, there is no theory for computing quantities like the right-weight (or the OTOCs) in interacting integrable systems. However, it is natural to expect that operator spreading should be captured by the quasiparticles of the underlying integrable model, similar to the quasiparticle picture of entanglement spreading [CC06, CC07, FC08, AC17a, AC17b, Alb18, Alb20]. Thermodynamics and hydrodynamics in integrable systems can entirely be understood in terms of quasiparticles. This is the basis of the recent framework of generalized hydrodynamics (GHD) [BCDNF16, CADY16c, Doy19]. Within a given (generalized) equilibrium state, quasiparticles with quantum number λ (called rapidity) move ballistically with a velocity v_λ, with an associated diagonal diffusion constant D_λ due to random collisions with other quasiparticles in the thermal background. Both v_λ and D_λ can be computed analytically in a given generalized equilibrium state. These quasiparticles are known control to transport properties and entanglement scaling, so it is natural to expect them to control operator spreading as well. Let us assume phenomenologically that the right-weight couples to quasiparticles propagating from the position of the initial operator in a featureless (infinite temperature) background, with an unknown weight ω_λ (normalized so that $\int d\lambda \omega_\lambda = 1$). This means that we expect the

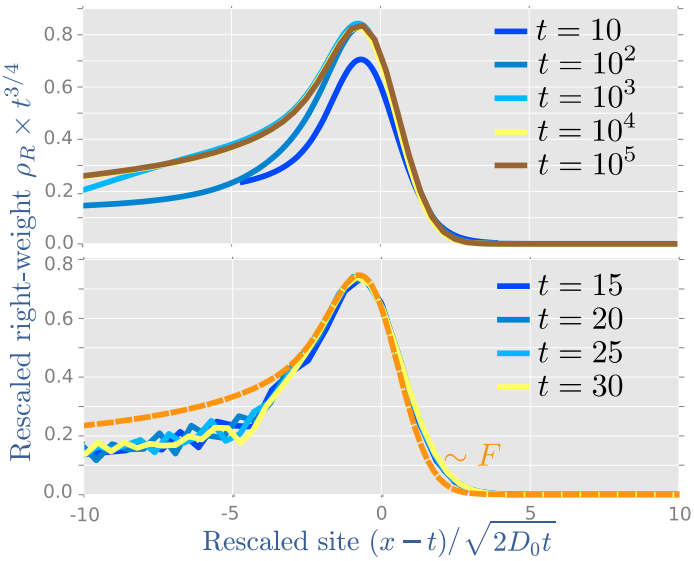

Figure 4.4. Scaling of the front for the XXZ spin chain with $\Delta = 1/2$ and $\mathcal{O}_0 = \sigma_0^z$. Top panel: collapse of right-weight from the model (4.8) for different times and asymptotic form $F(u)$. Here ω_λ was chosen to be Gaussian, though its precise form does not matter. Bottom panel: collapse of right-weight from TEBD at short times.

right-weight to be given by

$$\rho_R(x,t) \sim \int d\lambda \omega_\lambda \frac{1}{\sqrt{4\pi D_\lambda t}} e^{-\frac{(x-v_\lambda t)^2}{4D_\lambda t}}. \tag{4.8}$$

The weight ω_λ is an unknown function in general. On general grounds, we expect the operator front to be described by the fastest quasiparticle excitation in the system [GHKV18a]. This would correspond to $\omega_\lambda = \delta(\lambda - \lambda_0)$, with λ_0 the rapidity corresponding to the fastest quasiparticle, and $\rho_R(x,t) = \frac{1}{\sqrt{4\pi D_0 t}} e^{-\frac{(x-v_B t)^2}{4D_0 t}}$, with $D_0 = D_{\lambda_0}$, $v_B = v_{\lambda_0}$. This would be a Gaussian front, as in 1d chaotic systems [NVH18b, VKRPS18b](in particular the height of the front should decay as $\sim t^{-1/2}$). Our numerical data is however not consistent with this picture for the times we can access: (1) We find numerically that the speed of the front is slightly lower than v_{λ_0}, (2) The diffusion constant associated with the diffusive broadening of the front in Fig. 4.3 does not coincide with the GHD predictions for D_0, (3) The oper-

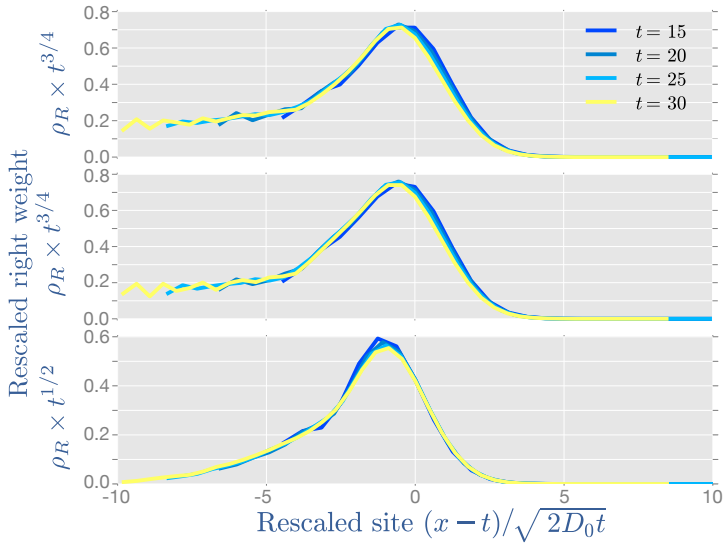

Figure 4.5. Collapse of the right-weight for various operators $\mathcal{O}_0$ for the XXZ model with $\Delta = 1/2$. Top panel: $\mathcal{O}_0$ given by the energy density on site 0. Middle panel: local charge of a non-conserved operator that couples to conserved charges $\mathcal{O}_0 = \sigma_0^+\sigma_1^- + \text{h.c.}$. Bottom panel: local charge of a non-conserved operator that does not couple to any conserved charge $\mathcal{O}_0 = \sigma_0^x$. In this last case, we find that the height of the front scales as $t^{-1/2}$.

ator front observed numerically is clearly non-Gaussian (Fig. 4.4), and in particular, its height decays as $\sim t^{-3/4}$ (instead of $\sim t^{-1/2}$).

All those observations indicate that, at least for times accessible within TEBD, the right-weight couples more generically to a continuum of quasiparticles with rapidity near λ_0. In fact, eq. (4.8) predicts a universal form for the operator front as long as ω_λ is non-zero within a finite neighborhood of λ_0. The asymptotic behavior of (4.8) at long times can then be obtained through a saddle point analysis. Expanding all quantities near the front, we have $v_\lambda = v_B - w(\lambda - \lambda_0)^2 + \ldots$, $D_\lambda = D_0 + \ldots$, and $\omega_\lambda = \omega_0 + \ldots$, where $w > 0$ since by assumption v_B is the maximum velocity. Plugging these expressions into eq. (4.8) and changing variables, we find that

$$\rho_R(x,t) \sim t^{-3/4} F\left(u\right), \tag{4.9}$$

where $u \equiv (x - v_B t)/\sqrt{2D_0 t}$, with the *universal* scaling function

$$F(u) = \int \frac{d\eta}{\sqrt{2\pi}} \mathrm{e}^{-\frac{1}{2}(u+\eta^2)^2}. \tag{4.10}$$

This intermediate-time scaling form is one of our main results. It is entirely independent of the weight ω_λ, as long as the right-weight couples to a continuum of quasiparticles with rapidity near $\lambda = \lambda_0$. The height of the operator front decays as $t^{-3/4}$ rather than decaying as $t^{-1/2}$ as in chaotic systems, with the associated non-Gaussian scaling function (4.10). In particular, we have $F(u) \sim 1/\sqrt{|u|}$ as $u \to -\infty$, indicating a fat tail behind the front that scales as $t^{-3/4} \times u^{-1/2} \sim \frac{1}{\sqrt{t}} \frac{1}{\sqrt{v_B t - x}}$.

As shown in Fig. (4.4), eq (4.8) approaches the scaling form (4.9) at long times only ($t \sim 10^4$) for generic functions ω_λ, making it challenging to observe numerically. However, we find that our TEBD data collapses very well against the scaling (4.9), even though the resulting collapse is not fully converged to the scaling function (4.10) at those times (Fig. (4.4)). Our TEBD data very clearly indicates a non-Gaussian front, with the height decaying with an exponent consistent with $t^{-3/4}$.

In Fig. 4.5 we show results of the right-weight for various choices of initial operators in the XXZ spin chain. Operators corresponding to conserved charges, such as energy, are expected to have a right-weight that scales as in (4.9). Other operators such as $\mathcal{O}_0 = \sigma_0^+ \sigma_1^- + \text{h.c.}$ are not conserved, but do couple to hydrodynamic modes (in this case energy), and thus are expected to scale as in (4.9) as well. To see this note that one may introduce the projector onto hydrodynamic modes $\mathcal{P} = \sum_{i,j} |I_i\rangle\!\rangle C^{-1}_{ij} \langle\!\langle I_j|$, where the sum goes over all pairs of conserved charges, $\{|I_i\rangle\!\rangle\}$ is the set of all conserved charges in vector form (using the notation from Sec. 4.1), and $C_{ij} = \langle\!\langle I_i | I_j \rangle\!\rangle \equiv 2^{-L} \mathrm{tr}(I_i I_j)$. Thus any operator $\mathcal{O}$ with $\mathcal{P}|\mathcal{O}\rangle\!\rangle \neq 0$ is expected to have a corresponding right-weight scaling as in (4.9) (at least for intermediate times). In comparison, the last panel in Fig. 4.5 shows the right-weight of the operator σ^x; this operator manifestly does not couple to any hydrodynamic modes as it breaks the

$U(1)$ symmetry. The behavior of this operator is quite unlike that described above: it has a Gaussian front that closely resembles what one would see in a chaotic system. In particular, the height of the front scales down as $t^{-1/2}$ rather than as $t^{-3/4}$. The anomalous scaling observed in Figs. 4.4-4.5 is stable against increasing bond dimension (data shown for $\chi_{\mathrm{MAX}} = 256$).

Our results do not settle the asymptotic late-time behavior of the right-weight in integrable systems. It seems plausible that for *generic* operators there will be some non-hydrodynamic piece (that does not couple to single quasiparticles) in addition to the hydrodynamic piece—we have no reason to expect that the coupling to single quasiparticles exhausts the operator weight. Assuming there is some such non-hydrodynamic piece, the $t^{-1/2}$ peak of the non-hydrodynamic part of the front will eventually dominate the $t^{-3/4}$ peak due to quasiparticles. We do not see any sign of this in our numerics, but we do not have access to late enough times to address this asymptotic question. Whether the quasiparticles capture *all* the operator weight, for some reason we do not yet understand, or whether there is instead a late-time crossover to a Gaussian front, is an interesting question for future work.

Table 4.1 summarizes the various scalings for the width and height of the operator weight for generic operators, in integrable, chaotic and non-interacting systems. We also note that our prediction for the operator front (4.9) in interacting integrable systems also applies to the front of standard two-point correlation functions. Linear response correlation functions admit a hydrodynamic decomposition in terms of quasiparticles as in eq. (4.8), so our argument carries over to such correlation functions. It will be interesting to check this prediction in future work.

4.3 Operator front in chaotic systems

We now briefly contrast our findings for interacting integrable systems to chaotic (non-integrable) chains. In chaotic systems, the operator front is expected to broaden

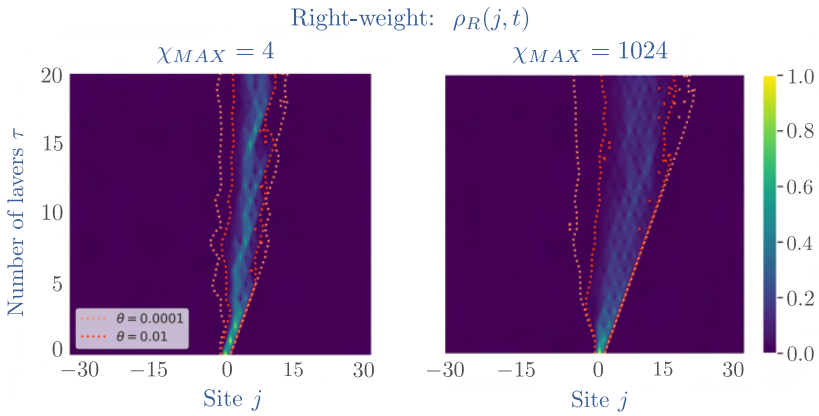

Figure 4.6. Truncation errors on the right-weight for random circuit dynamics. Here we show a single Haar random circuit realization. Left panel: $\chi_{\text{MAX}} = 4$. Right panel: $\chi_{\text{MAX}} = 1024$. The dashed lines are contour lines of the right-weight with threshold θ. For small bond dimension, the operator front slows down, and stops at finite time. This is an artifact of truncation errors, that can be postponed to longer times by increasing the bond dimension.

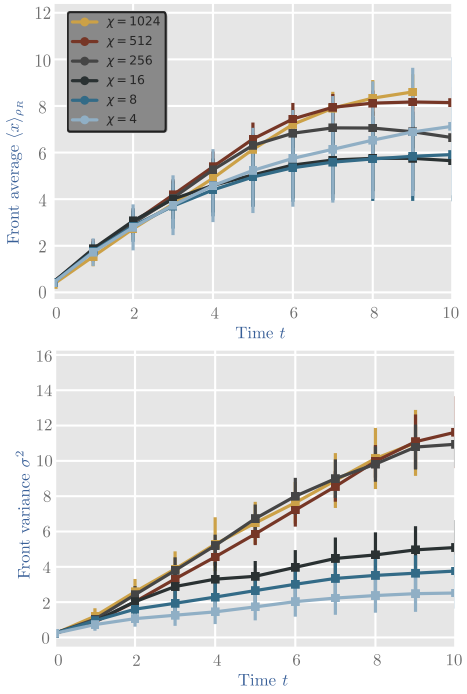

Figure 4.7. Slow-down in operator spreading due to truncation errors. Top panel: average front position vs time averaged over different circuit realizations and for various maximum bond dimensions χ_{MAX}. Bottom panel: same but for the front variance.

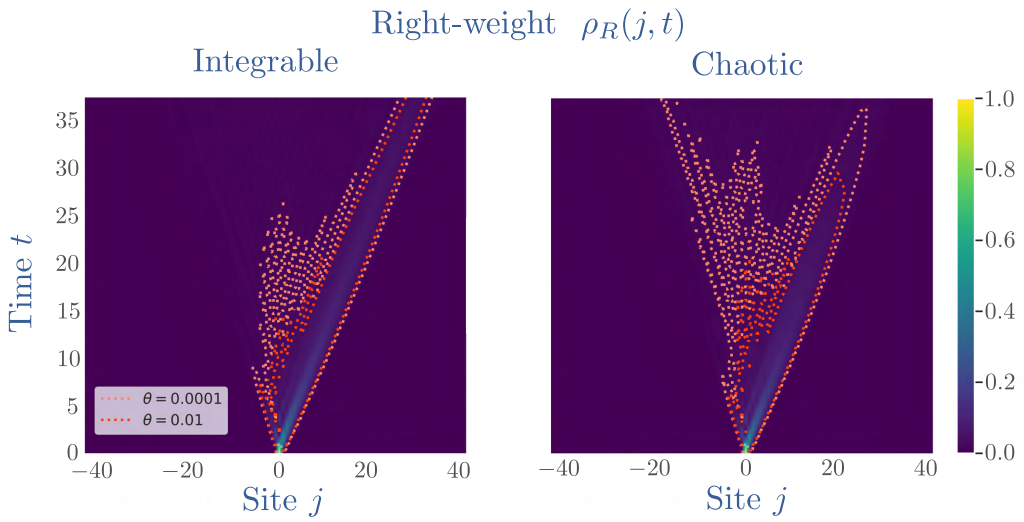

Figure 4.8. Comparison of integrable vs. chaotic dynamics in operator spreading. Left (Right): XXZ model at $\Delta = 1/2$ and an homogeneous (staggered) magnetic field of $h_z = 0.1$. Results at $\chi_{\text{MAX}} = 64$.

diffusively [NVH18b, VKRPS18b] as in integrable systems (albeit for very different reasons [GHKV18a]), but with a Gaussian scaling function. As we will show below, the effects of truncation errors using finite dimension MPOs are even more drastic for chaotic systems. In practice, this provides yet another way to distinguish integrability and chaos using finite bond dimension numerics, but this also makes accessing the true operator front properties of chaotic systems numerically very challenging.

We first study random Haar quantum circuits where each two-site gate is independently drawn from the ensemble of Haar random matrices of size $q^2 \times q^2$, with q the local Hilbert space dimension. Our results will focus on the case $q = 2$ corresponding to spin$-1/2$ systems. The seminal works [NVH18b, VKRPS18b] analyzed this setup analytically and characterized operator spreading exactly. Our main motivation here is to study operator front broadening in this setup numerically, to illustrate the effects of truncation errors due to finite bond dimension. Our results indicate the following two features present in quantum chaotic models at finite bond dimensions: 1) artificial slow-down of operator spreading as shown in Figs. 4.6-4.7 (see also Ref.[HPL19]); and

2) a front that broadens sub-diffusively and eventually stops broadening altogether, as shown in Fig. 4.7 (see also [XS20] for similar results in the chaotic kicked Ising model). In Fig. 4.8 we show how, even close to integrability, this slow-down in operator spreading becomes patent when studying the XXZ model for $\Delta = 1/2$ and a staggered magnetic field along the $z-$ direction of $h_z = 0.1$. Taking instead an homogeneous magnetic field of the same strength, in which case the system remains integrable, the front spreads ballistically at all times following the trace of the fastest quasiparticles in the system.

Those findings are consistent across all non-integrable models we have considered. We have also studied the chaotic Ising chain Hamiltonian given by:

$$H = J \sum_j \sigma_j^z \sigma_{j+1}^z + h_z \sigma_j^z + h_x \sigma_j^x. \tag{4.11}$$

For simplicity we set again $J = 1$. To ensure we are far into the non-integrable regime, we set $h_x = (1 + \sqrt{5})/4$ and $h_z = (5 + \sqrt{5})/8$, as in Ref.[KH13]. Our simulations for the computation of the right-weight in this case require a time step $dt \lesssim 0.01$. In contrast with the integrable case analyzed in the previous section, the present non-integrable model yields a front that evades our MPO simulations entirely: the entire light cone structure vanishes after the maximum bond dimension is reached, after which the front fails to spread at all. We note that this phenomenon is absent in the integrable case (see middle panel in Fig. 4.1). In fact, the maximum bond dimension in both the TFI model as well as in the XXZ model is reached at around the same time in both cases. This hints at a possible connection already put forward in Ref.[Picvcv07] between operator entanglement growth and integrability.

CHAPTER 5

CONCLUSION

In this Thesis we have studied universal properties in the dynamics of quantum many-body systems. First, inspired by random matrix theory and the physics of random quantum circuits we have studied a model of random tree tensor networks that display an entanglement phase transition from area law to logarithmic law as a function of the bond dimension. Our results indicate that the universality class of these *mean-field* entanglement transitions corresponds to the n-state Potts model living on a Cayley tree.

Next, in order to better understand the dynamics of integrable systems we have analyzed in great detail transport in the Rule 54 cellular automaton, verifying recent formulas using the framework of generalized hydrodynamics.

In the third Chapter we have studied transport in *near-integrable* models, that is, models that weakly break integrability. Our motivation here was to better understand transport in more experimentally realistic scenarios, where different sources of noise ultimately destroy the conservation of charges. We proposed an experimentally relevant and simple scheme based on the relaxation-time approximation that is able to capture universal properties of these systems, such as Fermi Golden's Rule for the decay rate of nonconserved charges and diffusion of conserved charges (when momentum is not conserved). With the aim to understand better transport in near-integrable systems we studied two simple models of these systems, corresponding to backscattering in the Rule 54 and in the classical hard-rod gas. We argued that transport in the noisy version of Rule 54 displays some pathological features in that

Fermi Golden Rule is strictly speaking not satisfied in our set-up and that, owing to slow equilibration, transport is not governed by a single decay rate, challenging the relaxation-time approximation scheme proposed earlier. Nevertheless we manage to analytically extract the *self-diffusion* constant of the tracer particles (corresponding to the diagonal components of the diffusion matrix). In the case of backscattering in the hard-rod gas, we manage to study analytically transport (in the limit of small noise). Our results shed light on the role of the off-diagonal components of the diffusion matrix – they are nonzero in general, in the presence of interactions (as in the hard-rod gas). Moreover, as far as we are aware, our resulting model is the first of its kind: it possesses infinitely many local conserved charges despite not being integrable.

Lastly, we have studied operator spreading in both integrable and quantum chaotic systems. We have provided evidence of a novel signature that would in principle allow one to distinguish integrable from chaotic systems: the height of the right-weight decays anomalously in the former (up to accessible times), while in the latter does so consistent with a gaussian front. Further, we have found while tensor network simulations allow one to extract the exponentially decaying tail of the front, the entire front suffers from severe truncation errors at fixed bond dimension already at reasonably short times.

APPENDIX A

QUANTUM CHANNEL DESCRIPTION OF NOISY RULE 54

A.1 Setting up the Kraus operators

Our model is defined as follows: after each unitary step $\hat{F}$, we convert with certain probability p a right mover into a left mover and viceversa. This will preserve the total number of particles N_+, but not the imbalance N_-. It is easy to realize that the minimum set of Kraus operators implementing this operation at each unit cell j is two and must be of the form

$$\begin{aligned} \hat{K}_{\mu_j=1} &= \mathbb{1}_j - \hat{\Pi}_j + \sqrt{1-p}\hat{\Pi}_j, \\ \hat{K}_{\mu_j=2} &= \sqrt{p}\hat{\Pi}_j \hat{S}_j \hat{\Pi}_j, \end{aligned} \tag{A.1a}$$

with $j \in \mathbb{Z}$. Here $\hat{\Pi}$ projects onto a given (to be determined) subspace composed of right/left movers while $\hat{S}$ swaps a right mover and a left mover within said subspace. The identity element in (A.1a) guarantees the completeness condition of Kraus operators. A full circuit layer is thus given by $\hat{\rho}(t+1) = \sum_{\{\vec{\mu}\}} \hat{K}_{\vec{\mu}} \hat{F}^\dagger \hat{\rho}(t) \hat{F} \hat{K}_{\vec{\mu}}^\dagger$, with $\vec{\mu} = (\mu_1, \mu_2, ..., \mu_L)$ and we define $\hat{K}_{\vec{\mu}} \equiv \bigotimes_{i=1}^{L} \hat{K}_{\mu_i}$. The structure of the model, in particular the fact that the density of right and left movers depend on three sites (two unit cells) already tells us that we should make sure that not only at a given unit cell N_+ is preserved, but also at its adjacent cells. To keep matters simple we consider the operator $\hat{S}_j$ that swaps the states $|\underset{j}{\square\square\blacksquare}\rangle$ (corresponding to one right mover) and $|\underset{j}{\blacksquare\square\square}\rangle$ (corresponding to one left mover). That is, $\hat{S}_j = \hat{\sigma}_j^+ \underset{j+1/2}{\square} \hat{\sigma}_{j+1}^- + \text{h.c.}$. Having

found $\hat{S}$ we can determine $\hat{\Pi}$. After some trial and error we find that the most general projector that still preserves N_+ must be of the form

$$\begin{aligned}\hat{\Pi}_i = \alpha(&\underset{i-1\ \ i\ \ i+1}{\blacksquare\square\square\blacksquare\blacksquare} + \underset{i-1\ \ i\ \ i+1}{\blacksquare\blacksquare\square\square\blacksquare}) \\ +\beta(&\underset{i-1\ \ i\ \ i+1\ i+2}{\square\square\square\blacksquare\square\square} + \underset{i-1\ \ i\ \ i+1\ i+2}{\square\square\blacksquare\square\square\square}) \\ +\gamma(&\underset{i-1\ \ i\ \ i+1\ i+2}{\blacksquare\square\square\blacksquare\square\blacksquare} + \underset{i-1\ \ i\ \ i+1\ i+2}{\blacksquare\square\blacksquare\square\square\blacksquare})\end{aligned} \tag{A.2}$$

with $\alpha, \beta, \gamma \in \{0, 1\}$. Note that these Kraus operators are symmetric, $\hat{K}_{\mu_i}^\dagger = \hat{K}_{\mu_i}^T = \hat{K}_{\mu_i}$. This work considers the simplest case with $\alpha = 1, \beta = \gamma = 0$, for which Kraus operators mutually commute with each other, $[\hat{K}_{\mu_i}, \hat{K}_{\mu_j}] = 0$ for any i, j (this is not true for the other possible choices). This will permit us to *encode* dissipation in a single circuit layer. Note that this circuit has a natural interpretation as an extension of the Rule 54 cellular automaton when including noise of strength p and as such we can simulate it classically as well. For details on the numerical implementation of the quantum channel, we refer to "Numerical details" section of the Appendix.

A.2 Perturbative expansion of the quantum channel

Let $\vec{\rho}_-$ the density of left movers in vector form, i.e. $\vec{\rho}_- \equiv 1/L\vec{N}_-$. Time evolution for t time steps gives $\vec{\rho}_-^{(t)} = \Phi^{(t)}\vec{\rho}_-^{(0)}$ with the map

$$\Phi^{(t)} \equiv \left(\sum_{\{\vec{\mu}\}} \hat{K}_{\vec{\mu}}\hat{F}^\dagger \otimes \hat{K}_{\vec{\mu}}\hat{F}^\dagger\right)^t, \tag{A.3}$$

where we have implicitly made use of the properties $\hat{K}_{\vec{\mu}}^\dagger = \hat{K}_{\vec{\mu}}^T = \hat{K}_{\vec{\mu}}$ and $\hat{F}^\dagger = \hat{F}^T$. At this step it is useful to start a perturbative expansion in p of $\sum_{\{\vec{\mu}\}} \hat{K}_{\vec{\mu}} \otimes \hat{K}_{\vec{\mu}}$. Let us denote $\hat{\Theta}_i \equiv \hat{\Pi}_i\hat{S}_i = \hat{\Pi}_i\hat{S}_i\hat{\Pi}_i$. Carrying out the expansion we get

$$\sum_{\{\vec{\mu}\}} \hat{K}_{\vec{\mu}} \otimes \hat{K}_{\vec{\mu}} = \hat{K}_{(0,0,\ldots,0)} \otimes \hat{K}_{(0,0,\ldots,0)} + \sum_{i=1}^{L} \hat{K}_{(0,0,\ldots,0,\underset{i}{1},0,\ldots,0)} \otimes \hat{K}_{(0,0,\ldots,0,\underset{i}{1},0,\ldots,0)} + \mathcal{O}(p^2). \tag{A.4}$$

Let us consider the first term. This gives us

$$\begin{aligned}\hat{K}_{(0,0,\ldots,0)} \otimes \hat{K}_{(0,0,\ldots,0)} &= \prod_{i=1}^{L} \left(\mathbb{1} + \hat{\Pi}_i \sum_{n=1}^{\infty} (-1)^n p^n \binom{\frac{1}{2}}{n} \right) \otimes \prod_{i=1}^{L} \left(\mathbb{1} + \hat{\Pi}_i \sum_{n=1}^{\infty} (-1)^n p^n \binom{\frac{1}{2}}{n} \right) \\ &= \mathbb{1} - \frac{p}{2} \sum_{i=1}^{L} \left(\mathbb{1} \otimes \hat{\Pi}_i + \hat{\Pi}_i \otimes \mathbb{1} \right) + \mathcal{O}(p^2).\end{aligned} \tag{A.5}$$

The second term takes also a very simple form

$$\hat{K}_{(0,0,\ldots,0,\underset{i}{1},0,\ldots,0)} \otimes \hat{K}_{(0,0,\ldots,0,\underset{i}{1},0,\ldots,0)} = p\hat{\Theta}_i \otimes \hat{\Theta}_i + \mathcal{O}(p^2). \tag{A.6}$$

Thus to first order in p we have

$$\sum_{\{\vec{\mu}\}} \hat{K}_{\vec{\mu}} \otimes \hat{K}_{\vec{\mu}} = \mathbb{1} + p \sum_{i=1}^{L} \left(\hat{\Theta}_i \otimes \hat{\Theta}_i - \frac{1}{2} \left(\mathbb{1} \otimes \hat{\Pi}_i + \hat{\Pi}_i \otimes \mathbb{1} \right) \right) + \mathcal{O}(p^2). \tag{A.7}$$

Plugging this into $\Phi^{(t)}$ we get

$$\begin{aligned}\Phi^{(t)} &= (\hat{F}^\dagger \otimes \hat{F}^\dagger)^t + \\ &+ p \sum_{i=1}^{L} \sum_{n=1}^{t} (\hat{F}^\dagger \otimes \hat{F}^\dagger)^{t-n} \left(\hat{\Theta}_i \otimes \hat{\Theta}_i - \frac{1}{2} \left(\mathbb{1} \otimes \hat{\Pi}_i + \hat{\Pi}_i \otimes \mathbb{1} \right) \right) (\hat{F}^\dagger \otimes \hat{F}^\dagger)^n + \mathcal{O}(p^2).\end{aligned} \tag{A.8}$$

Applying this to the local density of imbalance which we take it to be $\hat{\rho}_{-,l}$, with $l \in [1, L]$ we have

$$\hat{\rho}^{(t)}_{-,l} = \hat{\rho}^{0(t)}_{-,l} + p \sum_{i=1}^{L} \sum_{n=1}^{t} (\hat{F}^\dagger)^{t-n} \hat{\Theta}_i \hat{\rho}^{0(n)}_{-,l} \hat{\Theta}_i \hat{F}^{t-n} - (\hat{F}^\dagger)^{t-n} \hat{\Pi}_i \hat{\rho}^{0(n)}_{-,l} \hat{\Pi}_i \hat{F}^{t-n} + \mathcal{O}(p^2), \tag{A.9}$$

where $\hat{\rho}^{0(n)}_{-,l} \equiv (\hat{F}^\dagger)^n \hat{\rho}^{(0)}_{-,l} \hat{F}^n$ and we have made use of $[\hat{\rho}^{0(n)}_{-,l}, \hat{\Pi}_i] = 0 \; \forall i, l, n$. We seek an e.o.m. for the decaying charge. Let $\hat{N}_- = \sum_l \hat{\rho}_{-,l}$. Its discrete time derivative reads

$$\hat{N}_-^{(t+1)} - \hat{N}_-^{(t)} = p \sum_{i=1}^{L} (\hat{F}^\dagger)^t \hat{\Theta}_i \hat{N}_-^{(0)} \hat{\Theta}_i \hat{F}^t - (\hat{F}^\dagger)^t \hat{\Pi}_i \hat{N}_-^{(0)} \hat{\Pi}_i \hat{F}^t + \mathcal{O}(p^2), \tag{A.10}$$

where have used conservation of the global charge under the unperturbed dynamics, $[\hat{F}, \hat{N}_-] = 0$. Multiplying both sides of (A.10) by $\hat{N}_-^{(0)}$ and averaging over an homogeneous Gibbs state of fixed μ, $\langle \cdots \rangle \equiv 1/Z \mathrm{tr}[\cdots e^{-\mu \hat{N}_+}]$, we get

$$\begin{aligned} \langle (\hat{N}_-^{(t+1)} - \hat{N}_-^{(t)}) \hat{N}_-^{(0)} \rangle &= p \sum_{i=1}^{L} \langle \hat{\Theta}_i \hat{N}_-^{(0)} \hat{\Theta}_i \hat{N}_-^{(0)} \rangle - \langle \hat{\Pi}_i \hat{N}_-^{(0)} \hat{\Pi}_i \hat{N}_-^{(0)} \rangle + \mathcal{O}(p^2) \\ &= -2p \langle \hat{\Pi}_- \hat{N}_-^{(0)} \rangle + \mathcal{O}(p^2) \\ &= -2p \langle \hat{\Pi} \rangle + \mathcal{O}(p^2), \end{aligned} \tag{A.11}$$

where in the first line we have made use of $[\hat{F}, \hat{N}_+] = 0$, in the second line we have used

$$\hat{\Theta}_i \hat{\rho}_{-,j} \hat{\Theta}_i = (1 - 2\delta_{i,j}) \hat{\rho}_{-,j} \hat{\Pi}_i \tag{A.12}$$

and defined $\hat{\Pi}_- = \sum_i \hat{\Pi}_{-,i}$ with $\hat{\Pi}_{-,i} \equiv \hat{\Pi}_i \hat{\rho}_{-,i}$, and in the last line we have made use of $\hat{\rho}_{-,i} \hat{\Pi}_{-,i} = \hat{\Pi}_i$, and $\hat{\Pi} = \sum_i \hat{\Pi}_i$. Using the transfer matrix (2.40) we get

$$\langle \hat{\Pi}_i \rangle = 2 \frac{e^{3\mu}}{(1+e^\mu)^3 (3+e^\mu)}, \tag{A.13}$$

and so the derivative of the correlator at order p reads (taking time continuous)

$$\partial_t \frac{1}{L} \langle \hat{N}_-^{(t)} \hat{N}_-^{(0)} \rangle = -4p \frac{e^{3\mu}}{(1+e^\mu)^3 (3+e^\mu)} + \mathcal{O}(p^2). \tag{A.14}$$

In the following we shall see that the next to leading order terms $\mathcal{O}(p^2)$ cannot in fact be disregarded, as the small parameter controlling this expansion is pt and not

$p\tau^*$: the r.h.s. *does* depend on time through the term $\mathcal{O}(p^2)$. We shall discuss these higher order corrections next but before, let us state that in (A.14) at $t = 0$, terms of p^2 and higher order are zero (in general, at any time step t, only terms of at most order p^t can contribute; see below) and so one can extract a decay rate as

$$\partial_t \langle \hat{N}_-^{(t)} \hat{N}_-^{(0)} \rangle|_{t=0} = -\Gamma_{\text{s.t.}} \langle \hat{N}_-^{(t)} \hat{N}_-^{(0)} \rangle|_{t=0}, \tag{A.15}$$

where $\Gamma_{\text{s.t.}} = 2p\gamma_{\text{s.t.}}$ with

$$\gamma_{\text{s.t.}} = \frac{\langle \hat{\Pi} \rangle}{LG_{+,+}} = \frac{e^{2\mu}(3 + e^{\mu})}{(1 + e^{\mu})^3}. \tag{A.16}$$

where $G_{+,+} = 1/L\langle \hat{N}_-^2 \rangle$ is the current-current correlator of number of solitons in the integrable limit. The subscript s.t. here is to denote *short time*, given that the extracted decay rate is only an approximation that is valid at very short times (strictly, at $t = 0$).

APPENDIX B

DIFFUSIVE HYDRODYNAMICS FROM BACKSCATTERING

Here we rederive the formula for the diffusion constant of conserved modes within GHD used in the main text, Eq. (4), and which follows from Ref. [FGV20b] (see also [ZBK22]). Our starting point is the linearized Boltzmann equation Eq. (3),

$$\partial_t \delta\rho + A\partial_x \delta\rho = -\Gamma\delta\rho, \tag{B.1}$$

where the operators A and Γ act on velocity space as convolution, e.g. $A\delta\rho_k(x,t) = \int dk' A_{kk'}\delta\rho_{k'}(x,t)$. The densities of conserved charges in the hard-rod gas obey

$$q_n(x,t) = \int dk k^n \rho_k(x,t). \tag{B.2}$$

Similar relations would still hold for other integrable models; in particular, an identical relation holds in the Lieb-Liniger model – see e.g. Ref. [BD22]. We can recast the Boltzmann equation B.1 in terms of these charges as follows,

$$\partial_t \delta q_n + \sum_m A_{nm}\partial_x \delta q_m = -\sum_m \Gamma_{nm}\delta q_m, \tag{B.3}$$

where, analogously to the phase-space density, we assumed the above dynamics occurs above a state of fixed, homogeneous charge $q_n^* = \int dk k^n \rho_k^*$. Now the hydrodynamic matrices are expressed in the charge basis and have components e.g. $A_{nm} = \int dk dk' k^n A_{k,k'} k'^m$. We now use the method of hydrodynamic projections to

project Eq. (B.3) onto decaying charges, via the operator P, and conserved charges, via its complement, which we denote as $\bar{P} = 1 - P$. This results in the following two equations

$$\partial_t \bar{P}\delta\vec{q} + \bar{P}A\partial_x \delta\vec{q} = 0, \tag{B.4a}$$

$$\partial_t P\delta\vec{q} + PA\partial_x \delta\vec{q} = -P\Gamma P\delta\vec{q}. \tag{B.4b}$$

where the charge vector $\vec{q}$ has as components all the charges of the original integrable model. Note that we have implicitly assumed that dissipation will only act within the subspace of decaying charge (while in general, and in particular, for backscattering, decaying and conserved modes will be mixed by the integrable dynamics). Applying the inverse of the dissipation operator on (B.4b) and solving recursively yields

$$\begin{aligned} P\delta\vec{q} &= -(P\Gamma P)^{-1}(\partial_t P\delta\vec{q} + PA\partial_x\delta\vec{q}) \\ &= -\partial_x (P\Gamma P)^{-1} PA\bar{P}\delta\vec{q} + \mathcal{O}(\{\partial_x^2, \partial_t\partial_x, \partial_t^2\}). \end{aligned} \tag{B.5}$$

Ignoring higher order gradient terms and plugging this into (B.4a) leads to

$$\partial_t \bar{P}\delta\vec{q} + \bar{P}A\partial_x \bar{P}\delta\vec{q} = \mathcal{D}\partial_x^2 \bar{P}\delta\vec{q}, \tag{B.6}$$

where

$$\mathcal{D} = \bar{P}A(P\Gamma P)^{-1}A\bar{P}. \tag{B.7}$$

We will show below that for the case of backscattering noise, there are no ballistic contributions as the matrix A will only couple decaying charges with conserved ones.

APPENDIX C

BACKSCATTERING IN THE HARD-ROD GAS

While the hydrodynamics of the hard-rod gas was originally solved assuming a (continuous) distribution of rods' velocities, we shall assume that a well-defined and analogous description exists in the presence of a discrete set of different velocities. This will facilitate computing the diffusion constant of the different particle species exactly, and in the limit of infinite number of such particle species, allow us to compute the structure factor of density in the continuum limit.

C.1 One particle species (two velocities)

Earlier works [Per69, BDS83, DS17b] had shown that the hydrodynamics of the hard-rod gas at the Euler scale obeys GHD equation

$$\partial_t \rho + \partial_x (v^{\text{eff}} \rho) = 0, \tag{C.1}$$

where

$$v_k^{\text{eff}}[\rho] = k + \frac{a \int_{k'} (k - k') \rho_{k'}(x,t)}{1 - a \int_{k'} \rho_{k'}(x,t)}, \tag{C.2}$$

with a the hard-rod's length. Within linear response we may take $\rho = \rho^* + \delta\rho$, with ρ^* some stationary state that is spatially homogeneous. For what follows we take this

state to be given by $\rho^* = n\frac{1}{2}(\delta(v-v_0)+\delta(v+v_0))$, with $n = N/(2L)$ the density of hard-rods in the system. In this stationary state the effective velocity is given by

$$v^{\text{eff}}_{[\rho^*]}(v_0) = \frac{v_0}{1-an} \equiv v^{\text{eff},*}. \tag{C.3}$$

Note that this effective velocity is precisely that of the Rule 54 cellular automaton when setting $v_0 = \pm 1$, $a = -1$ [GHKV18b]. Carrying this analogy further, we posit the GHD equation to be of the form:

$$\partial_t \delta\vec{\rho} + A\partial_x \delta\vec{\rho} = 0, \tag{C.4}$$

with $\vec{\rho} = (\rho_+, \quad \rho_-)$, with $\rho_\pm = \rho_R \pm \rho_L$, where $\rho_{R/L}$ is the density of particles moving at speed $v_0 = \pm 1$. In the linear response setup we're interested in we have $\rho_+ = n + \delta\rho$, $\rho_- = \delta\rho_-$, and where the operator A is given as [DS17b]

$$A = (1-\theta^* T)^{-1} v^{\text{eff},*} (1-\theta^* T), \tag{C.5}$$

where θ is the Fermi factor and we have implicitly assumed all quantities here are evaluated at the stationary state. The Fermi factor in vector form is given as

$$\vec{\theta^*} = (1-an)^{-1}\vec{\rho^*}, \quad \vec{\rho^*} = (n, \quad 0). \tag{C.6}$$

The counterpart in matrix form corresponds to the diagonal matrix constructed out of this vector. Likewise, we may view the dressed velocity as being a diagonal matrix with entries given by (C.3). The kernel acts as follows on a test function

$$T\psi(v) = -a\int dw \psi(w). \tag{C.7}$$

In the R/L basis the kernel should read [1]

$$T = -a \begin{pmatrix} 1 & 1 \\ 1 & 1 \end{pmatrix}. \tag{C.8}$$

In the presence of backscattering noise, the GHD equation takes the form

$$\partial_t \delta\vec{\rho} + A\partial_x \delta\vec{\rho} = -\Gamma\delta\vec{\rho}, \tag{C.9}$$

with, the decay matrix

$$\Gamma = \gamma \begin{pmatrix} 1 & -1 \\ -1 & 1 \end{pmatrix}, \tag{C.10}$$

with p the proba for a right/left mover to veer direction. Note that Γ has one zero mode and one decaying mode, which is found upon rotating Γ to the $\pm$ basis as

$$\Gamma \to O\Gamma O^{-1}, \tag{C.11}$$

with

$$O = \begin{pmatrix} 1 & 1 \\ 1 & -1 \end{pmatrix}. \tag{C.12}$$

The decaying mode corresponds to the ρ_- mode and has eigenvalue $\Gamma_{-,-} = 2\gamma$. To get the diffusion constant of positive movers we also rotate the A matrices onto the $+/-$ basis to find

$$A_{+,-} = 1, \;\; A_{-,+} = \frac{1}{(1-an)^2}. \tag{C.13}$$

The diffusion constant is given as

$$\mathcal{D}_{+,+} = A_{+,-}\Gamma^{-1}_{-,-}A_{-,+} = \frac{1}{2\gamma(1-an)^2} \equiv \frac{(v^{\text{eff}})^2}{2\gamma}. \tag{C.14}$$

---

[1] While in the continuum the diagonal components of matrix T are ill-defined, we will set these to be 1 in the discrete version of the model. It can be shown that the diffusion constant of quasiparticles and the structure factor will not depend on these diagonal (*gauge*) components.

Note that these are results are identical to those obtained in Rule 54 upon setting $a = -1$ [LPGV22].

C.2 Two particle species

The previous analysis can be generalized straightforwardly to the case of particles having four possible velocities (two of opposite sign) with backscattering. The corresponding hydrodynamic matrices now read

$$T = -a \begin{pmatrix} 1 & 1 & 1 & 1 \\ 1 & 1 & 1 & 1 \\ 1 & 1 & 1 & 1 \\ 1 & 1 & 1 & 1 \end{pmatrix}, \tag{C.15}$$

$$\Gamma = \gamma \begin{pmatrix} 1 & -1 & 0 & 0 \\ -1 & 1 & 0 & 0 \\ 0 & 0 & 1 & -1 \\ 0 & 0 & -1 & 1 \end{pmatrix}, \tag{C.16}$$

$$O = \begin{pmatrix} 1 & 1 & 0 & 0 \\ 1 & -1 & 0 & 0 \\ 0 & 0 & 1 & 1 \\ 0 & 0 & 1 & -1 \end{pmatrix}. \tag{C.17}$$

where the rotation matrix is defined so as to rotate to the $\pm$ basis within each speed sector. We stick to the convention that the top left block in the O matrix defines a subspace of e.g. velocity $\pm v_1$ and the bottom right block defines a different subspace of velocity $\pm v_2$. The Fermi factor (in matrix form) reads in the R/L basis

$$\theta = \frac{1}{1 - an} \frac{n}{4} \mathbb{1}_{4\times 4}, \tag{C.18}$$

where we've chosen the background state to be that where all velocities are equally likely to simplify the analysis (we will extend to arbitrary distribution and number of particle species below). With this we can find the A matrix in the $\pm$ basis using (C.5). For reference we write it down

$$A = \frac{1}{1-an}\begin{pmatrix} \overset{(+,1)}{0} & \overset{(-,1)}{(1-\frac{an}{2})v_1} & \overset{(+,2)}{0} & \overset{(-,2)}{-\frac{an}{2}v_2} \\ \frac{1-\frac{an}{2}}{1-an}v_1 & 0 & \frac{an}{2(1-an)}v_1 & 0 \\ 0 & -\frac{an}{2}v_1 & 0 & (1-\frac{an}{2})v_2 \\ \frac{an}{2(1-an)}v_2 & 0 & \frac{1-\frac{an}{2}}{1-an}v_2 & 0 \end{pmatrix} \begin{matrix} (+,1) \\ (-,1) \\ (+,2) \\ (-,2) \end{matrix} \tag{C.19}$$

with $(\pm, i)$ corresponding to the sector with $\pm v_i$ velocity. The diffusion matrix written in this basis reads

$$\mathcal{D}_{(+,i),(+,j)} = \sum_k A_{(+,i),(-,k)}\Gamma^{-1}_{(-,k),(-,k)}A_{(-,k),(+,j)}, \tag{C.20}$$

with $\Gamma_{(-,i),(-,i)} = 2\gamma$. The diffusion matrix has off-diagonal entries now owing to the interaction between the two different particle species. The matrix components read

$$\mathcal{D}_{(+,i),(+,j)} = \frac{1}{2\gamma}\frac{1}{4(1-an)^3} \times \begin{cases} (2-an)^2v_1^2 - (anv_2)^2, & i=j=1, \\ (2-an)^2v_2^2 - (anv_1)^2, & i=j=2, \\ an(2-an)(v_i^2 - v_j^2), & i \neq j. \end{cases} \tag{C.21}$$

The diagonal components of this matrix may be negative for some choice of parameters. This is fine so long as $\mathcal{D} \geq 0$. This can be checked by diagonalizing $\mathcal{D}$ and checking that its eigenvalues are nonnegative. We've confirmed this and found the eigenvalues to be $\{(v_1^{\text{eff}})^2, (v_2^{\text{eff}})^2\} \times 1/2\gamma$. The corresponding eigenmodes read

$\{(-\phi,\ \ 1),(1,\ \ -\phi)\}$ with $\phi \equiv -1 + \frac{2}{an}$. This crucially implies $\rho_+ \equiv \rho_{(+,1)} + \rho_{(+,2)}$ is not a diffusive mode. Instead, these correspond to

$$\delta\vec{\tilde{\rho}} = W^{-1}\delta\vec{\rho}, \tag{C.22}$$

with $\delta\vec{\rho} = \begin{pmatrix} \delta\rho_{(+,1)} & \delta\rho_{(+,2)} \end{pmatrix}$, and

$$W = \begin{pmatrix} -\phi & 1 \\ 1 & -\phi \end{pmatrix}. \tag{C.23}$$

the matrix of eigenvectors of $\mathcal{D}$. We are interested in the quantity $S(x,t) = \langle \delta\rho(x,t)\delta\rho(0,0)\rangle^c$, with $\delta\rho = \delta\rho_{(+,1)} + \delta\rho_{(+,2)}$ corresponding to the density of particles. First we compute the C matrix which reads [DS17b]

$$C = (1-\theta^* T)^{-1}\rho^*(1-T\theta^*)^{-1}. \tag{C.24}$$

At variance with the A matrix, the C matrix, written in the $+,-$ basis is *not simply* given by a rotation of C by O, and instead this picks up a factor of 2 (as can be checked by explicitly computing C and A). Explicitly

$$C = \begin{array}{c} \begin{matrix} \text{(+,1)} & \text{(-,1)} & \text{(+,2)} & \text{(-,2)} \end{matrix} \\ \begin{pmatrix} \frac{1}{4}n(2-2an+(an)^2) & 0 & \frac{1}{4}an^2(-2+an) & 0 \\ 0 & \frac{n}{2} & 0 & 0 \\ \frac{1}{4}an^2(-2+an) & 0 & \frac{1}{4}n(2-2an+(an)^2) & 0 \\ 0 & 0 & 0 & \frac{n}{2} \end{pmatrix} \end{array} \begin{matrix} \text{(+,1)} \\ \text{(-,1)} \\ \text{(+,2)} \\ \text{(-,2)} \end{matrix} \tag{C.25}$$

Crucially, the $(+,1)$ and $(+,2)$ charges are correlated, while $(-,1)$ and $(-,2)$ are not. This means in particular we must take care of cross terms when expanding

$\delta\rho = \delta\rho_{(+,1)} + \delta\rho_{(+,2)}$ in the structure factor. We compute next each term appearing in $S(x,t)$, $S(x,t) = S_{1,1}(x,t) + S_{1,2}(x,t) + S_{2,1}(x,t) + S_{2,2}(x,t)$, with $S_{i,j}(x,t) = \langle \delta\rho_{(+,i)}(x,t)\delta\rho_{(+,j)}(0,0)\rangle^c$. We shall be interested in the C matrix projected onto the $\{(+,1),(+,2)\}$ subspace. Call it $C^{(+)}$. In the eigenmode basis this reads

$$\tilde{C}^{(+)} = (W^{-1})C^{(+)}(W^{-1})^T = \frac{n}{2}\frac{(an)^2}{4}\mathbb{1}_{2\times 2} = \frac{n}{4}\frac{1}{1+\phi}\mathbb{1}_{2\times 2}. \tag{C.26}$$

Note that the exact expression of $\tilde{C}$ depends on the choice of normalization factors of the eigenvectors forming matrix W but this is the one that yields the simplest expression for $\tilde{C}$. Then,

$$\begin{aligned} S_{1,1}(x,t) &= \phi^2\tilde{S}_{1,1}(x,t) - \phi\tilde{S}_{1,2}(x,t) - \phi\tilde{S}_{2,1}(x,t) + \tilde{S}_{2,2}(x,t) \\ &\asymp \phi^2\tilde{C}^{(+)}_{1,1}g(x,2\mathcal{D}_1 t) + \tilde{C}^{(+)}_{2,2}g(x,2\mathcal{D}_2 t) \\ &= \frac{n}{4(1+\phi)}\left(\phi^2 g(x,2\mathcal{D}_1 t) + g(x,2\mathcal{D}_2 t)\right), \end{aligned} \tag{C.27}$$

where $\mathcal{D}_i = (v_i^{\text{eff}})^2/2\gamma$, and $\asymp$ denotes the limit $t \gg 1/\gamma$, and $g(x,\sigma^2) = \frac{e^{-\frac{x^2}{2\sigma^2}}}{\sqrt{2\pi\sigma^2}}$. As a sanity check we confirm $\int dx S_{1,1}(x,t) = C_{1,1}$. We can compute the rest of the terms contributing to $S(x,t)$ and we find

$$\begin{aligned} S_{1,2}(x,t) &\asymp -\frac{n\phi}{4(1+\phi)}(g(x,2\mathcal{D}_1 t) + g(x,2\mathcal{D}_2 t)), \\ S_{2,1}(x,t) &\asymp -\frac{n\phi}{4(1+\phi)}(g(x,2\mathcal{D}_1 t) + g(x,2\mathcal{D}_2 t)), \\ S_{2,2}(x,t) &\asymp \frac{n}{4(1+\phi)}(g(x,2\mathcal{D}_1 t) + \phi^2 g(x,2\mathcal{D}_2 t)). \end{aligned} \tag{C.28}$$

These results also fulfill the sum rule $\int dx S_{i,j}(x,t) = C_{i,j}$. Equipped with these results we get the structure factor of the density

$$\begin{aligned} S(x,t) &\asymp \frac{n}{2}\left(\frac{1-\phi^2}{1+\phi^2}\right)^2 (g(x,2\mathcal{D}_1 t) + g(x,2\mathcal{D}_2 t)) \\ &= \frac{n}{2}(1-an)^2(g(x,2\mathcal{D}_1 t) + g(x,2\mathcal{D}_2 t)). \end{aligned} \tag{C.29}$$

So, indeed, we find that the structure factor of the density is given by an equal superposition of the two gaussians.

C.3 m-particle species (arbitrary distribution)

For arbitrary number of particles species and arbitrary even velocity distributions, so that $\{v_i \to p_i/2, -v_i \to p_i/2\}$, with $p_i \in [0,1]$, the corresponding A matrix components read (found by inspection from analyzing smaller instances)

$$A_{(+,i),(-,j)} = \begin{cases} \frac{-1+anp_i}{-1+an} v_i, & i = j \\ \frac{an}{-1+an} p_i v_j, & i \neq j. \end{cases} \tag{C.30}$$

$$A_{(-,i),(+,j)} = \begin{cases} \frac{1-an(1-p_i)}{(-1+an)^2} v_i, & i = j \\ \frac{an}{(-1+an)^2} p_i v_i, & i \neq j. \end{cases} \tag{C.31}$$

Which results in the diffusion matrix

$$\mathcal{D}_{(+,i),(+,i)} = \frac{1}{2\gamma(1-an)^3} \left((1 - an + (an)^2 p_i) v_i^2 - (an)^2 p_i \langle v^2 \rangle \right), \tag{C.32}$$

$$\mathcal{D}_{(+,i),(+,j\neq i)} = \frac{anp_i}{2\gamma(1-an)^3} \left(v_i^2 + (1+an) v_j^2 - an \langle v^2 \rangle \right), \tag{C.33}$$

with $\langle v^2 \rangle = \sum_k p_k v_k^2$. Note that in the absence of interactions the diffusion matrix is purely diagonal. The next step is to determine the eigenmode matrix that diagonalizes $\mathcal{D}$. This has the rather simple form

$$W_{i,j} = \begin{cases} 1 - anp_i, & i = j \\ -anp_i, & i \neq j. \end{cases} \tag{C.34}$$

The charge-charge matrix for arbitrary distribution has components

$$
\begin{aligned}
C_{(+,i),(+,j)} &= \begin{cases} np_i(1-anp_i+(an)^2p_i), & i=j, \\ -(2-an)an^2p_ip_j, & i\neq j, \end{cases} \\
C_{(-,i),(-,j)} &= np_i\delta_{i,j}, \\
C_{(+,i),(-,j)} &= 0 = C_{(-,i),(+,j)}.
\end{aligned}
\tag{C.35}
$$

Note that the sum rule in this case takes a very simple form

$$
\sum_{i,j} C_{(+,i),(+,j)} = n(1-an)^2. \tag{C.36}
$$

Written in the basis of eigenmodes in the + subspace the charge-charge matrix reads

$$
\tilde{C}^{(+)} = n(an)^2 \mathrm{diag}(p_1, p_2, \cdots, p_m). \tag{C.37}
$$

The structure factor matrix has components

$$
\begin{aligned}
S_{i,j}(x,t) &= n(an)^2 \times \\
&\times \begin{cases} \left(p_i - \frac{1}{an}\right)^2 p_i g(x, \mathcal{D}_i t) + \sum_{k\neq i} p_i^2 p_k g(x, 2\mathcal{D}_k t), & i=j \\ p_ip_j\left(\left(p_i-\frac{1}{an}\right)g(x,2\mathcal{D}_it) + \left(p_j-\frac{1}{an}\right)g(x,2\mathcal{D}_jt) + \sum_{k\neq i,j} p_k g(x,2\mathcal{D}_k t)\right), & i\neq j. \end{cases}
\end{aligned}
\tag{C.38}
$$

After some lengthy algebra we find the structure factor of density $S(x,t) = \sum_{i,j} S_{i,j}(x,t)$

$$
S(x,t) = n(1-an)^2 \langle g(x, 2\mathcal{D}t)\rangle, \tag{C.39}
$$

where

$$
\langle g(x,2\mathcal{D}t)\rangle \equiv \sum_i p_i g(x, 2\mathcal{D}_i t). \tag{C.40}
$$

This is the expression quoted in the main text. This expression fulfills the sum rule, $\sum_x S(x,t) = \sum_{i,j} C^{(+)}_{i,j} = n(1-an)^2$. In the continuum limit we simply replace $p_i \to p(v)$ and the sum by an integral. I.e. the structure factor is given as

$$\boxed{S(x,t) = (1-an)^2 \int dv \rho^*(v) g(x, 2\mathcal{D}(v)t), \quad \mathcal{D}(v) \equiv \frac{(v^{\text{eff}})^2}{2\gamma},} \tag{C.41}$$

with $\rho^*(v) = p(v)n$ the background particle density.

BIBLIOGRAPHY

[AABS19] Dmitry A Abanin, Ehud Altman, Immanuel Bloch, and Maksym Serbyn. Colloquium: Many-body localization, thermalization, and entanglement. *Reviews of Modern Physics*, 91(2):021001, 2019.

[AC17a] Vincenzo Alba and Pasquale Calabrese. Entanglement and thermodynamics after a quantum quench in integrable systems. *Proceedings of the National Academy of Sciences*, 114(30):7947–7951, 2017.

[AC17b] Vincenzo Alba and Pasquale Calabrese. Rényi entropies after releasing the néel state in the xxz spin-chain. *Journal of Statistical Mechanics: Theory and Experiment*, 2017(11):113105, 2017.

[AF17] Vincenzo Alba and Maurizio Fagotti. Prethermalization at low temperature: The scent of long-range order. *Phys. Rev. Lett.*, 119:010601, Jul 2017.

[AL18] Fabien Alet and Nicolas Laflorencie. Many-body localization: An introduction and selected topics. *Comptes Rendus Physique*, 19(6):498–525, 2018.

[Alb18] Vincenzo Alba. Entanglement and quantum transport in integrable systems. *Physical Review B*, 97(24):245135, 2018.

[Alb20] Vincenzo Alba. Diffusion and operator entanglement spreading. *arXiv preprint arXiv:2006.02788*, 2020.

[ARS01] Changrim Ahn, Chaiho Rim, and Ryu Sasaki. Integrable quantum field theories and their applications. *Integrable Quantum Field Theories and their Applications*, 2001.

[BAC19] Alvise Bastianello, Vincenzo Alba, and Jean-Sébastien Caux. Generalized hydrodynamics with space-time inhomogeneous interactions. *Phys. Rev. Lett.*, 123:130602, Sep 2019.

[Bat] Murray T. Batchelor. The bethe ansatz after 75 years. *Physics Today 1 January 2007; 60 (1): 36–40.*

[BB92] VV Bazhanov and RJ Baxter. New solvable lattice models in three dimensions. *Journal of Statistical Physics*, 69(3):453–485, 1992.

[BCA19] Yimu Bao, Soonwon Choi, and Ehud Altman. Theory of the Phase Transition in Random Unitary Circuits with Measurements, Aug 2019.

[BCA20] Yimu Bao, Soonwon Choi, and Ehud Altman. Theory of the phase transition in random unitary circuits with measurements. *Physical Review B*, 101(10):104301, 2020.

[BCDNF16] Bruno Bertini, Mario Collura, Jacopo De Nardis, and Maurizio Fagotti. Transport in out-of-equilibrium xxz chains: Exact profiles of charges and currents. *Phys. Rev. Lett.*, 117:207201, Nov 2016.

[BCK15] G. P. Brandino, J.-S. Caux, and R. M. Konik. Glimmers of a quantum kam theorem: Insights from quantum quenches in one-dimensional bose gases. *Phys. Rev. X*, 5:041043, Dec 2015.

[BCR+19] Alberto Biella, Mario Collura, Davide Rossini, Andrea De Luca, and Leonardo Mazza. Ballistic transport and boundary resistances in inhomogeneous quantum spin chains. *Nature Communications*, 10(1):4820, 2019.

[BD17] Denis Bernard and Benjamin Doyon. Diffusion and signatures of localization in stochastic conformal field theory. *Phys. Rev. Lett.*, 119:110201, Sep 2017.

[BD22] Isabelle Bouchoule and Jérôme Dubail. Generalized hydrodynamics in the one-dimensional bose gas: theory and experiments. *Journal of Statistical Mechanics: Theory and Experiment*, 2022(1):014003, jan 2022.

[BDD20] Isabelle Bouchoule, Benjamin Doyon, and Jerome Dubail. The effect of atom losses on the distribution of rapidities in the one-dimensional Bose gas. *SciPost Phys.*, 9:44, 2020.

[BDNDL20a] Alvise Bastianello, Jacopo De Nardis, and Andrea De Luca. Generalised hydrodynamics with dephasing noise. *arXiv preprint arXiv:2003.01702*, 2020.

[BDNDL20b] Alvise Bastianello, Jacopo De Nardis, and Andrea De Luca. Generalized hydrodynamics with dephasing noise. *Phys. Rev. B*, 102:161110, Oct 2020.

[BDS83] C. Boldrighini, R. L. Dobrushin, and Yu. M. Sukhov. One-dimensional hard rod caricature of hydrodynamics. *Journal of Statistical Physics*, 31(3):577–616, 1983.

[BDZ08] Immanuel Bloch, Jean Dalibard, and Wilhelm Zwerger. Many-body physics with ultracold gases. *Reviews of modern physics*, 80(3):885, 2008.

[BEGR15] Bruno Bertini, Fabian H. L. Essler, Stefan Groha, and Neil J. Robinson. Prethermalization and thermalization in models with weak integrability breaking. *Phys. Rev. Lett.*, 115:180601, Oct 2015.

[BEGR16] Bruno Bertini, Fabian H. L. Essler, Stefan Groha, and Neil J. Robinson. Thermalization and light cones in a model with weak integrability breaking. *Phys. Rev. B*, 94:245117, Dec 2016.

[Bet31] Hans Bethe. Zur theorie der metalle. *Zeitschrift für Physik*, 71(3):205–226, 1931.

[BGR20] Marlon Brenes, John Goold, and Marcos Rigol. Ballistic vs diffusive low-frequency scaling in the xxz and a locally perturbed xxz chain, 2020.

[BHMK+21] B. Bertini, F. Heidrich-Meisner, C. Karrasch, T. Prosen, R. Steinigeweg, and M. Žnidarič. Finite-temperature transport in one-dimensional quantum lattice models. *Rev. Mod. Phys.*, 93:025003, May 2021.

[BHML+12] C. J. Bolech, F. Heidrich-Meisner, S. Langer, I. P. McCulloch, G. Orso, and M. Rigol. Long-time behavior of the momentum distribution during the sudden expansion of a spin-imbalanced fermi gas in one dimension. *Phys. Rev. Lett.*, 109:110602, Sep 2012.

[BK17] Fabian R. A. Biebl and Stefan Kehrein. Thermalization rates in the one-dimensional hubbard model with next-to-nearest neighbor hopping. *Phys. Rev. B*, 95:104304, Mar 2017.

[BKP21] Berislav Buča, Katja Klobas, and Tomaž Prosen. Rule 54: Exactly solvable model of nonequilibrium statistical mechanics. *arXiv preprint arXiv:2103.16543*, 2021.

[BLGR20] Marlon Brenes, Tyler LeBlond, John Goold, and Marcos Rigol. Eigenstate thermalization in a locally perturbed integrable system. *arXiv preprint arXiv:2004.04755*, 2020.

[BLV21] Alvise Bastianello, Andrea De Luca, and Romain Vasseur. Hydrodynamics of weak integrability breaking. *Journal of Statistical Mechanics: Theory and Experiment*, 2021(11):114003, nov 2021.

[Bre99] Kevin F Brennan. *The physics of semiconductors: with applications to optoelectronic devices*. Cambridge university press, 1999.

[BS97] C. Boldrighini and Y. M. Suhov. One-dimensional hard-rod caricature of hydrodynamics: "navier–stokes correction"for local equilibrium initial states. *Communications in Mathematical Physics*, 189(2):577–590, 1997.

[BVKM17] Vir B. Bulchandani, Romain Vasseur, Christoph Karrasch, and Joel E. Moore. Solvable hydrodynamics of quantum integrable systems. *Phys. Rev. Lett.*, 119:220604, Nov 2017.

[CADY16a] Olalla A. Castro-Alvaredo, Benjamin Doyon, and Takato Yoshimura. Emergent hydrodynamics in integrable quantum systems out of equilibrium. *Phys. Rev. X*, 6:041065, Dec 2016.

[CADY16b] Olalla A. Castro-Alvaredo, Benjamin Doyon, and Takato Yoshimura. Emergent hydrodynamics in integrable quantum systems out of equilibrium. *Phys. Rev. X*, 6:041065, Dec 2016.

[CADY16c] Olalla A Castro-Alvaredo, Benjamin Doyon, and Takato Yoshimura. Emergent hydrodynamics in integrable quantum systems out of equilibrium. *Physical Review X*, 6(4):041065, 2016.

[CBM18] Xiangyu Cao, Vir B. Bulchandani, and Joel E. Moore. Incomplete thermalization from trap-induced integrability breaking: Lessons from classical hard rods. *Phys. Rev. Lett.*, 120:164101, Apr 2018.

[CC06] Pasquale Calabrese and John Cardy. Time dependence of correlation functions following a quantum quench. *Phys. Rev. Lett.*, 96:136801, Apr 2006.

[CC07] Pasquale Calabrese and John Cardy. Entanglement and correlation functions following a local quench: a conformal field theory approach. *Journal of Statistical Mechanics: Theory and Experiment*, 2007(10):P10004, 2007.

[CDD+19] Jean-Sébastien Caux, Benjamin Doyon, Jérôme Dubail, Robert Konik, and Takato Yoshimura. Hydrodynamics of the interacting Bose gas in the Quantum Newton Cradle setup. *SciPost Phys.*, 6:70, 2019.

[CDLV18] Mario Collura, Andrea De Luca, and Jacopo Viti. Analytic solution of the domain-wall nonequilibrium stationary state. *Phys. Rev. B*, 97:081111, Feb 2018.

[Che15] Alain Chenciner. Poincaré and the three-body problem. In *Henri Poincaré, 1912–2012*, pages 51–149. Springer, 2015.

[CNPS19] Amos Chan, Rahul M. Nandkishore, Michael Pretko, and Graeme Smith. Unitary-projective entanglement dynamics. *Phys. Rev. B*, 99:224307, Jun 2019.

[DBD20] Joseph Durnin, M. J. Bhaseen, and Benjamin Doyon. Non-Equilibrium Dynamics and Weakly Broken Integrability. *arXiv e-prints*, page arXiv:2004.11030, April 2020.

[DBD21] Joseph Durnin, M. J. Bhaseen, and Benjamin Doyon. Nonequilibrium dynamics and weakly broken integrability. *Phys. Rev. Lett.*, 127:130601, Sep 2021.

[Deu91] Josh M Deutsch. Quantum statistical mechanics in a closed system. *Physical review a*, 43(4):2046, 1991.

[Deu18] Joshua M Deutsch. Eigenstate thermalization hypothesis. *Reports on Progress in Physics*, 81(8):082001, 2018.

[DGM08] S. N. Dorogovtsev, A. V. Goltsev, and J. F. F. Mendes. Critical phenomena in complex networks. *Rev. Mod. Phys.*, 80:1275–1335, Oct 2008.

[DKPR16] Luca D'Alessio, Yariv Kafri, Anatoli Polkovnikov, and Marcos Rigol. From quantum chaos and eigenstate thermalization to statistical mechanics and thermodynamics. *Advances in Physics*, 65(3):239–362, 2016.

[DNBD18] Jacopo De Nardis, Denis Bernard, and Benjamin Doyon. Hydrodynamic diffusion in integrable systems. *Phys. Rev. Lett.*, 121:160603, Oct 2018.

[DNBD19] Jacopo De Nardis, Denis Bernard, and Benjamin Doyon. Diffusion in generalized hydrodynamics and quasiparticle scattering. *SciPost Phys.*, 6(4):049, 2019.

[DNMKI20] Jacopo De Nardis, Marko Medenjak, Christoph Karrasch, and Enej Ilievski. Universality classes of spin transport in one-dimensional isotropic magnets: the onset of logarithmic anomalies. *arXiv preprint arXiv:2001.06432*, 2020.

[Doy19] Benjamin Doyon. Lecture notes on generalised hydrodynamics. *arXiv preprint arXiv:1912.08496*, 2019.

[Doy20] Benjamin Doyon. Lecture notes on generalised hydrodynamics. *SciPost Physics Lecture Notes*, Aug 2020.

[DS17a] Benjamin Doyon and Herbert Spohn. Drude weight for the lieb-liniger bose gas. *SciPost Physics*, 3(6):039, 2017.

[DS17b] Benjamin Doyon and Herbert Spohn. Dynamics of hard rods with initial domain wall state. *Journal of Statistical Mechanics: Theory and Experiment*, 2017(7):073210, jul 2017.

[DYC18] Benjamin Doyon, Takato Yoshimura, and Jean-Sébastien Caux. Soliton gases and generalized hydrodynamics. *Phys. Rev. Lett.*, 120:045301, Jan 2018.

[EKMR14] F. H. L. Essler, S. Kehrein, S. R. Manmana, and N. J. Robinson. Quench dynamics in a model with tuneable integrability breaking. *Phys. Rev. B*, 89:165104, Apr 2014.

[Fag17] Maurizio Fagotti. Higher-order generalized hydrodynamics in one dimension: The noninteracting test. *Phys. Rev. B*, 96:220302, Dec 2017.

[FC08] Maurizio Fagotti and Pasquale Calabrese. Evolution of entanglement entropy following a quantum quench: Analytic results for the x y chain in a transverse magnetic field. *Physical Review A*, 78(1):010306, 2008.

[FGV19] Aaron J Friedman, Sarang Gopalakrishnan, and Romain Vasseur. Integrable many-body quantum floquet-thouless pumps. *Physical review letters*, 123(17):170603, 2019.

[FGV20a] Aaron J. Friedman, Sarang Gopalakrishnan, and Romain Vasseur. Diffusive hydrodynamics from integrability breaking. *Phys. Rev. B*, 101:180302, May 2020.

[FGV20b] Aaron J. Friedman, Sarang Gopalakrishnan, and Romain Vasseur. Diffusive hydrodynamics from integrability breaking. *Phys. Rev. B*, 101:180302, May 2020.

[FKNV23] Matthew P. A. Fisher, Vedika Khemani, Adam Nahum, and Sagar Vijay. Random quantum circuits. *Annual Review of Condensed Matter Physics*, 14(1):335–379, 2023/04/24 2023.

[FVVY21] Ruihua Fan, Sagar Vijay, Ashvin Vishwanath, and Yi-Zhuang You. Self-organized error correction in random unitary circuits with measurement. *Physical Review B*, 103(17):174309, 2021.

[FWS20] Matthew Fishman, Steven R. White, and E. Miles Stoudenmire. The itensor software library for tensor network calculations, 2020.

[Gal13] Giovanni Gallavotti. *Statistical mechanics: A short treatise*. Springer Science & Business Media, 2013.

[Gau83] Michel Gaudin. *La fonction d'onde de Bethe*, volume 1. Elsevier Masson, 1983.

[GE16] Christian Gogolin and Jens Eisert. Equilibration, thermalisation, and the emergence of statistical mechanics in closed quantum systems. *Reports on Progress in Physics*, 79(5):056001, 2016.

[GH19] Michael J. Gullans and David A. Huse. Scalable probes of measurement-induced criticality, Sep 2019.

[GHKV18a] Sarang Gopalakrishnan, David A. Huse, Vedika Khemani, and Romain Vasseur. Hydrodynamics of operator spreading and quasiparticle diffusion in interacting integrable systems. *Phys. Rev. B*, 98:220303, Dec 2018.

[GHKV18b] Sarang Gopalakrishnan, David A. Huse, Vedika Khemani, and Romain Vasseur. Hydrodynamics of operator spreading and quasiparticle diffusion in interacting integrable systems. *Phys. Rev. B*, 98:220303, Dec 2018.

[Gop18a] Sarang Gopalakrishnan. Operator growth and eigenstate entanglement in an interacting integrable floquet system. *Phys. Rev. B*, 98:060302, Aug 2018.

[Gop18b] Sarang Gopalakrishnan. Operator growth and eigenstate entanglement in an interacting integrable floquet system. *Phys. Rev. B*, 98:060302, Aug 2018.

[GV19] Sarang Gopalakrishnan and Romain Vasseur. Kinetic theory of spin diffusion and superdiffusion in x x z spin chains. *Physical review letters*, 122(12):127202, 2019.

[GZ18] Sarang Gopalakrishnan and Bahti Zakirov. Facilitated quantum cellular automata as simple models with non-thermal eigenstates and dynamics. *Quantum Science and Technology*, 3(4):044004, aug 2018.

[Has06] M. B. Hastings. Solving gapped hamiltonians locally. *Phys. Rev. B*, 73:085115, Feb 2006.

[HI98] Chin-Kun Hu and N. Sh. Izmailian. Exact correlation functions of Bethe lattice spin models in external magnetic fields. *Physical Review E*, 58(2):1644–1653, August 1998.

[HIA+23] Jesse C. Hoke, Matteo Ippoliti, Dmitry Abanin, Rajeev Acharya, Markus Ansmann, Frank Arute, Kunal Arya, Abraham Asfaw, Juan Atalaya, Joseph C. Bardin, Andreas Bengtsson, Gina Bortoli, Alexandre Bourassa, Jenna Bovaird, Leon Brill, Michael Broughton, and et al. Quantum information phases in space-time: measurement-induced entanglement and teleportation on a noisy quantum processor, 2023.

[HKM13] Yichen Huang, C. Karrasch, and J. E. Moore. Scaling of electrical and thermal conductivities in an almost integrable chain. *Phys. Rev. B*, 88:115126, Sep 2013.

[HLF+07] S. Hofferberth, I. Lesanovsky, B. Fischer, T. Schumm, and J. Schmiedmayer. Non-equilibrium coherence dynamics in one-dimensional bose gases. *Nature*, 449(7160):324–327, 09 2007.

[HNQ+16] P. Hayden, S. Nezami, X.-L. Qi, N. Thomas, M. Walter, and Z. Yang. Holographic duality from random tensor networks. *JHEP*, 2016(11):9, January 2016.

[HPL19] Kévin Hémery, Frank Pollmann, and David J. Luitz. Matrix product states approaches to operator spreading in ergodic quantum systems. *Phys. Rev. B*, 100:104303, Sep 2019.

[HRS04] V. Hunyadi, Z. Rácz, and L. Sasvári. Dynamic scaling of fronts in the quantum xx chain. *Phys. Rev. E*, 69:066103, Jun 2004.

[JHR06] P. Jung, R. W. Helmes, and A. Rosch. Transport in almost integrable models: Perturbed heisenberg chains. *Phys. Rev. Lett.*, 96:067202, Feb 2006.

[JYVL19] Chao-Ming Jian, Yi-Zhuang You, Romain Vasseur, and Andreas W. W. Ludwig. Measurement-induced criticality in random quantum circuits, 2019.

[KB21a] Katja Klobas and Bruno Bertini. Entanglement dynamics in rule 54: exact results and quasiparticle picture. *SciPost Physics*, 11(6):107, 2021.

[KB21b] Katja Klobas and Bruno Bertini. Exact relaxation to gibbs and non-equilibrium steady states in the quantum cellular automaton rule 54. 2021.

[KB21c] Katja Klobas and Bruno Bertini. Exact relaxation to gibbs and non-equilibrium steady states in the quantum cellular automaton rule 54. *SciPost Physics*, 11(6):106, 2021.

[KBI97] Vladimir E Korepin, Nicholay M Bogoliubov, and Anatoli G Izergin. *Quantum inverse scattering method and correlation functions*, volume 3. Cambridge university press, 1997.

[KH13] Hyungwon Kim and David A. Huse. Ballistic spreading of entanglement in a diffusive nonintegrable system. *Phys. Rev. Lett.*, 111:127205, Sep 2013.

[KHN18] Vedika Khemani, David A. Huse, and Adam Nahum. Velocity-dependent lyapunov exponents in many-body quantum, semiclassical, and classical chaos. *Phys. Rev. B*, 98:144304, Oct 2018.

[KMHM14] C. Karrasch, J. E. Moore, and F. Heidrich-Meisner. Real-time and real-space spin and energy dynamics in one-dimensional spin-$\frac{1}{2}$ systems induced by local quantum quenches at finite temperatures. *Phys. Rev. B*, 89:075139, Feb 2014.

[KMPV18] Katja Klobas, Marko Medenjak, Tomaz Prosen, and Matthieu Vanicat. Time-dependent matrix product ansatz for interacting reversible dynamics. *arXiv preprint arXiv:1807.05000*, 2018.

[KPHM17] C. Karrasch, T. Prosen, and F. Heidrich-Meisner. Proposal for measuring the finite-temperature drude weight of integrable systems. *Phys. Rev. B*, 95:060406, Feb 2017.

[KS12] Andreas Knauf and Yakov G Sinai. *Classical nonintegrability, quantum chaos*, volume 27. Birkhäuser, 2012.

[KSMM22] Jin Ming Koh, Shi-Ning Sun, Mario Motta, and Austin J. Minnich. Experimental realization of a measurement-induced entanglement phase transition on a superconducting quantum processor, 2022.

[KT74] Shigetoshi Katsura and Makoto Takizawa. Bethe Lattice and the Bethe Approximation. *Progress of Theoretical Physics*, 51(1):82–98, 01 1974.

[Kub57] Ryogo Kubo. Statistical-mechanical theory of irreversible processes. i. general theory and simple applications to magnetic and conduction problems. *Journal of the Physical Society of Japan*, 12(6):570–586, 1957.

[KVGP20] Katja Klobas, Matthieu Vanicat, Juan P Garrahan, and Tomaž Prosen. Matrix product state of multi-time correlations. *Journal of Physics A: Mathematical and Theoretical*, 53(33):335001, 2020.

[KVH18a] Vedika Khemani, Ashvin Vishwanath, and David A. Huse. Operator spreading and the emergence of dissipative hydrodynamics under unitary evolution with conservation laws. *Phys. Rev. X*, 8:031057, Sep 2018.

[KVH18b] Vedika Khemani, Ashvin Vishwanath, and David A Huse. Operator spreading and the emergence of dissipative hydrodynamics under unitary evolution with conservation laws. *Physical Review X*, 8(3):031057, 2018.

[KWE11] Marcus Kollar, F. Alexander Wolf, and Martin Eckstein. Generalized gibbs ensemble prediction of prethermalization plateaus and their relation to nonthermal steady states in integrable systems. *Phys. Rev. B*, 84:054304, Aug 2011.

[KWW06] T. Kinoshita, T. Wenger, and D. Weiss. A quantum newton's cradle. *Nature*, 440:900, 2006.

[LCF18] Yaodong Li, Xiao Chen, and Matthew PA Fisher. Quantum zeno effect and the many-body entanglement transition. *Physical Review B*, 98(20):205136, 2018.

[LCF19] Yaodong Li, Xiao Chen, and Matthew P. A. Fisher. Measurement-driven entanglement transition in hybrid quantum circuits. *Phys. Rev. B*, 100:134306, Oct 2019.

[LCLF20] Yaodong Li, Xiao Chen, Andreas WW Ludwig, and Matthew Fisher. Conformal invariance and quantum non-locality in hybrid quantum circuits. *arXiv preprint arXiv:2003.12721*, 2020.

[LEG+15] Tim Langen, Sebastian Erne, Remi Geiger, Bernhard Rauer, Thomas Schweigler, Maximilian Kuhnert, Wolfgang Rohringer, Igor E. Mazets, Thomas Gasenzer, and Jörg Schmiedmayer. Experimental observation of a generalized gibbs ensemble. *Science*, 348(6231):207–211, 2015.

[LF21] Yaodong Li and Matthew PA Fisher. Statistical mechanics of quantum error correcting codes. *Physical Review B*, 103(10):104306, 2021.

[LGS16a] Tim Langen, Thomas Gasenzer, and Jörg Schmiedmayer. Prethermalization and universal dynamics in near-integrable quantum systems. *Journal of Statistical Mechanics: Theory and Experiment*, 2016(6):064009, jun 2016.

[LGS16b] Tim Langen, Thomas Gasenzer, and Jörg Schmiedmayer. Prethermalization and universal dynamics in near-integrable quantum systems. *Journal of Statistical Mechanics: Theory and Experiment*, 2016(6):064009, 2016.

[LHMG+09] S. Langer, F. Heidrich-Meisner, J. Gemmer, I. P. McCulloch, and U. Schollwöck. Real-time study of diffusive and ballistic transport in spin-$\frac{1}{2}$ chains using the adaptive time-dependent density matrix renormalization group method. *Phys. Rev. B*, 79:214409, Jun 2009.

[LHMHM11] Stephan Langer, Markus Heyl, Ian P. McCulloch, and Fabian Heidrich-Meisner. Real-time energy dynamics in spin-$\frac{1}{2}$ heisenberg chains. *Phys. Rev. B*, 84:205115, Nov 2011.

[LLP81] LD Landau, EM Lifshitz, and LP Pitaevskij. *Course of theoretical physics. vol. 10: Physical kinetics*. Oxford, 1981.

[LM13] Elliott H Lieb and Daniel C Mattis. *Mathematical physics in one dimension: exactly soluble models of interacting particles*. Academic Press, 2013.

[LM18] Cheng-Ju Lin and Olexei I. Motrunich. Out-of-time-ordered correlators in a quantum ising chain. *Phys. Rev. B*, 97:144304, Apr 2018.

[LMMR14] Jonathan Lux, Jan Müller, Aditi Mitra, and Achim Rosch. Hydrodynamic long-time tails after a quantum quench. *Phys. Rev. A*, 89:053608, May 2014.

[LP83] EM Lifschitz and LP Pitajewski. Physical kinetics. In *Textbook of theoretical physics. 10*. 1983.

[LPGV22] Javier Lopez-Piqueres, Sarang Gopalakrishnan, and Romain Vasseur. Integrability breaking in the rule 54 cellular automaton. *Journal of Physics A: Mathematical and Theoretical*, 55(23):234005, may 2022.

[LPS68] J. L. Lebowitz, J. K. Percus, and J. Sykes. Time evolution of the total distribution function of a one-dimensional system of hard rods. *Phys. Rev.*, 171:224–235, Jul 1968.

[LPV23] Javier Lopez-Piqueres and Romain Vasseur. Integrability breaking from backscattering. *Phys. Rev. Lett.*, 130:247101, Jun 2023.

[LPWGV21a] Javier Lopez-Piqueres, Brayden Ware, Sarang Gopalakrishnan, and Romain Vasseur. Hydrodynamics of nonintegrable systems from a relaxation-time approximation. *Phys. Rev. B*, 103:L060302, Feb 2021.

[LPWGV21b] Javier Lopez-Piqueres, Brayden Ware, Sarang Gopalakrishnan, and Romain Vasseur. Operator front broadening in chaotic and integrable quantum chains. *Phys. Rev. B*, 104:104307, Sep 2021.

[LPWV20] Javier Lopez-Piqueres, Brayden Ware, and Romain Vasseur. Mean-field entanglement transitions in random tree tensor networks. *Phys. Rev. B*, 102:064202, Aug 2020.

[LRP22] Oliver Lunt, Jonas Richter, and Arijeet Pal. *Quantum Simulation Using Noisy Unitary Circuits and Measurements*, pages 251–284. Springer International Publishing, Cham, 2022.

[LSM+12] S. Langer, M. J. A. Schuetz, I. P. McCulloch, U. Schollwöck, and F. Heidrich-Meisner. Expansion velocity of a one-dimensional, two-component fermi gas during the sudden expansion in the ballistic regime. *Phys. Rev. A*, 85:043618, Apr 2012.

[LŽP17] Marko Ljubotina, Marko Žnidarič, and Tomaž Prosen. Spin diffusion from an inhomogeneous quench in an integrable system. *Nature communications*, 8(1):1–6, 2017.

[Mac07] Joseph Maciejko. An introduction to nonequilibrium many-body theory. *Lecture Notes, Springer*, 2007.

[MKP17] Marko Medenjak, Katja Klobas, and Tomaz Prosen. Diffusion in deterministic interacting lattice systems. *Phys. Rev. Lett.*, 119:110603, Sep 2017.

[MMGS13] Matteo Marcuzzi, Jamir Marino, Andrea Gambassi, and Alessandro Silva. Prethermalization in a nonintegrable quantum spin chain after a quench. *Phys. Rev. Lett.*, 111:197203, Nov 2013.

[MMGS16] M. Marcuzzi, J. Marino, A. Gambassi, and A. Silva. Prethermalization from a low-density holstein-primakoff expansion. *Phys. Rev. B*, 94:214304, Dec 2016.

[MMM09] Marc Mezard, Marc Mezard, and Andrea Montanari. *Information, physics, and computation*. Oxford University Press, 2009.

[MPV87] Marc Mézard, Giorgio Parisi, and Miguel Virasoro. *Spin glass theory and beyond: An Introduction to the Replica Method and Its Applications*, volume 9. World Scientific Publishing Company, 1987.

[MR18] Krishnanand Mallayya and Marcos Rigol. Quantum quenches and relaxation dynamics in the thermodynamic limit. *Phys. Rev. Lett.*, 120:070603, Feb 2018.

[MR19] Krishnanand Mallayya and Marcos Rigol. Heating rates in periodically driven strongly interacting quantum many-body systems. *Phys. Rev. Lett.*, 123:240603, Dec 2019.

[MRDR19] Krishnanand Mallayya, Marcos Rigol, and Wojciech De Roeck. Prethermalization and thermalization in isolated quantum systems. *Physical Review X*, 9(2):021027, 2019.

[MS20] Frederik S. Møller and Jörg Schmiedmayer. Introducing iFluid: a numerical framework for solving hydrodynamical equations in integrable models. *SciPost Phys.*, 8:41, 2020.

[NC02] Michael A Nielsen and Isaac Chuang. Quantum computation and quantum information, 2002.

[NDMP22] Jacopo De Nardis, Benjamin Doyon, Marko Medenjak, and Miłosz Panfil. Correlation functions and transport coefficients in generalised hydrodynamics. *Journal of Statistical Mechanics: Theory and Experiment*, 2022(1):014002, jan 2022.

[Neu29] J v Neumann. Beweis des ergodensatzes und des h-theorems in der neuen mechanik. *Zeitschrift für Physik*, 57(1):30–70, 1929.

[Nie82] Bernard Nienhuis. Exact critical point and critical exponents of O(n) models in two dimensions. *Phys. Rev. Lett.*, 49:1062–1065, Oct 1982.

[NNZ+22] Crystal Noel, Pradeep Niroula, Daiwei Zhu, Andrew Risinger, Laird Egan, Debopriyo Biswas, Marko Cetina, Alexey V. Gorshkov, Michael J. Gullans, David A. Huse, and Christopher Monroe. Measurement-induced quantum phases realized in a trapped-ion quantum computer. *Nature Physics*, 18(7):760–764, 2022.

[NR02] Onuttom Narayan and Sriram Ramaswamy. Anomalous heat conduction in one-dimensional momentum-conserving systems. *Phys. Rev. Lett.*, 89:200601, Oct 2002.

[NRVH17] A. Nahum, J. Ruhman, S. Vijay, and J. Haah. Quantum Entanglement Growth under Random Unitary Dynamics. *Physical Review X*, 7(3):031016, July 2017.

[NVH18a] Adam Nahum, Sagar Vijay, and Jeongwan Haah. Operator spreading in random unitary circuits. *Phys. Rev. X*, 8:021014, Apr 2018.

[NVH18b] Adam Nahum, Sagar Vijay, and Jeongwan Haah. Operator spreading in random unitary circuits. *Physical Review X*, 8(2):021014, 2018.

[Orú14] Román Orús. A practical introduction to tensor networks: Matrix product states and projected entangled pair states. *Annals of Physics*, 349:117–158, 2014.

[PCC+20] Mohit Pandey, Pieter W Claeys, David K Campbell, Anatoli Polkovnikov, and Dries Sels. Adiabatic eigenstate deformations as a sensitive probe for quantum chaos. *arXiv preprint arXiv:2004.05043*, 2020.

[Per69] J. K. Percus. Exact solution of kinetics of a model classical fluid. *The Physics of Fluids*, 12(8):1560–1563, 1969.

[PGSGG+10] D Pérez-García, M Sanz, C E González-Guillén, M M Wolf, and J I Cirac. Characterizing symmetries in a projected entangled pair state. *New Journal of Physics*, 12(2):025010, Feb 2010.

[Picvcv07] Toma ž Prosen and Marko Žnidarič. Is the efficiency of classical simulations of quantum dynamics related to integrability? *Phys. Rev. E*, 75:015202, Jan 2007.

[PK05] T. Platini and D. Karevski. Scaling and front dynamics in ising quantum chains. *The European Physical Journal B - Condensed Matter and Complex Systems*, 48(2):225–231, Nov 2005.

[PKS+19] Sebastian Paeckel, Thomas Köhler, Andreas Swoboda, Salvatore R Manmana, Ulrich Schollwöck, and Claudius Hubig. Time-evolution methods for matrix-product states. *Annals of Physics*, 411:167998, 2019.

[PMM16] Tomaž Prosen and Carlos Mejía-Monasterio. Integrability of a deterministic cellular automaton driven by stochastic boundaries. *Journal of Physics A: Mathematical and Theoretical*, 49(18):185003, 2016.

[Pol77] Alexander M Polyakov. Hidden symmetry of the two-dimensional chiral fields. *Physics Letters B*, 72(2):224–226, 1977.

[PSSV11] Anatoli Polkovnikov, Krishnendu Sengupta, Alessandro Silva, and Mukund Vengalattore. Colloquium: Nonequilibrium dynamics of closed interacting quantum systems. *Rev. Mod. Phys.*, 83:863–883, Aug 2011.

[PV22] Andrew C. Potter and Romain Vasseur. *Entanglement Dynamics in Hybrid Quantum Circuits*, pages 211–249. Springer International Publishing, Cham, 2022.

[RDO08a] Marcos Rigol, Vanja Dunjko, and Maxim Olshanii. Thermalization and its mechanism for generic isolated quantum systems. *Nature*, 452(7189):854–858, 2008.

[RDO08b] Marcos Rigol, Vanja Dunjko, and Maxim Olshanii. Thermalization and its mechanism for generic isolated quantum systems. *Nature*, 452(7189):854–858, 04 2008.

[RPvK18a] Tibor Rakovszky, Frank Pollmann, and C. W. von Keyserlingk. Diffusive hydrodynamics of out-of-time-ordered correlators with charge conservation. *Phys. Rev. X*, 8:031058, Sep 2018.

[RPvK18b] Tibor Rakovszky, Frank Pollmann, and C. W. von Keyserlingk. Diffusive hydrodynamics of out-of-time-ordered correlators with charge conservation. *Phys. Rev. X*, 8:031058, Sep 2018.

[RSB+13] J. P. Ronzheimer, M. Schreiber, S. Braun, S. S. Hodgman, S. Langer, I. P. McCulloch, F. Heidrich-Meisner, I. Bloch, and U. Schneider. Expansion dynamics of interacting bosons in homogeneous lattices in one and two dimensions. *Phys. Rev. Lett.*, 110:205301, May 2013.

[Rue78] David Ruelle. What are the measure describing turbulence? *Progress of Theoretical Physics Supplement*, 64:339–345, 1978.

[SBDD19] M. Schemmer, I. Bouchoule, B. Doyon, and J. Dubail. Generalized hydrodynamics on an atom chip. *Phys. Rev. Lett.*, 122:090601, Mar 2019.

[Sch11a] Ulrich Schollwöck. The density-matrix renormalization group in the age of matrix product states. *Annals of physics*, 326(1):96–192, 2011.

[Sch11b] Ulrich Schollwoeck. The density-matrix renormalization group in the age of matrix product states. *Annals of Physics*, 326(1):96 – 192, 2011. January 2011 Special Issue.

[SJS+17] R. Steinigeweg, F. Jin, D. Schmidtke, H. De Raedt, K. Michielsen, and J. Gemmer. Real-time broadening of nonequilibrium density profiles and the role of the specific initial-state realization. *Phys. Rev. B*, 95:035155, Jan 2017.

[Spo82] Herbert Spohn. Hydrodynamical theory for equilibrium time correlation functions of hard rods. *Annals of Physics*, 141(2):353–364, 1982.

[Spo14] Herbert Spohn. Nonlinear fluctuating hydrodynamics for anharmonic chains. *Journal of Statistical Physics*, 154(5):1191–1227, Mar 2014.

[SR10] Lea F. Santos and Marcos Rigol. Onset of quantum chaos in one-dimensional bosonic and fermionic systems and its relation to thermalization. *Phys. Rev. E*, 81:036206, Mar 2010.

[Sre94] Mark Srednicki. Chaos and quantum thermalization. *Physical review e*, 50(2):888, 1994.

[Sre99] Mark Srednicki. The approach to thermal equilibrium in quantized chaotic systems. *Journal of Physics A: Mathematical and General*, 32(7):1163, 1999.

[SRN19] Brian Skinner, Jonathan Ruhman, and Adam Nahum. Measurement-induced phase transitions in the dynamics of entanglement. *Physical Review X*, 9(3):031009, 2019.

[sup] *See Supplemental Material for numerical details and additional plots and containing Refs. [Doy20, ?, NR02, vB12, Spo14].*

[Sut04] Bill Sutherland. *Beautiful models: 70 years of exactly solved quantum many-body problems*. World Scientific, 2004.

[SVO18] Ramsés J Sánchez, Vipin Kerala Varma, and Vadim Oganesyan. Anomalous and regular transport in spin-1 2 chains: ac conductivity. *Physical Review B*, 98(5):054415, 2018.

[Tak99] M. Takahashi. *Thermodynamics of One-Dimensional Solvable Models*. Cambridge University Press, 1999.

[Tao14] Terence Tao. E pluribus unum: from complexity, universality. In *The Best Writing on Mathematics 2013*, pages 32–46. Princeton University Press, 2014.

[TKL+18a] Yijun Tang, Wil Kao, Kuan-Yu Li, Sangwon Seo, Krishnanand Mallayya, Marcos Rigol, Sarang Gopalakrishnan, and Benjamin L. Lev. Thermalization near integrability in a dipolar quantum newton's cradle. *Phys. Rev. X*, 8:021030, May 2018.

[TKL+18b] Yijun Tang, Wil Kao, Kuan-Yu Li, Sangwon Seo, Krishnanand Mallayya, Marcos Rigol, Sarang Gopalakrishnan, and Benjamin L. Lev. Thermalization near integrability in a dipolar quantum newton's cradle. *Phys. Rev. X*, 8:021030, May 2018.

[vAvEW+08] A. H. van Amerongen, J. J. P. van Es, P. Wicke, K. V. Kheruntsyan, and N. J. van Druten. Yang-yang thermodynamics on an atom chip. *Phys. Rev. Lett.*, 100:090402, Mar 2008.

[vB12] Henk van Beijeren. Exact results for anomalous transport in one-dimensional hamiltonian systems. *Phys. Rev. Lett.*, 108:180601, Apr 2012.

[Vid03] Guifré Vidal. Efficient classical simulation of slightly entangled quantum computations. *Phys. Rev. Lett.*, 91:147902, Oct 2003.

[vKRPS18a] C. W. von Keyserlingk, Tibor Rakovszky, Frank Pollmann, and S. L. Sondhi. Operator hydrodynamics, otocs, and entanglement growth in systems without conservation laws. *Phys. Rev. X*, 8:021013, Apr 2018.

[VKRPS18b] CW Von Keyserlingk, Tibor Rakovszky, Frank Pollmann, and Shivaji Lal Sondhi. Operator hydrodynamics, otocs, and entanglement growth in systems without conservation laws. *Physical Review X*, 8(2):021013, 2018.

[VLM+13] L. Vidmar, S. Langer, I. P. McCulloch, U. Schneider, U. Schollwöck, and F. Heidrich-Meisner. Sudden expansion of mott insulators in one dimension. *Phys. Rev. B*, 88:235117, Dec 2013.

[VPYL19] Romain Vasseur, Andrew C. Potter, Yi-Zhuang You, and Andreas W. W. Ludwig. Entanglement transitions from holographic random tensor networks. *Phys. Rev. B*, 100:134203, Oct 2019.

[VR16a] Lev Vidmar and Marcos Rigol. Generalized gibbs ensemble in integrable lattice models. *Journal of Statistical Mechanics: Theory and Experiment*, 2016(6):064007, 2016.

[VR16b] Lev Vidmar and Marcos Rigol. Generalized gibbs ensemble in integrable lattice models. *Journal of Statistical Mechanics: Theory and Experiment*, 2016(6):064007, 2016.

[VY19] Dinh-Long VU and Takato Yoshimura. Equations of state in generalized hydrodynamics. *SciPost Physics*, 6(2), Feb 2019.

[WVHC08] Michael M. Wolf, Frank Verstraete, Matthew B. Hastings, and J. Ignacio Cirac. Area laws in quantum systems: Mutual information and correlations. *Phys. Rev. Lett.*, 100:070502, Feb 2008.

[XS20] Shenglong Xu and Brian Swingle. Accessing scrambling using matrix product operators. *Nature Physics*, 16(2):199–204, 2020.

[YY69] Chen-Ning Yang and Cheng P Yang. Thermodynamics of a one-dimensional system of bosons with repulsive delta-function interaction. *Journal of Mathematical Physics*, 10(7):1115–1122, 1969.

[Zam80] AB Zamolodchikov. The tetrahedron equation and three-dimensional integrable systems. *Zh. Eksp. Teor. Fiz*, 79:641–664, 1980.

[ZBK22] Philip Zechmann, Alvise Bastianello, and Michael Knap. Tunable transport in the mass-imbalanced fermi-hubbard model. *Physical Review B*, 106(7), aug 2022.

[ZGW+20] Aidan Zabalo, Michael J Gullans, Justin H Wilson, Sarang Gopalakrishnan, David A Huse, and JH Pixley. Critical properties of the measurement-induced transition in random quantum circuits. *Physical Review B*, 101(6):060301, 2020.

[ZN19a] Tianci Zhou and Adam Nahum. Emergent statistical mechanics of entanglement in random unitary circuits. *Physical Review B*, 99(17):174205, 2019.

[ZN19b] Tianci Zhou and Adam Nahum. Emergent statistical mechanics of entanglement in random unitary circuits. *Phys. Rev. B*, 99:174205, May 2019.

[ZV04] M. Zwolak and G. Vidal. Mixed-state dynamics in one-dimensional quantum lattice systems: A time-dependent superoperator renormalization algorithm. *Phys. Rev. Lett.*, 93:207205, 2004.